
Electronic Theses and Dissertations, 2004-2019

2010

Dft Study Of Geometry And Energetics Of Transition Metal Systems

Satyender Goel
University of Central Florida

 Part of the [Chemistry Commons](#)

Find similar works at: <https://stars.library.ucf.edu/etd>

University of Central Florida Libraries <http://library.ucf.edu>

This Doctoral Dissertation (Open Access) is brought to you for free and open access by STARS. It has been accepted for inclusion in Electronic Theses and Dissertations, 2004-2019 by an authorized administrator of STARS. For more information, please contact STARS@ucf.edu.

STARS Citation

Goel, Satyender, "Dft Study Of Geometry And Energetics Of Transition Metal Systems" (2010). *Electronic Theses and Dissertations, 2004-2019*. 4316.

<https://stars.library.ucf.edu/etd/4316>

DFT STUDY OF GEOMETRY AND ENERGETICS OF TRANSITION METAL
SYSTEMS

by

SATYENDER GOEL

M.Sc. The University of Manchester, U.K. 2005

A dissertation submitted in partial fulfillment of the requirements
for the degree of Doctor of Philosophy
in the Department of Chemistry
in the College of Sciences
at the University of Central Florida
Orlando, Florida

Summer Term

2010

Major Professor: Artëm E. Masunov

© 2010 Satyender Goel

ABSTRACT

This dissertation focuses on computational study of the geometry and energetics small molecules and nanoclusters involving transition metals (TM). These clusters may be used for various industrial applications including catalysis and photonics. Specifically, in this work we have studied hydrides and carbides of *3d*-transition metal systems (Sc through Cu), small nickel and gold clusters. Qualitatively correct description of the bond dissociation is ensured by allowing the spatial and spin symmetry to break. We have tested applicability of new exchange-correlation functional and alternative theoretical descriptions (spin-contamination correction in broken symmetry DFT and ensemble Kohn-Sham (EKS)) as well. We studies TM hydrides and carbides systems to understand the importance of underlying phenomenon of bond breaking in catalytic processes. We have tested several exchange-correlation functionals including explicit dependence on kinetic energy density (τ -functionals) for the description of hydrides (both neutral and cationic) and carbides formed by *3d*-transition metals. We find M05-2x and BMK dissociation energies are in better agreement with experiment (where available) than those obtained with high level wavefunction theory methods, published previously. This agreement with experiment deteriorates quickly for other functionals when the fraction of the Hartree-Fock exchange in DFT functional is decreased. Higher fraction of HF exchange is also essential in EKS formalism, but it does not help when spin-adapted unrestricted approach is employed. We analyze the electron spin densities using Natural Bond Orbital population analysis and find that simple description of *3d* electrons as non-bonding in character is rarely correct.

Unrestricted formalism results in appreciable spin-contamination for some of the systems at equilibrium, which motivated us to investigate it further in details. In order to correct the spin contamination effect on the energies, we propose a new scheme to correct for spin contamination arising in broken-symmetry DFT approach. Unlike conventional schemes, our spin correction is introduced for each spin-polarized electron pair individually and therefore is expected to yield more

accurate energy values. We derive an expression to extract the energy of the pure singlet state from the energy of the broken-symmetry DFT description of the low spin state and the energies of the high spin states (pentuplet and two spin-contaminated triplets in the case of two spin-polarized electron pairs). We validate our spin-contamination correction approach by a simple example of H_2 and applied to more complex MnH system. Ensemble KS formalism is also applied to investigate the dissociation of C_2 molecule. We find that high fraction of HF exchange is essential to reproduce the results of EKS treatment with exact exchange-correlation functional.

We analyze the geometry and energetics of small nickel clusters (Ni_2 - Ni_5) for several lowest energy isomers. We also study all possible spin states of small nickel cluster isomers and report observed trends in energetics. Finally we determine the geometry and energetics of ten lowest energy isomers of four small gold clusters (Au_2 , Au_4 , Au_6 , and Au_8). We have also investigated the influence of cluster geometry, ligation, solvation and relativistic effects on electronic structure of these gold clusters. The effect of one-by-one ligand attachment in vacuum and solvent environment is also studied. Performance of five DFT functionals are tested as well; Local Spin Density Approximation (SVWN5), Generalized Gradient Approximation (PBE), kinetic energy density-dependent functional (TPSS), hybrid DFT (B3LYP), and CAM-B3LYP which accounts for long-range exchange effects believed to be important in the analysis of metal bonding in gold complexes and clusters. Our results exhibit the ligand induced stability enhancement of otherwise less stable isomers of Au_4 , Au_6 and Au_8 . Ligands are found to play a crucial role in determining the 2D \rightarrow 3D transition realized in small gold clusters. In order to select an appropriate theory level to use in this study, we investigate the effect of attachment of four different ligands (NH_3 , NMe_3 , PH_3 , PMe_3) on cluster geometry and energetics of Au_2 and Au_4 in vacuum and in solution. Our results benchmark the applicability of DFT functional model and polarization functions in the basis set for calculations of ligated gold cluster systems. We employ five different basis sets with increasing amount of polarization and

diffuse functions; LANL2DZ, LANL2DZ-P, def2-SVP, def2-TZVP, and def2-QZVP. We obtain $\text{NMe}_3 \approx \text{NH}_3 < \text{PH}_3 < \text{PMe}_3$ order of ligand binding energies and observe shallow potential energy surfaces in all molecules. Our results suggest appropriate quantum-chemical methodologies to model small noble metal clusters in realistic ligand environment to provide reliable theoretical analysis in order to complement experiments.

ACKNOWLEDGMENTS

As I complete my dissertation, I take the pleasant opportunity to convey my gratitude to the people who inspired me during my doctoral study.

My deepest gratitude goes to my family for their unflagging love, care and support throughout my life; this dissertation is simply impossible without them. I am indebted to my parents, my brother, sister and their family for their unconditional love and blessings.

I wish to express my sincere gratitude to my advisor, Prof. Atrëm E. Masunov, for his guidance during my research and study at University of Central Florida. I thank him for his contributions of time, ideas, and funding to make my PhD experience productive and stimulating.

I acknowledge my advisors at Los Alamos National Lab, Dr. Andrei Piryatinski, Dr. Sergei A. Ivanov and Dr. Sergei Tretiak for their support and intellectual insight during my one year co-op term at the lab.

I am grateful to my committee members for their detailed review, constructive criticism and valuable advices during my proposal and dissertation defense. I would like to thank my group members and collaborators for their advices and the fruitful discussions.

It is my pleasure to express my sincere acknowledgement to all of my friends who made my stay at UCF and Orlando full of joy. I specially thank all the staff members and my colleagues at NSTC.

At last but not the least, I gratefully acknowledge the financial support from I2Lab, Los Alamos National Lab, NanoScience Technology Center and Department of Chemistry, University of Central Florida which enabled me to successfully complete my dissertation.

TABLE OF CONTENTS

| | |
|---|-------------|
| LIST OF FIGURES | ix |
| LIST OF TABLES | xii |
| ABBREVIATIONS | xiii |
| CHAPTER 1: INTRODUCTION | 1 |
| 1.1 Transition metal hydrides and their ions | 5 |
| 1.2 Transition metal carbides | 8 |
| 1.3 Small nickel clusters | 11 |
| 1.4 Small gold clusters (bare and ligated) | 13 |
| CHAPTER 2: THEORY | 16 |
| 2.1 Density Functional Formalism and Exchange-correlation Functionals | 16 |
| 2.2 Basis sets and relativistic corrections..... | 22 |
| 2.3 Spin-Contamination Correction Development | 25 |
| 2.4 Spin-Contamination Correction Testing..... | 37 |
| 2.5 Ensemble Kohn-Sham approach: Example C_2 | 40 |
| CHAPTER 3: TRANSITION METAL HYDRIDES AND THEIR IONS | 45 |
| 3.1 TMH Binding Energies | 45 |
| 3.2 TMH Bond Lengths | 47 |
| 3.3 TMH Potential Energy Curves and spin gaps | 48 |
| 3.4 TMH Cations..... | 50 |
| 3.5 TMH Electronic Structure and Ionization Potential | 51 |
| 3.6 Conclusions..... | 53 |
| CHAPTER 4: TRANSITION METAL CARBIDES (TMC) AND SMALL NICKEL CLUSTERS | 70 |
| 4.1 TMC Binding Energies..... | 70 |
| 4.2 TMC Bond Lengths | 72 |
| 4.3 TMC Potential Energy Curves | 72 |
| 4.4 Small Nickel Cluster geometries and orbitals..... | 74 |
| 4.5 Conclusions..... | 77 |

| | |
|---|------------|
| CHAPTER 5: SMALL GOLD CLUSTERS WITH AND WITHOUT LIGANDS..... | 93 |
| 5.1 Benchmark study of Au ₂ and Au ₄ in presence of different ligands with several basis sets and DFT functionals | 94 |
| 5.2 Geometry and energetics of small gold clusters | 99 |
| 5.2.1 Bare gold clusters..... | 100 |
| 5.2.2 Ligands and solvent effect..... | 102 |
| 5.2.2.1 Relative stability of isomers..... | 102 |
| 5.2.2.2 Effect on cluster geometries | 104 |
| 5.2.2.3 Cluster energetics | 105 |
| 5.3 Conclusions..... | 106 |
| SUMMARY AND OUTLOOK | 119 |
| REFERENCES | 122 |
| LIST OF RELEVANT PUBLICATIONS..... | 140 |

LIST OF FIGURES

| | | |
|-------------|---|----|
| Figure 1.1 | Nano-catalysis; the structure of a heterogeneous catalyst illustrating the length scales and complexity involved in a heterogeneous catalyst. ‘adapted from www.inano.au.dk ’ ² | |
| Figure 1.2 | Visualization of a possible carbon nanotube growth mechanism(adapted from Ref 29). | 3 |
| Figure 1.3 | Fluorescent gold nanoparticles in solution and their application testing in bio-imaging, inset- picture showing configuration of fluorescent solution containing gold nanoparticles. (partial Figure was adapted from the work of Dr. Zheng ⁴)..... | 4 |
| Figure 2.1 | Potential Energy Curves for hydrogen dimer with and without spin-contamination correction from our new approach, along with CCSD and Yamaguchi correction..... | 43 |
| Figure 2.2 | Spin-corrected Potential Energy Curves of MnH with multiplicity 5 and 7, calculated by TPSS, BMK, and WFT19 methods. | 43 |
| Figure 2.3 | Potential energy curves with RKS, EKS and UKS approach compared with <i>ab-initio</i> and experimental data. Representative molecular orbitals with EKS occupations (range) and standard restricted KS occupations (in bracket) alongside interatomic distances. | 44 |
| Figure 3.1 | Deviations in Binding Energies from experimental data (Set III in Table 3.1.1) for neutral TMH with various DFT and WFT methods..... | 63 |
| Figure 3.2 | Deviations in Bond Lengths from experimental data for neutral TMH with various DFT and WFT methods..... | 63 |
| Figure 3.3 | Potential Energy Curves of ScH with multiplicity 1 and 3, calculated by non-relativistic TPSS, BMK, and WFT (21) methods. | 64 |
| Figure 3.4 | Potential Energy Curves of VH with multiplicity 3 and 5, calculated by non-relativistic TPSS, BMK, and WFT (20) methods..... | 64 |
| Figure 3.5 | Potential Energy Curves of MnH with multiplicity 5 and 7, calculated by non-relativistic TPSS, BMK, and WFT (19) methods. | 65 |
| Figure 3.6 | Potential Energy Curves of CrH with multiplicity 2,4 and 6, calculated by non relativistic TPSS, BMK, and WFT (19) methods. | 65 |
| Figure 3.7 | Potential Energy Curves of neutral TMH calculated by non-relativistic BMK..... | 66 |
| Figure 3.8 | Deviations in Binding Energies from experimental data (Set II in Table 3.4.1) for TMH cations with various DFT and WFT methods..... | 66 |
| Figure 3.9 | Deviations in Bond Lengths from experimental data for TMH cations with various DFT and WFT methods..... | 67 |
| Figure 3.10 | Potential Energy Curves of ScH ⁺ with multiplicity 2, calculated by non relativistic TPSS, BMK, and WFT (230) methods..... | 67 |
| Figure 3.11 | Potential Energy Curves of TiH ⁺ with multiplicity 3, calculated by non relativistic TPSS, BMK, and WFT (28) methods..... | 68 |
| Figure 3.12 | Potential Energy Curves of CrH ⁺ with multiplicity 5, calculated by non relativistic TPSS, BMK, and WFT (240) methods..... | 68 |

| | | |
|-------------|---|-----|
| Figure 3.13 | Potential Energy Curves of TMH cations calculated by non-relativistic BMK..... | 69 |
| Figure 4.1 | Potential Energy Curves of ScC in doublet and quartet spin state, calculated by non-relativistic TPSS, BMK, M05, M05-2x and WFT methods. a) ² ScC plot with all methods, b) ⁴ ScC plot with all methods. | 81 |
| Figure 4.2 | Potential Energy Curves of TiC in singlet and triplet spin state, calculated by non-relativistic TPSS, BMK and M05-2x methods. a) ¹ TiC plot with all methods, b) ³ TiC plot with all methods. | 82 |
| Figure 4.3 | Potential Energy Curves of VC in doublet and quartet spin state, calculated by non-relativistic TPSS, BMK, M05, M05-2x and WFT methods. a) ² VC plot with all methods, b) ⁴ VC plot with all methods. | 83 |
| Figure 4.4 | Potential Energy Curves of CrC in singlet, quintet and septet spin state, calculated by non-relativistic TPSS, BMK, M05, M05-2x and WFT methods. a) ³ CrC plot with all methods, b) ⁵ CrC plot with all methods, c) ⁷ CrC plot with all methods..... | 84 |
| Figure 4.5 | Potential Energy Curves of MnC in quartet spin state, calculated by non-relativistic TPSS, BMK, M05-2x and WFT methods. | 85 |
| Figure 4.6 | Potential Energy Curves of FeC in triplet and quintet spin state, calculated by non-relativistic TPSS, BMK, M05, M05-2x and WFT methods. a) ³ FeC plot with all methods, b) ⁵ FeC plot with all methods. | 86 |
| Figure 4.7 | Potential Energy Curves of CoC in doublet, quartet and sextet spin state, calculated by non-relativistic TPSS, BMK, M05, M05-2x and WFT methods. a) ² CoC plot with all methods, b) ⁴ CoC plot with all methods, c) ⁶ CoC plot with all methods. | 87 |
| Figure 4.8 | Potential Energy Curves of NiC in singlet, triplet spin state, calculated by non-relativistic TPSS, BMK, M05, M05-2x and WFT methods. a) ¹ NiC plot with all methods, b) ³ NiC plot with all methods. | 88 |
| Figure 4.9 | Potential Energy Curves of CuC in quartet, calculated by non-relativistic TPSS, BMK, M05, M05-2x and WFT methods. | 89 |
| Figure 5.1 | Representative geometries of Au ₂ and Au ₄ cluster with ligand attached as PMe ₃ . (a) Au ₂ (PMe ₃) ₂ , (b) Au ₄ (PMe ₃) ₂ , (c) Au ₄ (PMe ₃) ₄ , (d) Au ₄ (NMe ₃) ₄ | 108 |
| Figure 5.2 | Comparison of binding energy per Ligand in kcal/mol for geometries of Au ₂ and Au ₄ in partial and fully ligated form determined by DFT functional model. TZVP basis set has been used for all calculations..... | 109 |
| Figure 5.3 | Comparison of binding energy per Ligand in kcal/mol for geometries of Au ₂ and Au ₄ in partial and fully ligated form determined by basis set. TPSS/TPSS functional has been used for all calculations..... | 110 |
| Figure 5.4 | Lowest energy isomers (10) of small gold clusters (Au ₂ , Au ₄ , Au ₆ and Au ₈)..... | 112 |
| Figure 5.5 | Relative energies for different isomers of small gold clusters with ligands. Comparison displays variations starting from saturated isomer with least number of ligands to the saturated isomer with most number of ligands. The lowest energy isomer is taken as reference structure (zero energy) for comparison..... | 113 |
| Figure 5.6 | Geometries of two isomers of Au ₄ with ligand attachment from one (top) to full ligation (saturation, bottom)..... | 114 |

| | | |
|-------------|---|-----|
| Figure 5.7 | Geometries of four isomers of Au ₆ with ligand attachment from one (top) to full ligation (Last geometry in respective columns)..... | 115 |
| Figure 5.8 | Geometries of four isomers of Au ₈ with ligand attachment from one (top) to full ligation (Last in respective columns, saturation)..... | 116 |
| Figure 5.9 | Binding energies per ligand (kcal/mol) of different isomers of small gold cluster (Au ₂ , Au ₄ , Au ₆ , Au ₈) geometries with increase in number of ligands (PH ₃) with (right) and without (left) solvent. | 117 |
| Figure 5.10 | Bond length variation between gold-gold and gold-ligand bonds in different isomers of small gold clusters, when ligands are attached starting from one to full ligation (Saturation)..... | 118 |

LIST OF TABLES

| | | |
|-----------|---|-----|
| Table 2.1 | Spin corrected and uncorrected dissociation energies of MnH in kcal/mol calculated with BMK and compared with ab-initio and experiment. | 44 |
| Table 3.1 | Dissociation energies (kcal/mol) of neutral hydrides (TMH) and root mean square (rms) deviations from the experimental values..... | 55 |
| Table 3.2 | Equilibrium bond lengths (Å) of neutral hydrides (TMH) and root mean square (rms) deviations from the experimental values. | 56 |
| Table 3.3 | Dissociation energies (kcal/mol) of metal hydrides cations (TMH+) and root mean square (rms) deviations from the experimental values. | 57 |
| Table 3.4 | Equilibrium bond lengths (Å) of metal hydrides cations (TMH+) and root mean square (rms) deviations from the experimental values. | 58 |
| Table 3.5 | Alpha and beta bonding and non-bonding orbital hybridization coefficients obtained from NBO analysis for the neutral hydrides (TMH) calculated with BMK..... | 59 |
| Table 3.6 | Dipole moments (Debye) for neutral metal hydrides calculated with BMK and TPSS, compared with several WFT levels..... | 60 |
| Table 3.7 | Alpha and beta bonding and non-bonding orbital hybridization coefficients obtained from NBO analysis for the metal hydrides cations calculated with BMK. | 61 |
| Table 3.8 | Adiabatic ionization potential (IP) of neutral metal hydrides and their errors in comparison to experimental values. | 62 |
| Table 4.1 | Dissociation energies (kcal/mol) of neutral carbides (TMC) with various DFT functionals compared with ab-initio results and experimental data (where available)... | 79 |
| Table 4.2 | Equilibrium bond lengths (Å) of neutral carbides (TMC) with various DFT functionals compared with ab-initio results and experimental data (where available). | 80 |
| Table 4.3 | Geometries of Ni ₂ , Ni ₃ , Ni ₅ and four isomers of Ni ₄ with several spin states (singlet, triplet, quintet, septet, nonet, undectet, duodectet and tridectet) with their bondlengths (Å) and binding energy (kcal/mol) displayed on each structure. | 90 |
| Table 4.4 | Molecular orbitals of all stable spin states (singlet, triplet, quintet, septet and nonet) of Ni ₅ tabulated as per their distribution antibonding (<i>p</i> orbitals) on top as unoccupied, non-bonding (lone pairs, <i>d</i> orbitals) and bonding <i>s</i> orbitals the last..... | 91 |
| Table 5.1 | Binding energies and bond length for Au ₂ calculated with different DFT functionals and compared with experimental data. | 108 |
| Table 5.2 | Au-Au (Peripheral), Au-Au (Base) and Au-Ligand bond lengths for optimized structures of Au ₂ and Au ₄ clusters with different ligands. TPSS functional has been used for all calculations with different basis set. | 111 |
| Table 5.3 | Relative energies for different isomers of bare gold clusters. The lowest energy isomer is taken as reference structure (zero energy) for comparison. ‘NC- no convergence’ | 112 |

ABBREVIATIONS

| | |
|--------|--|
| CAM | : Coloumb-attenuated method |
| CCSD | : Couple Cluster Second Derivative |
| CPCM | : Conductor-like Polarizable Continuum Model |
| DFT | : Density Functional Theory |
| DFTB | : Density Functional Tight Binding |
| EAM | : Embedded Atom Method |
| ECP | : Effective Core Potential |
| EMT | : Effective Medium Theory |
| FCI | : Full Configuration Interaction |
| FON | : Fractional Occupation Number |
| GGA | : Generalized Gradient Approximation |
| GVB | : Generalized Valance Bond |
| HF | : Hartree-Fock |
| KS | : Kohn-Sham |
| LC | : Long Range Corrected |
| LDA | : Local Density Approximation |
| LSDA | : Local Spin Density Approximation |
| MCPF | : Modified Coupled Pair Functional |
| MCSCF | : Multi-Configurational Self-Consistent Field |
| MD | : Molecular Dynamics |
| MO | : Molecular Orbitals |
| MPHF | : Maximally Paired Hartree-Fock |
| MP4 | : Møller–Plesset Perturbation Theory 4 |
| MRCI | : Multi-Reference Configuration Interaction |
| MRSDCI | : Multi-Reference Single and Double Configuration Interaction |
| MSINDO | : Modified Symmetric-Orthogonalized Intermediate Neglect of Differential Overlap |
| NBO | : Natural Bond Order |
| NO | : Natural Orbitals |
| PEC | : Potential Energy Curve |

| | |
|------|--|
| SCF | : Self-Consistent Field |
| SOCI | : Spin-Orbit Configuration Interaction |
| TM | : Transition Metal |
| TMC | : Transition Metal Carbides |
| TMH | : Transition Metal Hydrides |
| TS | : Transition State |
| WFT | : Wave Function Theory |
| ZORA | : Zero Order Regular Approximation |

CHAPTER 1: INTRODUCTION

Transition metal nanoclusters present a peculiar case of systems intermediate between the molecules and solids. Unlike the molecules and solids, theory of metal nanoclusters is lacking a set of simple rules assisting in prediction of the stable structures, and the first principles simulations remain the only method of geometry prediction. The studies of Transition Metal (TM) systems present a challenge for theoretical description due to the presence of several closely spaced electron states which results in strong electron correlation.¹⁻³ For this reason molecules and clusters containing TMs require special attention to the theoretical methods used. This thesis is aimed at accurate theoretical description of small transition metal clusters using the recently developed methods of Density Functional Theory. Specifically, two classes of nanoclusters are considered Ni_2 - Ni_5 and Au_2 - Au_8 .

While atomic and magnetic structures of the nanoclusters are important for catalytic applications, the ability of the transition metals to form and break chemical bonds with atoms of other elements is even more important. We focus on this aspect in sections 1.1 and 1.2. This thesis reports an exhaustive study on diatomics of *3d*-series (Sc to Cu) transition metal bound to hydrogen or carbon atom. Further sections 1.1 and 1.2 give more details about the work carried in the past on Transition Metal Hydrides (TMH) and Transition Metal Carbides (TMC) respectively.

The interest in the transition metal clusters is based on their numerous applications, most of which belong to two areas: catalysis and photonics. Simplistically, a catalyst affects the transition state and chemical reaction path mainly by forming a complex with one of the reagents. Transition metals are perfect candidates for catalytic processes as they may be found in a variety of oxidation states. Due to their property of providing or withdrawing electrons from the reaction complex, they undergo oxidation/reduction to achieve electron

transfer. Despite many commercially favored properties like high chemoselectivity, regioselectivity and high activities, homogeneous catalysts suffer various drawbacks. Their engineering processes have limitations such as cumbersome catalyst recovery and product purification, deactivation via metal particle aggregation etc. These drawbacks are easily

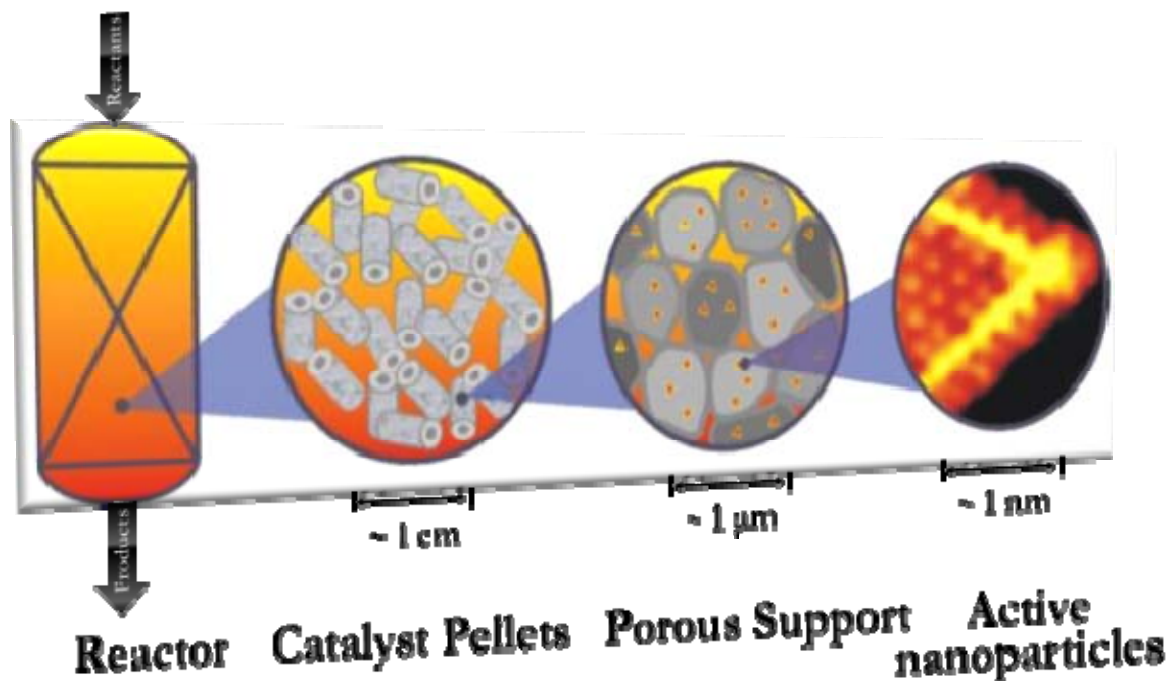


Figure 1.1 Nano-catalysis; the structure of a heterogeneous catalyst illustrating the length scales and complexity involved in a heterogeneous catalyst. 'adapted from www.inano.au.dk'

overcome by using heterogeneous catalysts due to their excellent stability and separability from the reaction mixture. Though they present an alternative to homogeneous catalysts but have their own limitations. These limitations include inferior catalytic performance and difficult isolation in filtration, which lead the search for more efficient catalyst. To overcome the limitations associated with these catalytic types, one needs to find a new catalytic system, which has activity comparable to homogeneous catalysis and recoverability comparable to heterogeneous catalyst. Nano-catalysis (Figure 1.1) emerged as the promising alternative

combining advantage of both the systems exhibiting unique activity and high selectivity. The interest in nanocatalysis stems from the fact that their properties are function of their dimension, size, chemical composition and morphology of the active catalyst nanoparticle. There have been considerable efforts made in recent decade to the design and controlled fabrication of these nanostructured materials. One of the major candidates for nanocatalysis are small metal clusters due to their several useful properties. To name a few characteristics of the small metal nanoclusters which can serve as effective catalysts are: (i) high surface to volume ratio, (ii) availability of active absorption and reactions sites, (iii) low energy barrier, (iv) wide range of coordination number and (v) easy migration and interatomic arrangements facilitates bond breaking.

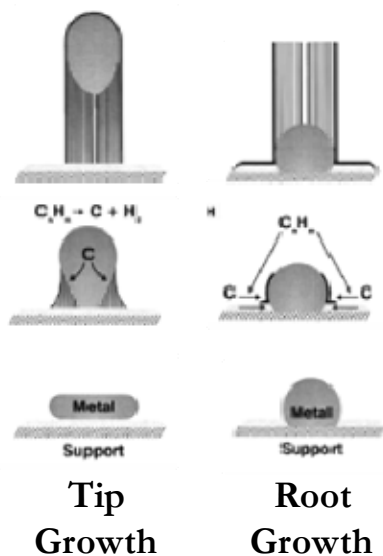


Figure 1.2 Visualization of a possible carbon nanotube growth mechanism(adapted from Ref 29).

Small nickel clusters have been studied extensively due to their potential use in carbon nanotubes (Figure 1.2) production. The research on carbon nanotubes in past two decades brought major breakthroughs in many fields due to their application in energy storage, energy conversion, field emission displays, sensors, conductive and high-strength

composites, interconnects, nanometer-sized semiconductor devices etc. Figure 1.2 above shows two mechanisms approaches of carbon nanotube growth catalyzed by metallic clusters. We detail the work investigating the small nickel clusters in section 1.3.

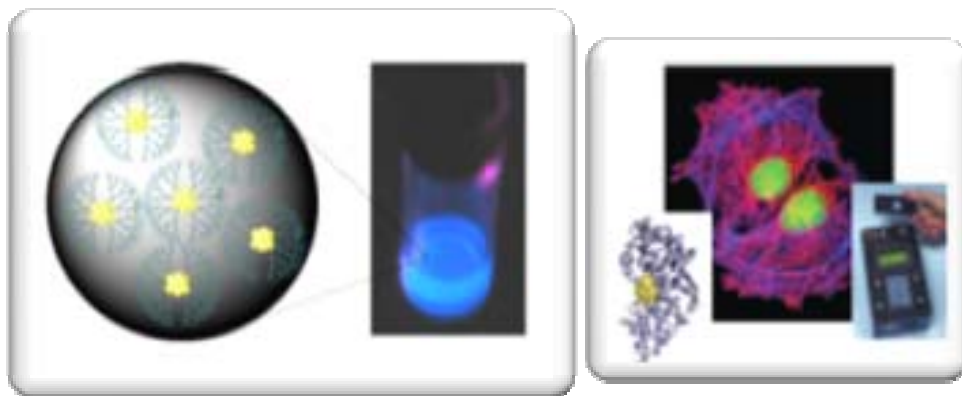


Figure 1.3 Fluorescent gold nanoparticles in solution and their application testing in bio-imaging, inset- picture showing configuration of fluorescent solution containing gold nanoparticles. (partial Figure was adapted from the work of Dr. Zheng⁴)

Gold is a precious metal known for its luster and value. While inert in bulk, it is excellent catalyst when scaled down to nanoparticles. Similar to other transition metal Nanoclusters, the chemical and physical properties of gold nanoclusters are also function of their size and morphology. Besides their catalytic activity, small gold clusters are also of wide interest due to their applications in photonics including bio-imaging and labeling (Figure 1.3). Their fluorescent capabilities and non-toxic nature makes them potential candidates for biological and synthetic chemistry research efforts for real world applications, if their size and structure can be controlled at the atomic level. Experimental studies cannot fully address the fundamental questions about cluster properties, whereas theoretical studies can provide invaluable microscopic insight into the electronic structure and dynamics of these nanoclusters. In view of the current scenario, we have broadened our vision of determining the geometry and energetics of bare metal clusters to include the effect of ligands on these

small clusters. We will provide the complete overview of small gold clusters in bare and ligated form in section 1.4.

1.1 Transition metal hydrides and their ions

Transition Metal Hydride (TMH) is small enough system to apply sophisticated and computationally demanding methods of the Wave Function Theory (WFT). This is one of the reasons why TM Hydrides and their positive ions have been investigated repeatedly both experimentally and theoretically in the series and individually. Availability of these results presents an excellent opportunity to validate new theoretical methods, including various Density Functional Theory approaches. Besides theoretical interest, chemical bonds between transition metal atom and hydrogen play an important role in surface chemistry and nanoparticle cluster catalysis, which fostered research on TM hydrides and their cations.⁵ The importance of TM hydrides, such as Iron hydride (FeH) in Astrophysics presents an additional motivation to study its spectroscopic constants and Potential Energy Curves (PEC).⁶⁻⁸ Ni is another important transition metal due to its catalytic properties. The electronic structure of NiH was investigated using SCF/CI methods three decades ago⁹ and, more recently with other multireference methods with or without relativistic effects.¹⁰⁻¹² Potential energy curves had been also calculated for other first row TM hydrides, including TiH,¹³⁻¹⁵ CoH,¹⁶ CuH,^{12, 17} VH,¹⁸ and ScH.¹⁹ Walch and Bauschlicher¹⁸ used CASSCF/SDCI method to account for both static and dynamic electron correlation effects in the ground state of most of the first row TM hydrides (TiH, VH, CrH, MnH, FeH, NiH). Related method MCSCF+SOCI was used by Koseki et al.²⁰ to study both ground and excited state PECs of the five first row TM hydrides (ScH, TiH, VH, CrH, MnH) recently.^{21, 22}

Besides the neutral TM hydrides, gas phase cations of transition metals attracted considerable interest as simplest compounds containing TM in different oxidation states in the hope that this study can help in understanding the behavior of more complicated systems. TM compounds of interest include systems used in surface and homogeneous catalysis⁵ and metallo-enzymes.²³ The comparison of bond energies and bond lengths of first row (Sc-Zn) transition metal hydrides calculated with modified coupled pair functional method (MCPF)²⁴ and generalized valence bond (GVB)²⁵ formalisms had shown a good agreement with experiment. A few extensive PES studies have been carried out for TM hydride positive ions such as (FeH⁺),²⁶ (CoH⁺),¹³ (CrH⁺)²⁷ and (TiH⁺).²⁸

In the past decade TM hydrides had been used to investigate the accuracy and efficiency of Density Functional Theory methods. Ziegler and Li studied TM hydride cations by using Local density approximations (LDA) and GGA.²⁹ They found bond lengths to be in agreement with experimentally determined values but their dissociation energies were less accurate. Barone et. al. used pure and hybrid DFT functionals BLYP and B3LYP to study transition metal complexes which includes first row TM hydrides and their cations.³⁰ B3LYP was found to give accurate dissociation energies, but somewhat overestimate the bond lengths and dipole moments. In a detailed study of *3d* transition metal systems including monohydrides, Furche and Perdew¹ did not reproduce these dissociation energies, even though they used the same functionals and basis sets. Presumably, their SCF procedure systematically converged to a different local minimum with broken symmetry DFT, whereas symmetry-adapted UKS was used by Barone et. al. Among various semilocal (LSDA, BP86, PBE, TPSS) and hybrid density functionals (B3LYP, hTPSS), Furche and Perdew recommend semilocal DFT functional TPSS. Their recommendation was based on the price/performance ratio, even though the hybrid functionals achieve lower mean absolute

error in bond energies. Jensen et. al.³ investigated performance of five different density functionals (B3LYP, BP86, PBE0, PBE, BLYP) for diatomics of first row transition metal systems. They concluded that success of a functional is system specific, which meant all of these functional are more accurate for certain system and less accurate for others. Jensen et. al. suggested an alternative way to get to the correct energies by taking arithmetic average of the functional which were under- and over-estimating the energies. Baker and Pulay studied metal hydrides MH and methylates MCH₃ (both neutral and cations) with two new functionals OLYP and O3LYP,³¹ but found no advantage of those as compared to BLYP and B3LYP. Riley and Merz recently published DFT study with 12 different functionals on several small TM molecules including 5 TM hydrides.³² They concluded that inclusion of exact exchange generally gave more accurate results consistently for heat of formation and ionization energies in TM systems. They also found B3LYP/6-31G** to be the best for ionization potentials, and PBE0/6-31G** to be the best for heat of formations.

DFT studies mentioned above used different basis sets and exchange-correlation functionals, and more importantly different protocols to obtain SCF solutions. The protocol included spin-adapted or broken-symmetry approach, wavefunction stability check, and initial guess. All these details might result in the large differences in calculated values for TM systems. Yet, they were rarely mentioned explicitly. Only a few papers mentioned how the lowest-energy SCF solution was obtained. For instance, Truhlar et. al.³³ reported using orbitals from CrMn as initial guess for Cr₂ to obtain the broken symmetry solution. Another example was constrained DFT calculations of Ni₂ and NiH by Diaconu et. al.,³⁴ where orbitals obtained from Ni atom were used as initial guess. The symmetry of electronic states was reported by Barone et. al.,³⁵ which indicated that lower-energy broken symmetry solutions were not attempted. On the other hand Furche et.al.¹ systematically considered all

possible microstates, corresponding to distribution of the metal valance electrons over $4s$ and $3d$ shells, converged them individually in SCF procedure and selected the one with the lowest energy.

Also, the studies described above were employing spin-polarized (or unrestricted) KS formalism and ignored spin contamination. Spin contamination played a major role in describing energy deviation of the systems with possibility of exhibiting more than one multiplicity, largely in complex systems involving TM compounds. In this study we have used both pure meta-GGA and hybrid meta-GGA exchange-correlation functionals TPSS and BMK to compare their performance with WFT methods and experimental data. To provide the insight into some of the important concepts we will focus here on TMH and TMH^+ (first row of transition metals) and examine the lowest states in several spin multiplicities and analyze variations in bond energies, bond lengths and electron densities. Potential energy curves and effect of spin correction are discussed. The DFT results are compared to experiment and WFT calculations.

1.2 Transition metal carbides

Transition metal carbides (TMC) were investigated repeatedly due to their importance in various scientific processes like catalysis. These investigations contributed to understanding the nature of chemical interaction between metal atoms and the other atomic species present in the reaction involving metal catalyst. Though, numerous theoretical attempts have been made to study these TMC's in past, their correct description was not completely understood due to the limited availability of experimental data. We could only find one theoretical investigation for complete $3d$ -metal monocarbides along with monoxides done by Gutsev et. al.³⁶ in past. Although research groups of Shim et. al.^{37, 38}, Maclagan et.

al.^{39, 40} and Borin et. al.⁴¹ explored few of these systems in detail in various independent efforts; the research group Mavridis et. al.⁴²⁻⁵⁰ presented a systematic independent ab-initio study of complete $3d$ -TMC series and listed existing energetics data for the ground states of $3d$ -TMC.

The valance characteristics of the transition metal atom gave rise to a multitude of potential bonding schemes, which presented a great challenge for their theoretical description. In view of the near-degeneracy problems due to the presence of several low lying electronic states, it was suggested to apply high-level quantum chemical methods to get the correct description⁴¹. Kalemios et. al.⁴⁶ provided the detailed description of ScC with ab-initio multireference methods and large basis set. Besides the electronic structure of low lying states of ScC, they also predicted the potential energy surface for all the states. They concluded doublet to be the ground state with a charge transfer happening in all the states from metal center to the carbon. They have recently reported *ab-initio* results for CuC.⁴⁴

Hack et. al.³⁹ compared different theory levels including density functional methods for TiC and reported the presence of singlet and triplet very close to each other, triplet being the lowest. They determined the properties of TiC were sensitive to type of theory level used and hybrid DFT functional perform reasonable in predicting most of the observables. In another study of TiC done by Tomonari and Tanaka,⁵¹ they found singlet to be the ground state and triplet is just 0.057 eV away. They also emphasized on careful selection of theory levels to study TMC, due to their observation about MRSDCI level giving wrong energetics due to size-inconsistency error. Besides Kalemios et. al.⁴² and Maclagan et. al.,³⁹ Majumdar and Balasubramanian⁵² reported their investigations for VC, where they found quartet and doublet spin states were nearly degenerate, latter being more favourable. There were several spin states considered for more complex CrC in past and all recent ab-initio and DFT

studies^{36, 37, 40, 42} reports triplet to be the ground state, followed by quintet. The ground state of MnC is reported^{41, 43} to be quartet, which can be derived from the ground state interaction of Mn and C atom.

There was experimental data available⁵³ for FeC, being extensively explored for its importance in astrophysics, reporting triplet as ground state. This was further confirmed in *ab-initio* studies by Shim et. al.,³⁸ Tzeli et. al.⁴⁸ and Itono et. al.,⁵⁴ where they reported the electronic structure and bonding strengths of FeC in various states. CoC was also investigated experimentally⁵⁵ and theoretically,^{36, 41, 49} and reported to have doublet ground state. NiC is another industrially important system due to its prime catalytic properties. We found comparatively good amount of literature^{36, 38, 50, 56, 57} investigating NiC including sequential studies by Shim et. al.³⁸ and Mavridis et. al.⁵⁰ It was reported to possess two low lying states (singlet and triplet), singlet being the lowest ground state. Finally, the last system in *3d*-TMC series, CuC was investigated less often except one recent *ab-initio* study by Kalemios et.al.⁴⁴ and one DFT study by Gutsev et. al.³⁶ in past. Both report quartet as the ground state lying significantly lower in energy than the doublet.

In chapter four, we report our investigations for the complete series of *3d*-TMC, with latest DFT functionals to predict the ground state and bonding strength for these molecules. We have considered several spin multiplicities of *3d*-series (Sc-Cu) transition metal carbides (diatomics) and compared our results with existing experimental and quantum chemical data in chapter four of this thesis. We have also plotted potential energy curves for each of the spin state of these TMC along with *ab-initio* curves for comparison.

1.3 Small nickel clusters

Nickel system received most attention, among 3d-TM clusters, both experimentally and theoretically. Although there are complexities involved in its description due to its unfilled 3d electrons, it is an excellent system to explore and validate new theoretical approaches. In the past three decades, we have seen wide interest in small nickel clusters as their properties are a function of their size and composition. Besides their catalytic importance, the chemical, physical, electronic and magnetic properties, related to their geometry, play an important role in furnishing information for the transition from nanoclusters to the bulk. Though the geometry of small nickel clusters holds the key to new behaviours, it is yet challenging to determine these shapes with usual spectroscopic techniques. There are experimental efforts made in past with different techniques to correctly describe Ni₂ to Ni₅,^{12, 58-62} which serves the ground for theoretical comparison.

Recently, Arvizu et. al.⁶³ reported several different topologies of small nickel clusters Ni₂- Ni₅ in their GGA based DFT study. They determined structural properties, binding energies, adiabatic ionization potential, etc. in order to facilitate the future experimental studies on these small clusters. To address the dilemma between ground state multiplicities of these nickel clusters they tested five spin states (singlet, triplet, quintet, septet, nonet) for each of the cluster under study. Other computational investigations of these clusters with LDA^{64, 65} and GGA⁶⁶ DFT methods were reported to predict the structural parameters. Petkov et. al.⁶⁷ have presented the effect of impurity on structure, stability, electronic and magnetic properties of Ni₄, and discussed 6 different symmetries (Planar D_{2h}, C_{2v}, non-planar C_{3v}, T_d, C_{2v}, C_s) of bare Ni₄ cluster. He reported C_s to be the most stable geometry of Ni₄ and found John-Teller distortion in T_d symmetry of Ni₄. In another attempt to study the structural and magnetic properties of nickel clusters Ni₂-Ni₁₃, Xie et. al.⁶⁸ discussed the

stability induced due to John-Teller distortion in these clusters. They have described the presence of John Teller effect in high symmetry clusters due to heavy degeneracy. They also reported the new ground state structure in case of Ni_5 and Ni_7 in C_{2v} and C_2 symmetry respectively.

Apart from DFT, the other techniques were also employed to investigate these clusters, including molecular dynamic (MD) simulations,⁶⁹ the embedded-atom method (EAM),⁷⁰ and effective medium theory (EMT).⁷¹ The MD simulation technique employed by Chenglin Luo⁶⁹ used density functional tight binding (DFTB) framework to study these clusters. Considering complexities involved in transition metal clusters, DFTB method emerged as a good alternative to *ab-initio*, providing a compromise between accuracy and computational speed. On the other hand EMT studies by Nygren et. al.⁷¹ reported fair estimation of binding energies for their study of $\text{Ni}_4 - \text{Ni}_9$. The stability study of small clusters comprising of ≤ 150 atoms was done with EAM method specially developed to study metal interactions. Grigoryan et. al.⁷⁰ reported four lowest energy isomers of all the clusters from 2-150 and determined structural information for each individual cluster, but described only the trends observed.

In this thesis, we have investigated the small nickel clusters Ni_2 - Ni_5 with modern hybrid DFT functional BMK. We have considered all multiplicities possible for these clusters ranging from singlet to tridectet and determined their geometry and energetics. We present our prediction of lowest energy state in Chapter Four and compared our results with existing experimental and theoretical data. We have also studied various isomers of Ni_4 to determine its ground state geometry.

1.4 Small gold clusters (bare and ligated)

Recently, there has been a significant interest in the research focused on the synthesis, characterization and theoretical analysis of gold clusters and nanoparticles, as their potential applications encompass ever increasing areas of modern technology and scientific advances, ranging from biological luminophores to the components of plasmonic devices and catalysis. Gold nanoclusters (typically smaller than 20 gold atoms) hold promise for the great advances in materials science as they are increasingly viewed as basic elements for assembly of nanoarchitectures having specific emergent properties. In this size regime, the metal clusters become molecular species with discrete electronic states and possible strong fluorescence properties. Several experimental studies done in the past^{72, 73} exploited the high polarizability, optical spectra and emission properties of these molecular-scale noble metal clusters. However, the assignment of the observed spectra is tedious without the detailed knowledge of geometries and energy levels. As the shape and size of nanoclusters define their optical properties, there has been a considerable effort^{4, 63, 74-95} to understand the factors that control the geometry. For example, computational studies of several bare gold nanoclusters (Au_N) suggest transition from 2D planar structures ($N < 11$) to 3D systems for $N \geq 13$.^{90, 95, 96} The review series by Pyykkö⁹⁶⁻⁹⁸ along with other comprehensive reviews by Daniel and Astruc,⁹⁹ and Häkkinen⁸⁸ gives an excellent insight of the theoretical work carried out in this area over the last few years.

Gold chemistry is strongly influenced by relativistic effects arising due to its tendency to form close metal-metal interaction. These effects play major role in gold binding as compared to other atoms in the same group.¹⁰⁰ We have considered relativistic effects including ZORA, Spin-Orbit coupling and found negligible effect on small gold clusters energetics. Small gold clusters can be put in different categories based on number of atoms

in the cluster. We have investigated small gold clusters with less than 10 atoms in this study, specifically Au₂, Au₄, Au₆, Au₈ and their isomers.

In contrast to the large body of research on bare small gold clusters (Au_n, n<20) much less attention was given to ligation and solvation of these clusters. These factors are important to be considered in order to interpret the most experimental studies. However, these factors also increase the computational complexity. So far, only two attempts have been made to target a couple of these small gold nanoclusters^{89,101} in the presence of solvent and ligands. There was much confusion in the literature about the transition from 2D→3D geometry taking place at n>13 or less. In past decade numerous theoretical studies^{63, 88-95, 97} were carried to find the stable geometrical isomer for small clusters. The majority of these studies showed transition happening beyond thirteen atom cluster, while Young-Kyu Han⁴¹ just addressed this issue for Au₈ and concluded it to be planar. Olson et. al.^{85, 87} investigated DFT, plane wave DFT and *ab-initio* theories to test isomers of Au₆ and Au₈ and found all of them planar with DFT and two of the Au₈ isomers non-planar with *ab-initio* theory. Controversial planar-nonplanar (2D to 3D) geometrical transition for these small clusters can be addressed through ligation. Shafai et. al.¹⁰¹ reported Au₁₃ to be icosahedral (3D) in the most stable experimentally favorable geometry, and the discrepancy within theoretical prediction was due to the absence of ligand environment.¹⁰¹ This indicated that ligands play a key role in stability of these small gold nanoclusters. The previous studies^{93, 102, 103} showed the relative stability can change amongst three-dimensional isomers due to the ligand stabilization effect.

This thesis systematically explores the effect of ligand and solvation on small gold nanoclusters (Au₂, Au₄, Au₆ and Au₈) geometries and energetics. We not only study the importance of these factors for realistic simulations, but also resolve dilemma about the

lowest energy isomers and 2D→3D transition in small gold clusters. The only study¹⁰⁴ considering the effect of anions on binding energy of small gold clusters including one of the isomer of Au₆ establish that binding energy doesn't vary much beyond Au₂ for clusters ≤ Au₂₀. We have studied ten lowest energy isomers of four gold clusters in the presence of phosphine ligand with and without solvent. Our study considers one-by-one attachment of these ligands in order to investigate their effect on geometry and energetic of these clusters.

CHAPTER 2: THEORY

Many properties of the molecules in their electronic ground states are reproduced in the mean field approximation, also known as Hartree-Fock (HF) theory. In this approximation each electron is described by an orbital shaped in the mean field created by the density distribution of all other electrons. Electron repulsion is then composed of two terms: classical Coulomb energy and exchange energy E_{HFX} , resulting from the quantum nature of electrons. Electron correlation effects are missing from this picture. In order to account for these effects, post-HF *ab initio* Wavefunction Theory (WFT) methods are used. This Chapter details several flavours of DFT approach and the specifics of its computational implementation used in other chapters. However, for larger systems WFT is prohibitively expensive. A more computationally affordable alternative is presented by Density Functional Theory (DFT). In DFT the electron correlation is introduced by means of exchange-correlation functional E_{XC} , replacing exact exchange E_{HFX} in HF theory.

2.1 Density Functional Formalism and Exchange-correlation Functionals

Density Functional Theory (DFT) is one of the most widely used quantum chemical method for electronic structure calculations in solid-state physics. It is a well known approach to study ground state properties of many-body systems such as atoms, molecules, crystals and surfaces. Its applicability extends to the fields like biology and mineralogy. It is a versatile methodology to calculate energetics of complex systems due to the generality and flexibility of implemented fundamental concepts. DFT's framework is primarily build on Hohenberg-Kohn theorem¹⁰⁵ and Kohn-Sham equations.^{106, 107} Although DFT is a first principle approach to solve Schrödinger's wave equation. To describe DFT approach in general, we start with the Born-Oppenheimer approximation where atomic nuclei are treated

classically as fixed, and the electrons are moving in their electric potential v . Thus a many electron Schrödinger equation can be written as:

$$\hat{H}\Psi = [\hat{T} + \hat{V} + \hat{U}]\Psi = \left[\sum_i^N -\frac{\hbar^2}{2m} \nabla_i^2 + \sum_i^N V(\vec{r}_i) + \sum_{i<j}^N U(\vec{r}_i, \vec{r}_j) \right] \Psi = E\Psi \quad (1)$$

Where \hat{H} is the Hamiltonian, \hat{U} is the electron-electron interaction energy, N is the number of electrons, \hat{T} is the kinetic energy, \hat{V} is the potential energy from the nucleian field, E is the total energy and Ψ represents the wave function of the system.

Density Functional Theory is mapping many body problem with \hat{U} onto a single body problem without \hat{U} , where key variable remaining is the particle density $n(\mathbf{r})$. According to Hohnberg-Kohn (HK) theorem, electronic density $n(\mathbf{r})$ determines all ground state properties of multi-electron system, where energy of the ground state is a functional of electronic density. The HK equation describing ground state properties of many electron systems in terms of electron density is:

$$E[n(\mathbf{r})] = T[n] + V_{ext}[n] + V_{e-e}[n] = \int n(\mathbf{r})v_{ext}(\mathbf{r})d\mathbf{r} + F_{HK}[n] \quad (2)$$

where Hohnberg-Kohn functional $F_{HK}[n] = T[n] + V_{e-e}[n]$. Although HK approach is in principle exact, the form of $F_{HK}[n]$ is unknown. The approximate form of kinetic energy functioinal $T[n]$ is usually given by Kohn-Sham (KS) equations. KS equations mapped the real system into an auxiliary non-interacting reference system with the same density, where each electron moves in an effective 1-particle potential due to surrounding electrons. Kohn and Sham introduced the way to solve Schrödinger's wave equation by giving relation between particle density and corresponding potential to finally calculate the kinetic energy of non-interacting N particle system. The Kohn-Sham equation:

$$\left[-\frac{1}{2}\nabla^2 + V_{\text{eff}}(r) \right] \phi_i = \varepsilon_i \phi_i \quad (3)$$

where ϕ_i are KS orbitals, is the system of N effective one-particle equations, making up the total density $n(r) = \sum_i |\phi_i(r)|^2$.

There are several approximations for exchange-correlation functionals¹⁰⁸ in equation (2). In this form, Density functional theory (DFT)^{106, 107} has become a method of choice for the calculation of numerous properties of molecules and solids. Unlike modern semiempirical methods such as MSINDO¹⁰⁹ and DFTB,¹¹⁰ it does not require tedious empirical parameter fitting to produce acceptable results. Unlike WFT methods,¹¹¹ DFT accounts for electron-correlation not through increasing complexity of the wavefunction, but via approximate exchange-correlation functional. The need to improve exchange-correlation functionals arises from known deficiencies of DFT describing the so called strongly correlated systems where vacant and occupied electronic levels are approaching degeneracy (this effect is also known as static or non-dynamic electron correlation). This situation is observed in d - and f -electron systems or when chemical bonds are being stretched. Despite these limitations different exchange-correlation functionals are widely used for modeling of various systems. Early exchange-correlation functionals were dependent only on electron spin density (Local Spin Density Approximation, LSDA). Next generation of exchange-correlation functionals also included energy dependence on the gradient of the density (Generalized Gradient Approximation, GGA). Among the later developments are kinetic energy density dependent functionals which are also known as meta-GGA, including TPSS and BB95.^{112, 113} GGA and meta-GGA functionals are called semilocal functionals to distinguish them from LDA on one hand, and non-local functionals including orbital dependence on the other hand. One of the meta-GGA functional we used in our study, TPSS¹¹⁴ was designed to correct the too-large atomization energies and increase

the too-small jellium surface energies obtained with LSD (jellium is the term for model system of interacting electrons and a uniform background of positive charge). It had been shown to accurately predict bond energies and bond lengths in molecules, hydrogen-bonded complexes, and ionic solids.¹ Performance of TPSS approaches that of the hybrid PBE0 functional with a practical advantage of not including Hartree-Fock exchange.¹¹⁴

All LSDA, GGA and meta-GGA are known to underestimate band gaps in solids. On the other hand, Hartree Fock (HF) method yields an overestimated band gap. The electron correlation in DFT is introduced in terms of exchange-correlation functional E_{XC} , replacing exact exchange E_{HFX} in HF theory without increase in computational expense. Some empirical parameter fitting is typically involved in the design of the exchange-correlation functional in this formalism; it is largely system-independent. Although exact exchange is non-local and orbital-dependent, in DFT the functional E_{XC} is expressed in terms of the total electron density and its gradients (respectively local and semi-local approximation). Unlike exact exchange, E_{XC} includes repulsion of electron from its own density and does not vanish for one-electron systems. This property is known as self-interaction error, and it has both negative and positive effects. As negative result, in DFT bonds are too weak, while electrons are over-delocalized and do not interact with Coulomb asymptotic $\sim 1/r$ at large separations. On a positive side, self interaction is mimicking non-local part of electron correlation and should be retained to some degree. Practically useful step in balancing self-interaction error was made by Becke,¹¹⁵ who suggested to include a fraction of HF exchange energy in E_{XC} functional:

$$E_{XC} = aE_{HFX} + (1-a)E_{DFX} + E_C \quad (3)$$

where $a=0.2$ is an empirical parameter, E_{DFX} and E_C are exchange and correlation functionals including local and semi-local terms. The original (B3LYP)¹¹⁵ as well as more recent hybrid functionals often achieve chemical accuracy in properties predictions.^{116,117,118} We have benchmarked our *3d*-Transition Metal calculations with BMK (Boese-Martin for kinetics) a hybrid meta-GGA functional with 42% of HF exchange, which was designed to be superior in describing transition state (TS) properties as well as atomization energies, geometry and harmonic frequencies of the molecules in the ground state.¹¹⁹ BMK functional was developed based on diverse and balanced parameterization set including transition metal complexes and hydrogen-bonded systems. However performance of BMK for TM systems varies.¹²⁰ Besides, we have also studied our test set of transition metal carbides with M05 and M05-2x, new parameterized functionals recently developed by Truhlar and co-workers. The M05 ('Minnesota 2005')¹²¹ functional includes 28% of exact exchange and usually gives good results for transition metal complexes. M05-2x¹²¹ (includes 56% of HF exchange) improves the description of weak interactions or energy barriers by duplicating the exact exchange contribution.

Moderate computational costs raises hopes for DFT to be a good candidate for universal black-box approach of spectroscopic accuracy. However, extensive testing reveals various drawbacks in the commonly used DFT implementations and necessitates further improvements (see recent review¹²² for more details). One improvement important for spectroscopic predictions involves the construction of range-separated hybrid functionals,^{123,124} where fraction of HF exchange $a(r_{12})$ depends on the electron-electron distance according to the standard error function,¹²⁵ linear combination of gaussian functions or Yukawa potential.¹²⁶ To account for the long-range effects believed to be important in the

analysis of metal bonding in gold complexes and clusters,¹²⁷ we used Coulomb-attenuated method (CAM),¹²⁵ which varied HF exchange from 18% to 60% depending on interelectron distance.

Though DFT based on single determinant KS approach is most widely used quantum chemical method in recent times, it has difficulty in describing bond breaking/bond forming processes in strongly correlated systems like C_2 . The restricted Slater determinant contributes to artificial enhancement of the energy at large distance due near-degeneracy of the bonding and antibonding orbitals, and arising of the unphysical ionic terms. The unrestricted KS can correct the potential energy curve at all distances by considering different orbitals for different spins, at the expense of the spin-contamination, as discussed in Section 2.3. Another approach to account for this situation of so-called “strong correlation” is Ensemble KS (EKS) approach, proposed by Schipper et al.¹²⁸ In EKS approach, two or more Slater determinants are used instead of one determinant in KS formalism. These determinants present fractional contribution to the total electron density and differ by just one orbital, which becomes fractionally occupied. Unlike other implementations using the fractional occupation numbers (FON), in rigorous EKS theory the contributions of the Slater determinants to the ensemble are varied until the fractionally occupied orbitals become exactly degenerate.

Although EKS may improve the description of the wide range of systems, in rare occasions molecular system may not be described by a single ground state Slater determinant at all and EKS is the only choice. These systems are called non ν -representable.⁸² It was shown, that biradicals molecular systems CH_2 and C_2 are in fact non ν -representable even if exact exchange-correlation potential is used. They are well described, however, by EKS approach.¹²⁸ The dissociation in C_2 molecule was also studied by WFT at its highest, Full CI

level by Sherrill et al.⁸² In close similarity to EKS picture, they found that three different Slater determinant become the dominant contributors to the wave function at different interatomic distances along the dissociation pathway.

However, another question remains: can C_2 be accurately described by the approximate Exchange-Correlation DFT functionals that are in use today? We address this issue in this thesis by adopting EKS approach, implemented in a modified version of Gaussian 98 code, which was developed by Dr. Konstantin Kudin (unpublished) making use of FON capabilities of this code. The results are described in Section 2.5.

2.2 Basis sets and relativistic corrections

In this thesis all calculations of transition metal diatomics and small nickel clusters were done with Gaussian03¹¹⁴ program using all-electron Wachters+f^{129, 130} basis set. Spin-polarized (unrestricted) DFT was used throughout. Initial guess was generated by using Harris functional²⁷ which is the default option in Gaussian03. Self-consistent field (SCF) convergence threshold was set to 10^{-7} , and relaxed to 10^{-5} in a few problematic cases. Initial guess was followed by either geometry optimization or scan along interatomic distance to plot the potential energy curve. In some cases (CrH, VH) Harris guess lead to SCF convergence problems, and Hartree-Fock (HF) orbitals were used as a guess. In a few cases where geometry optimization was terminated due to convergence failure, converged KS orbitals were used as initial guess (BMK orbitals in case of TPSS nonconvergence and vice versa).

A potential complication in the study of systems with nearly degenerate energy levels is the danger of obtaining distinctly different SCF solutions. When different solutions are obtained for the equilibrium geometry and for the dissociation limit, the energy difference is

no longer physically meaningful. In order to ensure consistency of SCF solution for all geometries, we built entire potential energy curves and verified that it does not have discontinuities indicating the switch from one SCF solution to another. To avoid false SCF solutions with Fermi holes (i.e. virtual orbitals with energy lower than some of the occupied ones), a new SCF algorithm was employed, which makes use of fractional occupation numbers (FON) around the Fermi energy. This was accomplished by using keywords SCF=Fermi and IOp(5/22=5). In FON approach the orbital occupations are determined using the Fermi–Dirac function for a fictitious electron temperature, so that sum of occupation numbers equals to the correct number of electrons for the system.¹³¹ The electron temperature value was set to 3000 K at the initial SCF cycle, and lowered to 0 K in 10 SCF steps, so that the occupational numbers became integer at the final SCF cycles. The stability of the SCF solution was checked and KS orbitals were reoptimized (if unstable) using keyword Stable=Opt. Default integration grid was used for all the calculation.

Molden¹³² graphical interface was used to examine Kohn-Sham orbitals at the dissociation limit, as well as at the points where potential curves were found to be non-monotonic. For one case (CrH) in order to obtain SCF solution with the lower energy, spin-polarization of σ -bond had to be inverted to have minority spin density localized on H atom using the keyword Guess=Alter. Natural Bond Orbital's (NBO) analysis due to Weinhold¹³³ was used to interpret the electron density. The NBOs are obtained by unitary transformation of occupied molecular orbitals so that they block diagonalize the (alpha and beta) density matrices and give the best Lewis representation of electronic structure. Relativistic calculations were done with the second-order Douglas-Kroll approximations^{134, 135} using keyword Int=DKH

We used commercially available Gaussian09¹³⁶ software package for all the calculation of small gold clusters. We considered five different basis sets with increasing amount of polarization and diffuse functions: the LANL2DZ double-zeta quality basis set with the corresponding effective core potential (ECP),¹³⁷ LANL2DZ ECP augmented with single polarization function for each element (LANL2DZ-P),¹³⁸ the split valence basis set def2-SVP of Ahlrich^{139, 140} with polarization, the triple zeta valence def2-TZVP with polarization, and the quadruple zeta valence def2-QZVP¹⁴¹ with polarization on all atoms and corresponding ECP on gold. Several commonly used DFT^{106, 107} functionals were tested as well. Local Spin Density Approximation (LSDA) was represented by SVWN5 model, and the Generalized Gradient Approximation (GGA) functional family was represented by the PBE exchange–correlation form. Among the later developed types of DFT functionals, TPSS¹¹⁴ was our functional of choice for the kinetic energy density-dependent functional (meta-GGA). Currently popular and well-tested B3LYP¹¹⁵ functional was used as a representative of a hybrid DFT model. B3LYP explicitly contains a fraction (20%) of orbital exchange.¹¹² Finally, we have considered the long-range corrected (LC) functional CAM-B3LYP¹²⁵ which accounts for long-range exchange effects believed to be important in the analysis of metal bonding in gold complexes and clusters.¹²⁷ Solvation effects were simulated by using implicit CPCM solvation model¹⁴² as implemented in Gaussian 09 with methanol being a solvent of choice. Vacuum optimized geometries were used as initial guesses to optimize cluster geometries in the presence of the solvent. ChemCraft and GaussView visualization software packages were used for subsequent visualization of resulting molecular structures.

2.3 Spin-Contamination Correction Development

Difficulties in DFT description of strongly correlated systems are based on the fact that DFT was derived based on assumption of non-degenerate system,^{105, 107} while multireference WFT methods are capable to take degeneracy into account. DFT implementations are using Kohn-Sham formalism based on single Slater determinant. Modifications to the formalism may thus be necessary to describe near degenerate cases. One of these modifications can be illustrated on the example of multiplet states of transition metal atoms. Ziegler, Rauk and Baerends¹⁴³ suggested to calculate the energies of singlet and triplet states of TM atoms as linear combinations of energies for single Slater determinants built with different orbital occupations. They considered the four possible configurations of two electrons on two singly occupied molecular orbitals a and b , three triplet's and one singlet.

$$\|a_\alpha b_\alpha\|, \frac{1}{\sqrt{2}}(\|a_\alpha b_\beta\| + \|a_\beta b_\alpha\|), \|a_\beta b_\beta\|, \frac{1}{\sqrt{2}}(\|a_\alpha b_\beta\| - \|a_\beta b_\alpha\|) \quad (1)$$

While electron density represented by determinant $D_1 = \|a_\alpha b_\alpha\|$ corresponds to the triplet energy

$${}^{DFT}E(D_1) = E_T(D_1), \quad (2)$$

the energy of electron density represented by determinant $D_2 = \|a_\alpha b_\beta\|$ is the average of singlet and triplet energies:

$${}^{DFT}E(D_2) = \frac{1}{2}(E_T(D_2) + E_S(D_2)) \quad (3)$$

The pure singlet energy can be then expressed as:

$$E'_s = 2^{DFT}E(D_1) - {}^{DFT}E(D_2) \quad (4)$$

This method was extended to higher atomic multiplets with partly occupied p -shells^{144, 145} and d -shells.¹⁴⁶⁻¹⁴⁸ Although complex atomic orbitals and functionals dependent on current density are generally required to treat degenerate atomic multiplet states, Becke recently suggested a set of rules to obtain accurate results with standard real orbitals and exchange-correlation functionals.¹⁴⁸ Application of the sum rule eq (3) to the molecular systems is complicated by the “symmetry dilemma”.¹⁴⁹ While the symmetry-adapted spin-restricted orbitals form a proper basis for WFT treatment, single Slater determinant built on these orbitals does not always correspond to the lowest energy SCF solution. For instance, Benard¹⁵⁰ describes several TM molecules where spin-adapted solution incorrectly describes electronic structure and lower-energy broken-symmetry solutions exist. This issue had been extensively studied in the past¹⁵⁰⁻¹⁵³ and the general consensus seems to favor the lowest energy over correct symmetry.

A clear advantage of unrestricted (also known as spin-polarized or broken spin-symmetry) solution is qualitatively correct description of bond dissociation process.^{149, 154} Since exact exchange-correlation functional is not known, unrestricted Kohn-Sham (UKS) treatment improves approximate functionals by taking part of the static electron correlation into account. The situation can be seen as localization of α and β electrons on the left and right atoms of the dissociating bonds, respectively (left-right electron correlation). Broken symmetry (BS) UKS thus describes the transition from closed shell system to biradical smoothly, which is not possible with restricted KS.

Even for simplest diatomic H_2 restricted Kohn-Sham (RKS) approach does not describe bond dissociation correctly. It is possible, in principle to obtain correct dissociation

limit if the exact exchange-correlation functional was known. An attempt had been made to use linear response formalism to account for static electron correlation.¹⁵⁵ Although it helped in the dissociation limit, an unphysical dissociation barrier was obtained, presumably due to lack of double excitations in linear response. Another attempt used exact electron density obtained from WFT (full CI method) to restore the nearly exact exchange correlation potential.¹⁵⁶ That also resulted in unphysical barrier. It appears that BS-UKS ansatz in DFT is more applicable to systems with chemical bond dissociation. An attractive feature of the BS approach is that one obtains a ‘quasi-valence bond’ like description with semi-localized magnetic orbitals that reflect the interacting singly occupied molecular orbitals (MOs) of the subsystems. On the other hand for a complicated many-electron molecule, it is difficult to extract the magnetic orbitals from the results of a spin-unrestricted calculation.¹⁵⁷

A disadvantage of UKS approach is that spin-polarized Slater determinant is no longer an eigenfunction of the spin operator. Hence, the average value of $\langle \hat{S}^2 \rangle$ is not, generally equal to the correct value of $S_x(S_x+1)$.¹⁵⁸ Here S_x is $1/2$ of the difference in total numbers of α and β electrons. This situation is known as spin contamination and $\langle \hat{S}^2 \rangle$ is often used as its measure. The common rule¹⁵⁹ is to neglect spin contamination if $\langle \hat{S}^2 \rangle$ differs from $S_x(S_x+1)$ by less than 10%. As a result of spin contamination, molecular geometry may be distorted toward the high-spin state one, spin density often becomes incorrect, and electron energy differs from the pure spin state ones. While some researchers argue that this spin contamination in DFT should be ignored¹⁴⁹ others recognize it as a problem affecting the energy. Possible solutions to spin contamination problem includes constrained DFT^{34, 160} and spin contamination correction schemes.^{161, 162} The latter are discussed in detail below.

There are two general approaches to spin contamination problem found in the literature: one is to project UKS wavefunction of non-interacting system onto eigenfunctions of \hat{S}^2 operator, and another is to map the real system onto model system described by a model Hamiltonian. The example of the projection approach is PUHF method, implemented at semi-empirical level by Zerner et al.¹⁶³ While successful at description of spin-splitting in multicenter d -metal complexes, PUHF method was found not to be size-consistent, which resulted in errors of tens of kcal/mol for organic biradicals.¹⁶⁴⁻¹⁶⁶ Orbital optimization after spin-projection such as in extended HF method (EHF),¹⁶³ and in maximally paired Hartree Fock method (MPHF)¹⁶⁷ is expected to restore size consistency, but faces substantial difficulties in practical implementation. Half-projected HF method (HPHF) offers a more practical solution of the expense of retaining higher order spin-contamination.¹⁶⁸ Jayatilaka et. al. proposed minimize spin-contamination together with total energy using method of Langrange multipliers,¹⁶⁹ and Yamanaka et. al. developed the new generalized Hartree-Fock-Slater method using non-collinear magnetic orbitals.¹⁷⁰ An elegant formalism for optimization of spin-projected wave function, based on strongly orthogonal geminal approach was proposed recently,¹⁷¹ but no DFT extension to it exists to date. Lowdin¹⁷² introduced the extension of Hartree Fock by implementing projection operators to treat the systems with spin degeneracies or correlation effects, which is further developed by Zilberberg et. al.¹⁷³ to deal with broken-symmetry states and used by others¹⁷³ for their complex systems involving transition metals.

Another approach to treat spin contamination problem consists of mapping of the model Hamiltonian onto results of *ab-initio* calculations.¹⁷⁴ Typically, Heizenberg-Dirac-Van-Vleck phenomenological Hamiltonian is used (see Moreira et.al.¹⁷⁵ and references therein).

This Hamiltonian describes the isotropic interaction between localized magnetic moments S_i and S_j as:

$$\hat{H}_{Model} = -\sum_{i,j} J_{ij} S_i S_j \quad (5)$$

where J_{ij} is the exchange coupling constant. For instance, a system with two unpaired electrons, the coupling constant corresponds to singlet-triplet energy splitting:

$$J = E_S - E_T \quad (6)$$

Positive value of J corresponds to ferromagnetic, and negative value corresponds to anti-ferromagnetic coupling. The mapping procedure consists of empirical adjustment of the coupling constant to match the multiplet energies obtained from WFT or experiment.¹⁷⁶⁻¹⁷⁸

Since BS-DFT does not produce the energies of the pure spin states, the expression for J must account for spin contamination. The following three equations (eqs 7-9) are the results obtained from these methods:

$$J = \frac{\left({}^{DFT} E_{BS} - {}^{DFT} E_T \right)}{S_{max}^2} \quad (7)$$

$$J = \frac{\left({}^{DFT} E_{BS} - {}^{DFT} E_T \right)}{S_{max} (S_{max} + 1)} \quad (8)$$

$$J = \frac{\left({}^{DFT} E_{BS} - {}^{DFT} E_T \right)}{\langle S^2 \rangle_T - \langle S^2 \rangle_{BS}} \quad (9)$$

Above equations vary in their use, based on the overlap of two magnetic orbitals. In the case of small overlap Equation 7 is applicable, which has been derived by Ginsberg,¹⁷⁹ Noodleman,¹⁵² and Davidson.¹⁸⁰ When the overlap is large Equation 8 can be used as

justified by Bencini et al.¹⁸¹ and Ruiz et al.¹⁷⁷ and Illas et al.^{175, 176} Finally, Yamaguchi et. al.^{170, 182} derives Equation 9, which can be reduced to eq 7 and eq 8 in the weak and strong overlap regions, respectively.

Although eq (7-9) only require the average value of spin operator and hence can be used with standard quantum chemical programs with no code modifications, they did not lead to consistent agreement with experiment.¹⁸³ A more complicated expressions for variable spin-correction, including dependence of J on overlap between corresponding spin polarized orbitals p and q were also derived recently.^{157, 184} This approach was shown to result in more accurate J values for Cu^{2+} binuclear complexes.¹⁸⁴ However, this variable spin-correction approach had not been applied to systems with two or more correlated electron pairs.

The expectation value of spin operator $\langle \hat{S}^2 \rangle$ obtained in standard quantum-chemical programs corresponds to the hypothetical system of non-interactive electrons, introduced in Kohn-Sham approach, rather than physical system of interest. Correct $\langle \hat{S}^2 \rangle$ can be expressed, however, through the two-particle density matrix.^{185, 186} The $\langle \hat{S}^2 \rangle$ values in the cases studied were found to be up to one order of magnitude greater than non-interacting case, depending on the system. Alternatively true $\langle \hat{S}^2 \rangle$ can be calculated in terms of the overlap of the spatial parts of the corresponding orbitals.¹⁸⁷

Here we propose an alternative approach to variable spin-correction, based on canonical Natural Orbitals (NO).¹⁶⁶ First, let us consider a diatomic system AB with one correlated electron pair, such as stretched H_2 molecule. We assume that restricted Kohn-Sham formalism yields higher energy for this system than unrestricted one, as the case of H_2 molecule far from equilibrium. Unrestricted KS description produces the natural orbitals a, b

as eigenvectors of the total density matrix with the orbital occupation numbers n_a , n_b as corresponding eigenvalues. We further assume that $n_a < n_b$ which means that orbital a is antibonding, and orbital b is bonding NO. They are symmetry-adapted (a is Σ_u and b is Σ_g in case of H_2 molecule). Corresponding spin-polarized broken symmetry orbitals p , q can be expressed¹⁸⁸ as a linear combination of a and b using polarization parameter λ :

$$p = \frac{1}{\sqrt{1+\lambda^2}}(b + \lambda a); q = \frac{1}{\sqrt{1+\lambda^2}}(b - \lambda a) \quad (10)$$

This parameter is determined by the occupation numbers n_a and n_b as shown below. If alpha and beta electrons are localized on different parts of the molecule and do not overlap, the polarization parameter become unity and we arrive to Noodleman's weak interaction limit. In the general case of many-electron system the orbitals of the alpha set, besides being orthogonal to each other, are also orthogonal to the orbitals of the beta set for a single exception of the corresponding beta orbital. The spin polarized orbitals obtained with the most standard quantum chemistry codes do not possess this property, which is why one has to produce the corresponding spin-polarized orbitals from NOs. BS solution can still be written as the Slater determinant in the basis of these corresponding orbitals as:

$$B = 1/\sqrt{2} \left\| p_\alpha q_\beta \right\| = \frac{1}{\sqrt{2}} \left\| \begin{matrix} p_1 \alpha_1 p_2 \alpha_2 \\ q_1 \beta_1 q_2 \beta_2 \end{matrix} \right\| \quad (11)$$

Substitution of the corresponding orbitals from eq (10) into eq (11) separates the pure singlet and triplet components:

$$BS = \frac{1}{\sqrt{2}} \left\| \begin{matrix} p_1 \alpha_1 p_2 \alpha_2 \\ q_1 \beta_1 q_2 \beta_2 \end{matrix} \right\| = \frac{1}{(1+\lambda^2)} S + \frac{\lambda}{(1+\lambda^2)} T \quad (12)$$

$$= \frac{1}{(1+\lambda^2)} (b_1 b_2 - \lambda^2 a_1 a_2) \frac{\alpha_1 \beta_2 - \beta_1 \alpha_2}{\sqrt{2}} + \frac{\lambda}{(1+\lambda^2)} (a_1 b_2 - b_1 a_2) \frac{\alpha_1 \beta_2 + \beta_1 \alpha_2}{\sqrt{2}}, \quad (13)$$

where indexes 1 and 2 mark coordinates of the electrons. The first term in this expression contains the linear combination of the two closed-shell singlets, the lower closed shell singlet S_1 :

$$S_1 = b_1 b_2 \frac{\alpha_1 \beta_2 - \beta_1 \alpha_2}{\sqrt{2}} \quad (14)$$

and the higher closed shell singlet S_2 :

$$S_2 = a_1 a_2 \frac{\alpha_1 \beta_2 - \beta_1 \alpha_2}{\sqrt{2}} \quad (15)$$

while the second term is proportional to one of the possible triplet states: $T = T_0 \sqrt{2}$,

$$T_0 = \frac{(a_1 b_2 - b_1 a_2) \alpha_1 \beta_2 + \beta_1 \alpha_2}{\sqrt{2}} \quad (16)$$

This triplet contribution is the reason why UKS solution is spin contaminated. Therefore, we are looking to extract the energy of the singlet term from BS energy E_{BS} using the energy of the triplet. The expectation value of Kohn-Sham operator \hat{H} then becomes,

$$E_{BS} = \langle BS | \hat{H} | BS \rangle = \frac{1}{(1+\lambda^2)^2} \langle S | \hat{H} | S \rangle + \frac{\lambda^2}{(1+\lambda^2)^2} \langle T | \hat{H} | T \rangle + \frac{\lambda}{(1+\lambda^2)^2} (\langle S | \hat{H} | T \rangle + \langle T | \hat{H} | S \rangle) \quad (17)$$

The last two terms in eq (17) vanish out due to orthogonality of S and T states, introduced in eq (12). Using normalization condition and substituting the eq (18) into eq (12) one can obtain:

$$\langle S | S \rangle = \langle b_1 b_2 - \lambda^2 a_1 a_2 | b_1 b_2 - \lambda^2 a_1 a_2 \rangle = 1 + \lambda^4 \quad (18)$$

$$BS = \frac{\sqrt{1+\lambda^4}}{1+\lambda^2} \cdot S_0 + \frac{\lambda\sqrt{2}}{1+\lambda^2} \cdot T_0 \quad (19)$$

where

$$S_0 = \frac{S}{\sqrt{1+\lambda^4}} = \frac{1}{\sqrt{1+\lambda^4}} (S_1 + \lambda^2 S_2) \quad (20)$$

Hence the BS UKS energy can be written in terms of renormalized singlet and triplet S_0, T_0

as:

$$E_{BS} = \frac{1+\lambda^4}{(1+\lambda^2)^2} \langle S_0 | \hat{H} | S_0 \rangle + \frac{2\lambda^2}{(1+\lambda^2)^2} \langle T_0 | \hat{H} | T_0 \rangle, \quad (21)$$

In non-relativistic case, the energy of the triplet T_0 is the same as the energy E_T for the single determinant triplet $T_1 = a_1 a_1 \setminus b_2 a_2$;

$$E_T = \langle T_1 | \hat{H} | T_1 \rangle = \langle T_0 | \hat{H} | T_0 \rangle \quad (22)$$

Then the energy E_{S_0} of the pure singlet S_0 can be found from (22) as

$$E_{S_0} = \frac{(1+\lambda^2)^2}{1+\lambda^4} E_{BS} - \frac{2\lambda^2}{1+\lambda^4} E_T \quad (23)$$

This energy includes the non-dynamic electron correlation effects arising from the mixing of S_1 and S_2 states. In order to relate the polarization parameter λ to the occupation numbers n_a, n_b , we can expand the electron density matrix in the basis of a and b orbitals.

$$\rho(BS) = \begin{bmatrix} n_a & 0 \\ 0 & n_b \end{bmatrix}, \rho(S_1) = \begin{bmatrix} 0 & 0 \\ 0 & 2 \end{bmatrix}, \rho(S_2) = \begin{bmatrix} 2 & 0 \\ 0 & 0 \end{bmatrix}, \rho(T_0) = \begin{bmatrix} 1 & 0 \\ 0 & 1 \end{bmatrix} \quad (24)$$

From eq (19-20)

$$\rho(BS) = \frac{1}{1+\lambda^2} \rho(S_1) + \frac{\lambda^4}{(1+\lambda^2)^2} \rho(S_2) + \frac{2\lambda^2}{(1+\lambda^2)^2} \rho(T_0) \quad (25)$$

then

$$n_a = \frac{2\lambda^4}{(1+\lambda^2)^2} + \frac{2\lambda^2}{(1+\lambda^2)^2} = \frac{2\lambda^2}{1+\lambda^2} \quad (26)$$

$$n_b = \frac{2}{(1+\lambda^2)^2} + \frac{2\lambda^2}{(1+\lambda^2)^2} = \frac{2}{1+\lambda^2} \quad (27)$$

And finally

$$\lambda = \sqrt{2/n_b - 1} \quad (28)$$

$$E_{S_0} = \frac{4}{2n_b^2 + 4n_b + 4} E_{BS} - \frac{4n_b - 2n_b^2}{2n_b^2 + 4n_b + 4} E_T \quad (29)$$

Thus, for a system with one correlated electron pair one can obtain the pure singlet energy expressed in terms of energy of BS UKS solution, the occupation number of the bonding NO, and the energy of the triplet built on these bonding and antibonding NOs (as opposed to self-consistent KS orbitals). This expression is applicable to two –electron systems as well as to the systems which have in addition the unpolarized electron core or ferromagnetically coupled unpaired electrons.

We will turn next to the systems with two correlated electron pairs, In that case the eq. 17 can be written as:

$$E_{BS} = \left\langle BS_1 \cdot BS_2 \left| \hat{H} \right| BS_1 \cdot BS_2 \right\rangle \quad (30)$$

Using eq. 19,

$$BS_1 \cdot BS_2 = \left(\frac{\sqrt{1+\lambda_1^4}}{(1+\lambda_1^2)} S_{01} + \frac{\sqrt{2}\lambda_1}{(1+\lambda_1^2)} T_{01} \right) \left(\frac{\sqrt{1+\lambda_2^4}}{(1+\lambda_2^2)} S_{02} + \frac{\sqrt{2}\lambda_2}{(1+\lambda_2^2)} T_{02} \right) \quad (31)$$

$$= \frac{1}{(1+\lambda_1^2)(1+\lambda_2^2)} \left(\sqrt{1+\lambda_1^4} \sqrt{1+\lambda_2^4} S_{01} S_{02} + \sqrt{2}\lambda_2 \sqrt{1+\lambda_1^4} T_{02} S_{01} + \sqrt{2}\lambda_1 \sqrt{1+\lambda_2^4} T_{01} S_{02} + 2\lambda_1 \lambda_2 T_{01} T_{02} \right) \quad \text{----}(32)$$

Simplifying above eq. by replacing S_{01} and S_{02} :

$$S_{01} = \left(BS_1 - \frac{\sqrt{2}\lambda_1}{(1+\lambda_1^2)} T_{01} \right) \frac{(1+\lambda_1^2)}{\sqrt{1+\lambda_1^4}} \quad (33)$$

$$S_{02} = \left(BS_2 - \frac{\sqrt{2}\lambda_2}{(1+\lambda_2^2)} T_{02} \right) \frac{(1+\lambda_2^2)}{\sqrt{1+\lambda_2^4}} \quad (34)$$

$$= \frac{1}{(1+\lambda_1^2)(1+\lambda_2^2)} \left(\sqrt{1+\lambda_1^4} \sqrt{1+\lambda_2^4} S_{01} S_{02} + \sqrt{2}\lambda_2 (1+\lambda_1^2) T_{02} BS_1 + \sqrt{2}\lambda_1 (1+\lambda_2^2) T_{01} BS_2 + 2\lambda_1 \lambda_2 T_{01} T_{02} \right) \quad \text{----}(35)$$

Hence the BS UKS energy can be written in terms of renormalized singlet, triplet and mixture of triplet and BS state, $S_{01}S_{02}$, $T_{01}T_{02}$, $T_{02}BS_1$, $T_{01}BS_2$ as:

$$E_{BS} = \frac{(1+\lambda_1^4)(1+\lambda_2^4)}{(1+\lambda_1^2)^2(1+\lambda_2^2)^2} \langle S_{01}S_{02} | \hat{H} | S_{01}S_{02} \rangle + \frac{2\lambda_2^2(1+\lambda_1^2)^2}{(1+\lambda_1^2)^2(1+\lambda_2^2)^2} \langle T_{02}BS_1 | \hat{H} | T_{02}BS_1 \rangle + \frac{2\lambda_1^2(1+\lambda_2^2)^2}{(1+\lambda_1^2)^2(1+\lambda_2^2)^2} \langle T_{01}BS_2 | \hat{H} | T_{01}BS_2 \rangle - \frac{4\lambda_1^2\lambda_2^2}{(1+\lambda_1^2)^2(1+\lambda_2^2)^2} \langle T_{01}T_{02} | \hat{H} | T_{01}T_{02} \rangle \quad (36)$$

Then the energy E_{S_0} of the pure singlet $S_{01}S_{02}$ can be found from (36) as

$$E_{BS} \cdot (1+\lambda_1^2)^2(1+\lambda_2^2)^2 = (1+\lambda_1^4)(1+\lambda_2^4)E_{S_0} + 2\lambda_2^2(1+\lambda_1^2)^2 E_{T_{02}BS_1} + 2\lambda_1^2(1+\lambda_2^2)^2 E_{T_{01}BS_2} - 4\lambda_1^2\lambda_2^2 E_{T_{01}T_{02}} \quad (37)$$

$$\begin{aligned}
E_{S_0} = \frac{1}{(1 + \lambda_1^4)(1 + \lambda_2^4)} & \left(E_{BS} \cdot (1 + \lambda_1^2)^2 (1 + \lambda_2^2)^2 - 2\lambda_2^2 (1 + \lambda_1^2)^2 E_{T_{02}BS_1} \right. \\
& \left. - 2\lambda_1^2 (1 + \lambda_2^2)^2 E_{T_{01}BS_2} + 4\lambda_1^2 \lambda_2^2 E_{T_{01}T_{02}} \right)
\end{aligned} \tag{38}$$

Here we derive an expression to extract the energy of the pure singlet state from the energy of the broken symmetry DFT description of the low-spin state and energies of the high-spin states: pentuplet and two spin-contaminated triplets. Thus, unlike spin-contamination correction schemes by Noodleman¹⁵² and Yamaguchi,¹⁸² spin-correction is introduced for each correlated electron pair individually and therefore is expected to give more accurate results.

2.4 Spin-Contamination Correction Testing

The formalism outlined in the previous section was implemented in the following steps:

1. Run G03 Self Consistent Field (SCF) job to obtain BS spin-polarized MOs and convert them to NOs.
2. Read NO printout from Gaussian job and converts the fractionally occupied NOs into corresponding spin-polarized molecular orbitals (CMO). Script uses a threshold parameter (tol) to select one correlated electron pair. The spin polarization of the electron core is neglected by adjusting the threshold value to consider natural occupations integer.
3. Check if the spin-up orbital p to be the one largely localized on metal atom and, so that spin-down orbital q is predominantly localized on H atom; if not, switch them.
4. Make new alpha orbital set is made of doubly occupied NOs, orbital p , singly occupied NOs, and weakly occupied NOs. The new beta orbital set was identical, except that p was replaced with q . Use these orbitals to evaluate the energy with single SCF step and verify that it is close to BS energy obtained at step 1.
5. Calculate the energy of the triplet (high spin state, HS) is calculated with another single SCF step using the original NOs only.
6. Calculate the energy of the pure singlet using HS and BS energies according to equation 29 in section 2.3.

Here we studied Potential Energy Curves (PEC) for hydrogen dimer H_2 and transition metal hydride MnH to validate the spin-contamination correction approach described above. MnH calculations were done with Gaussian03¹¹⁴ program using all-electron Wachters+f^{129, 130} basis set. For H_2 we have used aug-cc-pVQZ basis set with CCSD and spin-polarized (unrestricted) DFT calculations.

Spin-correction described above in theory section is implemented as a combination of unix shell script and FORTRAN code. It reads Natural Orbitals (NO) printout from Gaussian03 job (keyword used was Punch=NO) and converts them into spin-polarized molecular orbitals. Script uses a threshold parameter to identify the correlated pair. The spin polarization of the electron core was neglected by adjusting the threshold value to consider natural occupations integer. The provision is made for the spin-up orbital p to be the one largely localized on metal atom and, so that spin-down orbital q is predominantly localized on H atom. The new alpha orbital set is made of doubly occupied NOs, orbital p , singly occupied NOs, and weakly occupied NOs. The new beta orbital set was identical, except that p was replaced with q . These orbitals were further used to evaluate the energy with single SCF step and verify that it is close to BS energy obtained at self-consistence. The energy of the triplet is calculated with another single SCF step using the original NOs only. It was used by the script to extract the energy of the pure singlet. The keywords used for single SCF step with the modified orbital set were SCF (MaxCycle=1) and Guess=Cards.

Figure 2.1 illustrates potential energy curves for H_2 with CCSD, BMK (uncorrected and corrected) and conventional Yamaguchi spin contamination correction based on S^2 value. One can see from the Figure 2.1 the difference appear at the shoulder of the potential energy surface, where uncorrected BMK curve significantly overestimate the energies. The corrected curve with our new spin-contamination correction code efficiently finds the point of difference and corrects the energy to give potential energy curve similar to that of wavefunction method CCSD. We have also plotted the conventional correction based spin operator by Yamaguchi et. al. for comparison purpose. Though both of the corrections are equally good in predicting energies at the accuracy of wavefunction theory level CCSD, our approach is based on actual occupation nos., which would perform better when number of

electron correlated pair will increase in the study. The further validation of the system with more than two electron correlation pairs will be discussed in future. In another attempt to check our new approach we considered more complex system MnH. Figure 2.2 illustrates potential energy curve of two spin states of transition metal hydride, MnH with pure and hybrid DFT functionals TPSS and BMK. Our results are compared with PEC of only available WFT method MCSCF+SOCl in Figure 2.2 to equilibrium bond length for M=5. Table 2.1 shows the correction, introduced in Section 2, stabilizes this spin state by 3.1 kcal/mol below M=7, in agreement with experimental value reported in Borane et. al.³⁵ Thus, spin-corrected BMK predicts the ground state for MnH to have the multiplicity of 5 and accurately reproduces experimental D_e .

Here we derived an expression to extract the energy of the pure singlet state expressed in terms of energy of BS UKS solution, the occupation number of the bonding NO, and the energy of the triplet built on these bonding and antibonding NOs (as opposed to self-consistent KS orbitals). Thus, unlike spin-contamination correction schemes by Noodleman and Yamaguchi, spin-correction is introduced for each correlated electron pair individually and thus expected to give more accurate results. Diatomics considered for this study were found to have only pair of fractionally occupied NOs, in addition to singly occupied and unpolarized MOs. Our approach successfully predicts the correct spin state as validated by dihydrogen and manganese hydride in this study. This opens the venue to study more complicated enzymatic systems involving transition metals, more accurately with the help of DFT. However, the energy correction for the systems considered in this thesis is expected to be small, and Spin Contamination Correction was not used in the rest of the study.

2.5 Ensemble Kohn-Sham approach: Example C₂

The unusual bonding nature of C₂ makes it a challenging system to describe with quantum chemical methods. There are several attempts^{82, 128, 189} made in the past to explain the bonding pattern in C₂. They all agree that conventional DFT functionals are not sufficient to explain the nature of C₂ binding at equilibrium distance and asymptotic limit correctly. In this study we have investigated the Ensemble Kohn-Sham approach combined with DFT functionals to explain the bond breaking in C₂. We determined that EKS combined with hybrid exchange-correlation functional MPW1K¹⁹⁰ with higher fraction of HF exchange is required to correctly describe the dissociation of this molecule.

It has been established that restricted KS solution is not enough to describe non- v -representable systems like C₂, due to strong correlation and high level of orbital degeneracies. Although unrestricted KS approach may assign unpaired electrons to the degenerate orbitals, it gives rise to a significant spin contamination. Our spin-contamination correction scheme introduced in section 2.3, can only treat one or two pairs of electrons, which is not sufficient for C₂. Abrams & Sherrill reports highly correlated full CI (FCI) approach is necessary to describe C₂ curves; they also emphasized the computational complexities involved in extending this study to larger systems of interest. Salahub et. al.¹⁸⁹ described existence of different stable ground states at different inter-atomic distances on the potential energy surface in spin-restricted regime. Where one state is stable below 1.2 Å, the other one is stable beyond 1.5 Å - 1.7 Å and there is mixture of these two configurations in between.

We have plotted potential energy curves for singlet spin state of C₂ with Gaussian 98 obtained in RKS and UKS formalism and also with Gaussian 98 modified to implement Ensemble KS approach. The exact potential energy curves obtained at FCI theory level is

plotted in Figure 2.3 for comparison along with experimental energy.⁸² Our RKS and EKS calculations are in good agreement with the experimental dissociation energy, while UKS overestimates the energy.

As one can see on Figure 2.3 RKS and UKS potential energy are not smooth. At interatomic distance close to 1.6 Å the RKS and UKS curve has a shoulder that corresponds to switching between two different SCF solutions, as discussed below: Analysis of electronic structure obtained with EKS formalism, results in a more complicated bonding pattern. Based on the fractional occupations, the range of interatomic distances studied here can be divided into four parts (i) 1.0 Å - 1.5 Å (ii) 1.6 Å - 1.9 Å (iii) 2.0 Å - 4.2 Å (iv) 4.3 Å - 6.0 Å. Figure 2.3 lists the occupancies of molecular orbitals in EKS method and RKS occupations (in bracket) are shown for comparison. At shorter C-C distances, are two π - π character making double bond.

At all the R_{C-C} considered, both bonding and anti-bonding combinations of C_{2s} orbitals (σ_{2s} and σ_{2s}^*) are doubly occupied and results in net zero bond order. However, σ_{2p} , π_{2p} , and π_{2p}^* orbitals change their occupancies. Around equilibrium R_{C-C} (case (i)) both π_{2px} and π_{2py} are doubly occupied and σ_{2p} is empty. This confirms C_2 as unique molecule with two π -bonds and no σ bond in its ground state. Abrams and Sherrill also determined the strong mixing of $|(core)2\sigma_g^2 2\sigma_u^2 1\pi_x^2 1\pi_y^2|$ and $|(core)2\sigma_g^2 1\pi_x^2 1\pi_y^2 3\sigma_g^2|$ at the equilibrium geometry, which appears only in this unique case of C_2 . This significant contribution of determinants changes with the distance in their Full CI study of C_2 from 0.8 Å to 3.0 Å.

At the narrow range of R_{C-C} (1.6 Å – 1.9 Å) the occupation number on two π_{2p} -orbitals remains equal, but reduces rapidly from 2 to 1, while σ_{2p} orbitals gains its occupation

from 0 to 2. These occupations change in continuous manner and result in a smooth curve. The RKS descriptions on the contrary, changes sharply from $|(core)2\sigma_g^2 2\sigma_u^2 1\pi_x^2 1\pi_y^2|$ to $(core)2\sigma_g^2 1\pi_x^2 1\pi_y^2 3\sigma_g^2|$, which results in unphysical shoulder on PEC. This behavior is in agreement with EKS study reported by Schipper et. al.¹²⁸ There the exact density in C₂ molecule was obtained at high WFT level and used to reverse engineer the exact exchange correlation potential.

We were not able to reproduce these fractional occupations with the common exchange-correlation functionals (PBE, B3LYP, PW91PW91, BLYP). Only the MPW1K functional developed in Truhlar's group to reproduce the transition states and including a larger fraction of HF exchange yields the results similar to exact F_{XC}.

All the studies so far, to our knowledge, have observed C₂ curve from short to intermediate distances on the potential energy surface. There was lack of description near asymptotic limit while analyzing the inter-atomic distances towards dissociation limit. The longer region at R_{C-C} (2.0 Å-4.2Å) retain π_{2px} and π_{2py} orbitals half-occupied, while σ_{2p} orbital is doubly occupied. Finally, at distances R_{C-C} \geq 4.3 Å the σ_{2p} orbital begins to lose electron density, while σ_{2p}^* , π_{2px} and π_{2py} increase their occupations. This represents a correct trend towards the dissociation limit, where σ/σ^* and π/π^* are exactly degenerate and should have equal occupation numbers. It would be interesting to compare our results with exact F_{XC}, but the longer range of distances was not considered by Schipper et. al.¹²⁸

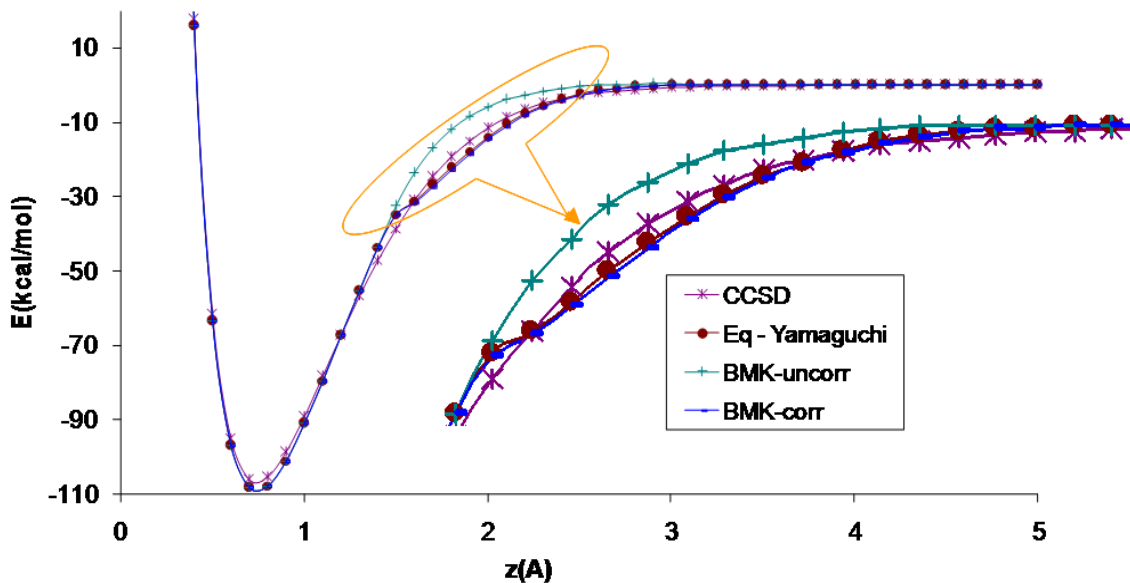


Figure 2.1 Potential Energy Curves for hydrogen dimer with and without spin-contamination correction from our new approach, along with CCSD and Yamaguchi correction.

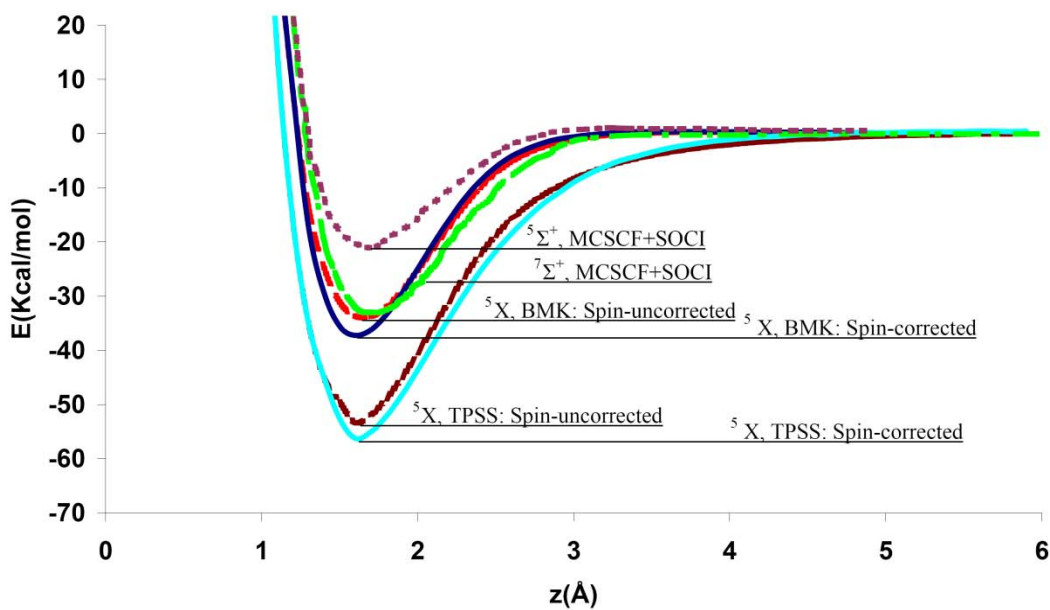


Figure 2.2 Spin-corrected Potential Energy Curves of MnH with multiplicity 5 and 7, calculated by TPSS, BMK, and WFT19 methods.

Table 2.1 Spin corrected and uncorrected dissociation energies of MnH in kcal/mol calculated with BMK and compared with ab-initio and experiment.

| | MnH |
|-------------------------|------|
| Multiplicity | 5 |
| BMK - Spin Uncorrected | 34.1 |
| BMK - Spin Corrected | 37.2 |
| MCSCF+SOC1 ^a | 21.8 |
| Experiment ^b | 39.0 |

(a)-Ref 94, (b)-Ref 93

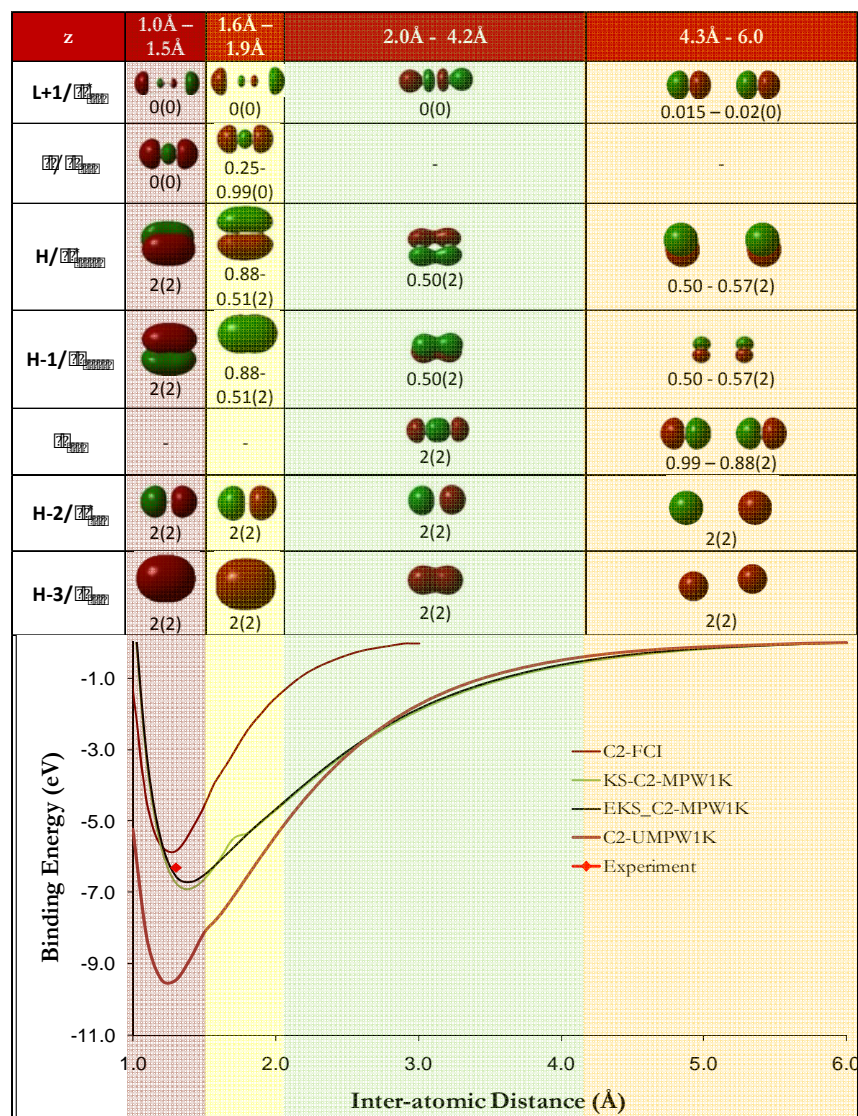


Figure 2.3 Potential energy curves with RKS, EKS and UKS approach compared with *ab-initio* and experimental data. Representative molecular orbitals with EKS occupations (range) and standard restricted KS occupations (in bracket) alongside interatomic distances.

CHAPTER 3: TRANSITION METAL HYDRIDES AND THEIR IONS

To provide the insight into some of the important concepts we investigated Transition Metal Hydrides (TMH) and their Cations (TMH⁺). We examined the lowest states in several spin multiplicities of these diatomics and analyzed variations in bond energies, bond lengths and electron densities. Potential energy curves and effect of spin correction are discussed. The DFT results are compared to experiment and WFT calculations. In this study we use both pure meta-GGA and hybrid meta-GGA exchange-correlation functionals TPSS and BMK to compare their performance with WFT methods and experimental data.

3.1 TMH Binding Energies

Dissociation energies for neutral hydrides in equilibrium geometry are reported in Table 3.1 and Figure 3.1. Comparison with three sets of experimental data and some of the published Wave Function Theory and DFT predictions are also listed. To calculate the root mean square (rms) deviations for all theoretical values, we used two sets of experimental data, compiled in Borane et. al.³⁵ and Furche et. al.¹ and we also compiled the third set from the original experimental papers for accuracy.

Based on rms values (three last columns on Table 3.1), BMK gives the best agreement with experiment, followed by two WFT methods. The other DFT methods range as follows. Among broken symmetry methods, the accuracy quickly deteriorates as the fraction of HF exchange decreases from BMK (42%) to B3LYP (20%) to TPSSh (10%) to TPSS (0%). Spin adapted (SA) formalism on the other hand, show only marginal improvement from pure BLYP to hybrid DFT (B3LYP). SA-B3LYP gives 80% lower rms value than BS-B3LYP but it is still twice less accurate than BS-BMK.

The individual values of deviations are plotted on Figure 3.1. One can see that BMK values are within 4 kcal/mol of experimental ones for almost all the systems (8 kcal/mol for CrH). Scalar relativistic correction does not improve the energies and deviations are similar to the one observed in non-relativistic BMK. TPSS strongly overbinds in all cases and the deviations are from 10 to 20 kcal/mol with ScH showing largest of all (48 kcal/mol), and 10% of HF exchange in TPSS does not improve the situation. Small fraction of HF exchange (TPSSh) helps only in case of NiH, while larger fraction helps in most cases. Spin-adapted formalisms (BLYP and B3LYP) are close to each other for all systems, except for MnH, but have no systematic deviations otherwise. All DFT methods agree for full and half-full d -shells (CuH and CrH), although this consensus is ~ 10 kcal/mol away from experimental value¹⁹¹⁻¹⁹⁷ in case of CrH. WFT and BMK are everywhere close to the baseline with MCPF slightly overbinding and MCSCF+SOC1 slightly underbinding. The first two (ScH, TiH) and last three systems (CoH, NiH, CuH) are especially well reproduced.

In the past, relativistic corrections were reported to be important in the systems involving $3d$ transition metals.^{33, 198, 199} We studied scalar relativistic effects on the dissociation energies with Douglas-Kroll¹³⁴ approximations and found them to be close to 2 kcal/mol. Moreover, we find that relativistic correction does not improve the agreement with experiment. This is in sharp contrast with s/d excitation energies in $3d$ atoms, which were reported to improve nearly twice when scalar-relativistic effects are taken into account. For the nickel hydride the scalar relativistic corrections of WFT theory level were calculated by Marian et.al.¹¹ He compared the results of the conventional perturbative method to the variational ones and found the coupling between the relativity and electron correlation to be very similar, despite the fact that relativity accounts for unusually large 0.36 eV increases in splitting between the nearly degenerate d^8s^2 and d^9s^1 - derived levels. Although Marian did not

discuss the binding energies, in a later work Roos et al. found the relativistic corrections to increase the dissociation energy by 2.5 kcal/mol for NiH and by 2.3 kcal/mol for CuH at CASPT2 level,¹² bringing it closer to the experimental values. We attribute the absence of improvement in our calculated D_e to the fact that spin-orbit effects are not accounted for. To take spin-orbit coupling into accounts Diaconu et. al.³⁴ used weighted averages over J components of the experimental data for easy comparison with the non-relativistic calculations. Unfortunately, the fine splitting in metal hydrides (necessary to use this technique) are only available for some of the hydrides (NiH,^{200,201} CoH,²⁰² FeH¹⁴), but not for others. Truhlar et. al.³³ correct their DFT binding energies by adding a Spin-Orbit (SO) corrections term defined by equation $\Delta E_{SO} = nE_{SO}(L) + E_{SO}(M) - E_{SO}(ML_n)$. Where, three different SO energies are defined for a general process given by $ML_n \rightarrow M + nL$. They have used atomic spectral information listed in Moore's books²⁰³ and equations from Herzberg's books²⁰⁴ to calculate spin-orbit effects for FeH and CoH to -0.12 and -0.37 kcal/mol.

3.2 TMH Bond Lengths

Equilibrium bond lengths are reported in Table 3.2 and Figure 3.2 Scalar relativistic corrections with BMK show smaller rms deviations, almost half of the ones compared to nonrelativistic-BMK and WFT method. Curiously, all non-relativistic methods demonstrate the same accuracy.

Table 3.2 includes experimental data available²⁰⁵⁻²⁰⁸ for six TMH systems out of nine in $3d$ -TM series. BMK relativistic bond lengths (Figure 3.2) for CrH, MnH, CoH and NiH are in very good agreement with experimental values, while WFT shows largest deviations for the same four systems. For FeH and CuH the deviation of 0.015 and 0.021 is obtained

with BMK-DKH, where WFT deviations are somewhat smaller (0.009 and 0.005 respectively).

3.3 TMH Potential Energy Curves and spin gaps

Potential Energy Curves (PEC) for neutral hydrides for ScH, VH, MnH and CrH in various multiplicities are reported in Figures 3.3 - 3.7 together with available MCSCF+SOC curves. All the curves for neutral *3d*-TM hydrides with non-relativistic BMK are plotted in Figure 3.8 for reference to the data in Table 3.1.

According to BMK the first two lowest multiplicities for ScH (Figure 3.3) are close in energy but differ in the bond length, so that singlet is more stable at the shorter, and triplet at longer bond length. On the contrary, TPSS overstabilizes singlet at all distances. Only singlet multiplicity is reported in the previous works^{1, 19, 35, 209} including WFT study by Koseki et. al.²² Two spin multiplicities are reported for VH at WFT²¹ (Figure 3.4). Both BMK and TPSS reproduce the ordering, although the spin gap in BMK is twice larger than in WFT. BMK result seems to be more reliable as it closely reproduces experimental D_e for the multiplicity 5. The two multiplicities for MnH (Figure 3.5) are almost degenerate in both BMK and TPSS, while WFT favors $M=7$ by 11 kcal/mol. Unlike the other TMH, MnH is found to have strong, more than 10%, spin contamination close to equilibrium bond length for $M=5$. The spin-contamination correction (detailed in chapter two) stabilizes this spin state by 3.5 kcal/mol below $M=7$, in disagreement with WFT. The corrected BMK dissociation energy is however, closer to the experimental value reported in Borane et. al.³⁵ Three Multiplicities of CrH are reported at WFT²⁰ (Figure 3.6), all with different dissociation limits. Both WFT and DFT predict the ground state to have the multiplicity of 6. BMK and

especially TPSS underestimate the spin gap at equilibrium, as compared to the *ab initio* results, while reproduce it fairly well at the dissociation limit.

The energy difference between the high and low spin states was studied previously by several authors and found to depend strongly on the fraction of HF exchange. This can be attributed to the fine balance between the negative HF exchange energy contribution from the electron of the same spin, which is opposite in sign to the electronic correlation contribution arising from the repulsion between any two electrons regardless of their spin. A method which includes the exchange and neglects the correlation (such as HF) will favor high multiplicities by maximizing the number of electrons with the same spin. To the contrary, self-interaction error in pure DFT favors low-spin states. Attempts to improve the relative spin-state energies description of density functionals include hybrid DFT schemes as well as DFT+U.²¹⁰ It was recently shown that DFT+U is capable of providing the qualitatively correct splitting in low- and high-spin iron porphyrins²¹⁰ and FeO⁺.²¹¹ However, when broken symmetry approach is adapted, the improvements obtained by the use of semiempirical +U correction can be accomplished by improving the form of the DFT functional.²¹² Conradie and Ghosh²¹³ studied Fe(+2) spin-crossover complexes and found that pure functionals such as BLYP, PW91 and BP86 unduly favor spin-coupled form (covalent description), while hybrid functionals such as B3LYP lean in the other direction. To correct the latter, they suggested reducing the amount of Hartree-Fock exchange in B3LYP from the standard 20% to 15%; the modified B3LYP functional has been found to give improved results. These calculations are in agreement with the recent review by Harvey.²¹⁴ He found an optimum exact exchange admixture of 15% to yield accurate results in many other cases. It appears that the large fraction of HF exchange is necessary for

correct prediction of the dissociation energies while smaller fraction is in better agreement with experimentally observed spin-gaps.

Spin contamination was observed in almost all TM neutral and ionic hydrides at intermediate distances. Spin contamination at the equilibrium was found to be less than 10% for all hydrides except in the case of MnH.

3.4 TMH Cations

Dissociation energies for cationic hydrides in equilibrium geometry are reported in Table 3.3 Comparison with two sets of experimental data and some of the published Wave Function Theory (WFT) and DFT predictions are also given. The experimental dissociation energies from ref.²¹⁵⁻²²⁰ are listed in the Table 3.4 as Set 2. Both Set 2 and Set 1 (compiled in Borane et. al.³⁵) were used to calculate the rms deviations for all theoretical values. Comparison with both the sets indicates BMK functional performs better than other XC functionals, while TPSS strongly overbinds in all cases. BMK values are superior to the best WFT data (when compared with new compilation), while hybrid B3LYP functionals demonstrates larger deviations. The deviations of predicted dissociation energies from experimental values (Set 2) are plotted on Figure 3.9 One can see that WFT underestimates the bonding energies, TPSS overbinds, and BMK is bracketed by these values for all TMH cations, except NiH⁺. All deviations at BMK level are within 6 kcal/mol.

Equilibrium bond lengths are reported in Table 3.4 and Figure 3.10 Table 3.4 includes experimental data²⁰⁵ for six TMH systems out of nine in *3d*-TM series. WFT performs considerably better than all the DFT methods for the bond lengths predictions; while BMK is superior to other functionals (except for CuH⁺ case).

Potential Energy Curves (PEC) of metal hydride cations for ScH⁺, TiH⁺ and CrH⁺ in various multiplicities are reported in Figures 3.11 – 3.12 and compared with available MCSCF+SOCl curves^{27, 28}. All the curves for 3*d*-TM hydride cations with non-relativistic BMK are plotted in Figure 3.4.6 for reference to the data in Table 3.4.

3.5 TMH Electronic Structure and Ionization Potential

Table 3.5 reports the Natural Bond Orbital (NBO) analysis of BMK spin densities respectively. The differences between the two methods are not significant and we will only discuss BMK in the following. The naive description of TM hydrides consist of 4*s* orbital involved in σ -bonding and the remaining non-bonding *d*-electrons coupled anti-ferromagnetically. Indeed, the highest spin state was found to be the most stable for all the neutral hydrides with two exceptions, ScH and MnH, where other multiplicities (1 and 7 respectively) are almost degenerate with the states of regular multiplicity (3 and 5). For that reason we consider the high spin states first.

As one can see from the Table 3.5, this naive description is accurate only for NiH and CuH. For FeH, CoH and CrH *s* and *d* orbitals hybridize close to 50/50 to form the bond, and for Sc, Ti, V hydrides one of the unpaired electrons occupies *s* orbital, and the covalent bond is formed by *d*-orbital of the majority (alpha) spin. The minority (beta) spin component of the covalent bond is still of *s*-character in these molecules. One exception is MnH in M=7 state, which in a simple picture would have zero bond order with the bonding electrons uncoupled. From NBO analysis, of the majority spin electrons the bond is ionic, and minority spin is covalent (mostly formed by *s* orbital). The low spin state of ScH has a lone pair on *s*-orbital. The remaining (VH, CrH, MnH) hydrides in the low spin states have

non-bonding electron of the minority spin on s orbital, while nonbonding electrons of majority spin are all on d -orbitals.

Dipole moments are reported in Table 3.6 for BMK and TPSS given by NBO analysis. BMK and TPSS values are compared with other WFT functionals for given multiplicities reported by Chong et. al.²⁴ One can see from the Table 3.6, BMK and TPSS values are not much different and are in close agreement with MCPF values for FeH, CoH, CuH and MnH (M=7). BMK and TPSS slightly overestimate the dipole moment values for ScH, TiH, VH and NiH in comparison to MCPF, and are close to CPF values (with the only exception of CrH).

Table 3.7 reports the Natural Bond Orbital analysis of BMK spin densities respectively for metal hydride cations. As can be seen from the Table 3.7, s electron is ionized during the formation of the cationic species, in all cases. Also, for all TMH⁺ systems all nonbonding electrons are d electrons in both the spins (alpha and beta). In the majority spin, ScH⁺, TiH⁺ and VH⁺ have s and d orbital hybridize close to 50/50, where as in remaining systems (MnH⁺, FeH⁺, CoH⁺, NiH⁺ and CuH⁺) s -orbital found to form covalent bond. In case of CrH⁺ d -orbital forms covalent bond, which is due to its half filled electronic configuration. The minority spin distribution for almost all the systems have close to 50/50 s and d hybridization except for CuH⁺, which shows covalent bond formation by d -orbital.

Table 3.8 gives the adiabatic and vertical ionization potential for BMK and TPSS along with experimental data. Our TPSS values of ionization potential differ from the results recently reported by Riley and Merz,³² with the same functional along with 11 other exchange-correlation functionals. The differences (and larger deviations from experiment) obtained in their study are likely to originate from using spin-adapted approach with default

orbital guess. The average unsigned error in our broken symmetry treatment is 0.141 and 0.269 eV for BMK and TPSS respectively.

3.6 Conclusions

We have used two exchange-correlation functionals including explicit dependence on kinetic energy density (τ -functionals) to study (both neutral and cationic) hydrides formed by *3d*-transition metals (Sc-Cu). One of the functionals selected contained large fraction of Hartree-Fock exchange (BMK), and another one was a pure DFT functional (TPSS). Watchers basis sets,¹²⁹ augmented with *f*-functions by Hay et. al.¹³⁰ were used. We have taken particular care to obtain the consistent SCF solution, including the stability analysis and Fermi smearing. In order to ensure the stability of Slater determinant in the entire range of interatomic distances, the potential energy curves were plotted and inspected for discontinuities. When found, the discontinuities were eliminated by using the lower energy orbitals as initial guess to continue the curve smoothly. The spin orbitals at the dissociation limit were inspected and reordered if necessary.

Qualitatively correct description of the bond dissociation was ensured by allowing the spatial and spin symmetry to break. This resulted in appreciable spin-contamination for some of the systems at equilibrium, and all the systems at intermediate interatomic distances. In order to correct the spin contamination effect on the energies, we used a new approach as described in chapter two. This approach differs from existing spin-correction schemes, which are based on the expectation value of the spin operator corresponding to the hypothetical non-interactive systems. Instead, our spin correction scheme is based on the energy of high spin determinant built on the Natural Orbitals of the total density and its contribution is evaluated from the occupation numbers of these orbitals.

Based on the described protocol, we report BMK dissociation energies that are in better agreement with experiment than those obtained with high level wavefunction theory methods, published previously. This agreement with experiment deteriorates quickly when the fraction of the Hartree-Fock exchange in DFT functional is decreased. Higher fraction of HF exchange does not necessarily help, however, when spin-adapted unrestricted approach is employed. We found no improvements in dissociation energies, when Scalar relativistic effects are taken into account in Douglas-Kroll approximation,¹³⁴ while bond distances showed twice lower RMS deviations after relativistic corrections. We analyzed the electron spin densities using Natural Bond Orbital population analysis and found that simple description of the chemical bond in metal hydrides as formed by $4s$ orbital of the metal with $3d$ -electrons keeping non-bonding character is rarely correct.

We also found that the average unsigned error for ionization potentials is much lower (0.14 and 0.27 eV for BMK and TPSS respectively) than previously reported owing to the careful SCF protocol employed. However, the spin gaps for the systems with multiple spin states considered is in disagreement with the wavefunction data available even after the spin-contamination correction.

Table 3.1 Dissociation energies (kcal/mol) of neutral hydrides (TMH) and root mean square (rms) deviations from the experimental values.

| | ScH | | TiH | | VH | | CrH | | | MnH | | FeH | CoH | NiH | CuH | rms deviations | | |
|-------------------------------|-------------|------|-------------|------|-------------|------|------|-------------|-------------------|-------------|-------------|-------------|-------------|-------------|------|----------------|-------|--|
| Multiplicity | 1 | 3 | 4 | 3 | 5 | 2 | 4 | 6 | 5 | 7 | 4 | 3 | 2 | 1 | Set1 | Set 2 | Set 3 | |
| BS-TPSS | 95.5 | 64.9 | 67.8 | 59.4 | 64.6 | 68.3 | 55.9 | 57.9 | 53.0 | 52.8 | 60.9 | 65.7 | 76.1 | 69.0 | 6.62 | 7.37 | 7.75 | |
| BS-BMK | 50.8 | 50.2 | 48.7 | 43.6 | 55.7 | 43.7 | 48.1 | 52.5 | 37.2 ^k | 34.8 | 41.0 | 46.4 | 59.5 | 61.8 | 1.79 | 1.06 | 1.38 | |
| SA-BLYP^a | 42.4 | | 55.7 | | 66.7 | | | 57.0 | | 26.5 | 42.3 | 47.4 | 68.1 | 66.2 | 3.93 | 2.44 | 2.90 | |
| SA-B3LYP^a | 40.2 | | 60.1 | | 63.8 | | | 54.0 | | 34.8 | 40.5 | 43.4 | 60.3 | 63.5 | 3.09 | 2.23 | 2.56 | |
| BS - B3LYP^b | 57.8 | | 66.8 | | 62.9 | | | 54.9 | | 39.4 | 55.3 | 61.6 | 60.9 | 62.7 | 4.97 | 3.67 | 4.12 | |
| BS-TPSSh^b | 62.8 | | 68.2 | | 64.2 | | | 55.9 | | 50.9 | 59.6 | 62.9 | 64.2 | 65.5 | 5.80 | 4.77 | 5.22 | |
| MCSCF+SOCF^c | 47.3 | | 43.3 | 36.6 | 42.7 | | 37.8 | 44.2 | 21.8 | 33.6 | | | | | 1.73 | 2.32 | 1.84 | |
| MCPF^d | 51.0 | | 47.3 | | 53.0 | | | 48.7 | 21.9 | 39.4 | 45.0 | 44.7 | 64.3 | 61.6 | 1.84 | 1.38 | 1.63 | |
| BS-TPSS:DKH | 95.2 | 64.1 | 71.8 | 58.3 | 66.0 | 65.9 | 56.9 | 59.0 | 50.5 | 51.7 | 61.8 | 67.1 | 71.9 | 71.7 | 6.93 | 7.52 | 7.91 | |
| BS-BMK:DKH | 51.9 | 49.0 | 49.1 | 45.6 | 51.9 | 50.4 | 46.0 | 54.2 | 33.9 | 33.7 | 40.8 | 42.9 | 60.7 | 63.9 | 1.85 | 1.19 | 1.42 | |
| Exp.-Set1^a | | | 45.2 | | 49.1 | | | 44.5 | | 39.0 | 34.4 | 42.9 | 56.5 | 60.0 | | | | |
| Exp.-Set2^b | 47.5 | | 50 | | 51.4 | | | 46.8 | | 31.1 | 39.2 | 48.4 | 61.3 | 63.4 | | | | |
| Exp.-Set3 | 47.5 | | 48.9 | | 49.1 | | | 44.5 | | 30.2 | 37.5 | 46.0 | 59.4 | 61.0 | | | | |
| | $\pm 2.0^e$ | | $\pm 2.1^f$ | | $\pm 1.6^g$ | | | $\pm 1.6^g$ | | $\pm 4.4^h$ | $\pm 1.9^i$ | $\pm 3.0^j$ | $\pm 3.0^j$ | $\pm 4.0^j$ | | | | |

(a)-Ref 30, (b)-Ref 1, (c)-Ref 19-21, (d)-Ref 225, (e)-Ref 209, (f)-Ref 208, (g)-Ref 210, (h)-Ref 211, (i)-Ref 212, (j)-Ref 207, (k)-Spin-Corrected, using the scheme detailed in Chapter 2

Table 3.2 Equilibrium bond lengths (Å) of neutral hydrides (TMH) and root mean square (rms) deviations from the experimental values.

| Multiplicity | ScH | | TiH | | VH | | CrH | | MnH | | FeH | CoH | NiH | CuH | rms |
|-------------------------------|-------|-------|-------|-------|-------|-------|-------|--------------------|-------|--------------------|--------------------|--------------------|--------------------|--------------------|--------|
| | 1 | 3 | 4 | 3 | 5 | 2 | 4 | 6 | 5 | 7 | 4 | 3 | 2 | 1 | |
| BS-TPSS | 1.798 | | 1.756 | 1.678 | 1.684 | 1.633 | 1.629 | 1.654 | 1.590 | 1.713 | 1.554 | 1.523 | 1.472 | 1.475 | 0.0080 |
| BS-BMK | 1.755 | 1.874 | 1.783 | 1.712 | 1.705 | 1.642 | 1.658 | 1.668 | 1.745 | 1.745 | 1.581 | 1.525 | 1.486 | 1.506 | 0.0079 |
| SA-BLYP^a | 1.743 | | 1.750 | | 1.681 | | | 1.652 | | 1.720 | 1.561 | 1.510 | 1.507 | 1.460 | 0.0080 |
| SA-B3LYP^a | 1.730 | | 1.744 | | 1.677 | | | 1.654 | | 1.723 | 1.561 | 1.510 | 1.509 | 1.460 | 0.0080 |
| BS - B3LYP^b | | | 1.760 | | | | | 1.663 | | 1.734 | 1.571 | 1.524 | 1.516 | 1.482 | 0.0084 |
| BS-TPSSh^b | | | | | | | | 1.659 | | 1.720 | 1.570 | 1.526 | 1.505 | 1.479 | 0.0076 |
| MCSCF+SOCI^c | 1.782 | | 1.852 | | 1.758 | | 1.658 | 1.676 | 1.644 | 1.702 | | | | | 0.0202 |
| MCPF^d | 1.800 | | 1.840 | | 1.740 | | | 1.700 | 1.644 | 1.770 | 1.580 | 1.532 | 1.439 | 1.458 | 0.0107 |
| BS-TPSS:DKH | 1.795 | | 1.754 | 1.677 | 1.681 | 1.637 | 1.621 | 1.646 | 1.582 | 1.709 | 1.555 | 1.506 | 1.455 | 1.456 | 0.0090 |
| BS-BMK:DKH | 1.756 | 1.875 | 1.783 | 1.714 | 1.728 | 1.747 | 1.659 | 1.660 | 1.652 | 1.740 | 1.574 | 1.513 | 1.467 | 1.484 | 0.0045 |
| Exp. | | | | | | | | 1.662 ^e | | 1.740 ^e | 1.589 ^f | 1.513 ^g | 1.475 ^e | 1.463 ^h | |

(a)-Ref 30, (b)-Ref 1, (c)-Ref 19-21, (d)-Ref 225, (e)-Ref 221, (f)-Ref 222, (g)-Ref 223, (h)-Ref 224

Table 3.3 Dissociation energies (kcal/mol) of metal hydrides cations (TMH+) and root mean square (rms) deviations from the experimental values.

| | ScH+ | TiH+ | VH+ | CrH+ | MnH+ | FeH+ | CoH+ | NiH+ | CuH+ | rms deviations | |
|-------------------------------|---------------------|---------------------|---------------------|---------------------|---------------------|---------------------|---------------------|---------------------|---------------------|----------------|-------|
| Multiplicity | 2 | 3 | 4 | 5 | 6 | 5 | 4 | 3 | 2 | Set 1 | Set 2 |
| BS-TPSS | 65.1 | 62.9 | 58.6 | 44.2 | 55.5 | 58.8 | 55.2 | 52.4 | 34.6 | 3.81 | 3.58 |
| BS-BMK | 57.8 | 55.7 | 48.4 | 37.0 | 45.3 | 54.5 | 50.2 | 35.0 | 22.6 | 1.43 | 1.14 |
| SA-B3LYP^a | 57.5 | 62.0 | 48.5 | 36.0 | 49.3 | 58.0 | 53.9 | 43.2 | 27.2 | 2.03 | 1.89 |
| MCPF^b | 54.0 | 51.0 | 47.0 | 27.8 | 40.8 | 49.1 | 40.7 | 36.4 | 15.9 | 1.22 | 1.29 |
| Exp. Set 1^a | 55.3 | 55.1 | 47.3 | 27.7 | 47.5 | 48.9 | 45.7 | 38.6 | 21.2 | | |
| Exp. Set 2 | 56.3±2 ^c | 54.3±3 ^d | 48.3±1 ^e | 31.6±2 ^f | 47.5±3 ^g | 48.9±1 ^h | 45.7±1 ⁱ | 38.7±2 ⁱ | 21.2±3 ⁱ | | |

(a)-Ref 30, (b)-Ref 225, (c)-Ref 231, (d)-Ref 238, (e)-Ref 232, (f)-Ref 233, (g)-Ref 234, (h)-Ref 235-236, 239, (i)-Ref 237

Table 3.4 Equilibrium bond lengths (Å) of metal hydrides cations (TMH⁺) and root mean square (rms) deviations from the experimental values.

| | ScH⁺ | TiH⁺ | VH⁺ | CrH⁺ | MnH⁺ | FeH⁺ | CoH⁺ | NiH⁺ | CuH⁺ | rms |
|-----------------------------|------------------------|------------------------|-----------------------|------------------------|------------------------|------------------------|------------------------|------------------------|------------------------|------------|
| Multiplicity | 2 | 3 | 4 | 5 | 6 | 5 | 4 | 3 | 2 | |
| BS-TPSS | 1.775 | 1.695 | 1.632 | 1.600 | 1.598 | 1.568 | 1.540 | 1.487 | 1.512 | 0.018 |
| BS-BMK | 1.791 | 1.713 | 1.648 | 1.609 | 1.633 | 1.589 | 1.540 | 1.496 | 1.508 | 0.013 |
| SA-B3LYP^a | 1.766 | 1.700 | 1.648 | 1.594 | 1.600 | 1.561 | 1.541 | 1.466 | 1.478 | 0.016 |
| MCPF^b | 1.829 | 1.740 | 1.661 | 1.604 | 1.652 | 1.603 | 1.547 | 1.487 | 1.445 | 0.002 |
| Exp. | 1.83 ^c | | 1.663 ^c | | 1.645 ^c | 1.598 ^c | 1.54 ^c | | 1.443 ^c | |

(a)-Ref 30, (b)-Ref 225, (c)-Ref 221

Table 3.5 Alpha and beta bonding and non-bonding orbital hybridization coefficients obtained from NBO analysis for the neutral hydrides (TMH) calculated with BMK.

| Systems | M | Alpha (TM) | | | | | | | | | Beta (TM) | | | | | | | | | | | | | | |
|------------|---|-------------|----------|----|----|-----------------|-------|-------|-------|-----------|-----------|-------------|----------|---|---|-----------------|---|---|---|---|------|----|----|----|------------------------------|
| | | Spin-Charge | Bond (%) | | | Non-bonding (%) | | | | | | Spin-Charge | Bond (%) | | | Non-bonding (%) | | | | | | | | | |
| | | | s | p | d | 1 | 2 | 3 | 4 | 5 | 6 | | s | p | d | 1 | 2 | 3 | 4 | 5 | | | | | |
| ScH | 1 | 0.26 | 18 | 5 | 77 | s 82 | | | | | | | | | | | | | | | 0.26 | 18 | 5 | 77 | s 82 |
| | 3 | -0.64 | 7 | 20 | 73 | d 100 | s 92 | | | | | | | | | | | | | | 1.28 | 70 | 6 | 24 | |
| TiH | 4 | -1.20 | 11 | 12 | 78 | d 100 | d 100 | s 89 | | | | | | | | | | | | | 1.76 | 70 | 5 | 25 | |
| VH | 3 | -0.82 | 66 | 3 | 31 | d 100 | d 100 | d 100 | | | | | | | | | | | | | 1.32 | 10 | 11 | 80 | s 90 |
| | 5 | -1.79 | 19 | 5 | 76 | d 100 | d 100 | d 100 | s 81 | | | | | | | | | | | | 2.25 | 72 | 3 | 25 | |
| CrH | 2 | -0.37 | 82 | 2 | 16 | d 100 | d 100 | d 85 | | | | | | | | | | | | | 0.70 | 25 | 3 | 72 | d 100 s 75 |
| | 4 | -1.34 | 59 | 2 | 39 | d 100 | d 100 | d 100 | d 100 | | | | | | | | | | | | 1.79 | 13 | 7 | 80 | s 87 |
| | 6 | -2.39 | 44 | 2 | 54 | d 100 | d 100 | d 100 | d 100 | s 56 d 44 | | | | | | | | | | | 2.78 | 71 | 3 | 26 | |
| MnH | 5 | -1.92 | 91 | 2 | 7 | d 100 | d 100 | d 100 | d 100 | d 93 | | | | | | | | | | | 2.32 | 9 | 9 | 82 | s 91 |
| | 7 | -2.58 | 0 | 0 | 0 | d 100 | d 100 | d 100 | d 100 | d 77 s 70 | | | | | | | | | | | 3.21 | 74 | 4 | 22 | |
| FeH | 4 | -1.37 | 92 | 2 | 6 | d 100 | d 100 | d 100 | d 100 | d 94 | | | | | | | | | | | 1.67 | 41 | 2 | 57 | d 100 s 59 d 40 |
| CoH | 3 | -0.88 | 92 | 1 | 7 | d 100 | d 100 | d 100 | d 100 | d 93 | | | | | | | | | | | 1.13 | 55 | 1 | 44 | d 100 d 100 d 54 s 45 |
| NiH | 2 | -0.36 | 93 | 1 | 5 | d 100 | d 100 | d 100 | d 100 | d 95 | | | | | | | | | | | 0.72 | 73 | 2 | 25 | d 100 d 100 d 100 d 100 |
| CuH | 1 | 0.15 | 92 | 2 | 6 | d 100 | d 100 | d 100 | d 100 | d 94 | | | | | | | | | | | 0.15 | 92 | 2 | 6 | d 100 d 100 d 100 d 100 d 94 |

Table 3.6 Dipole moments (Debye) for neutral metal hydrides calculated with BMK and TPSS, compared with several WFT levels.

| System | M | Dipole Moments | | | | |
|------------|---|----------------|------|-------------------|------------------|-------------------|
| | | BMK | TPSS | SDCI ^a | CPF ^a | MCPF ^a |
| ScH | 1 | 1.9 | 2.5 | 1.4 | 1.8 | 1.6 |
| | 3 | 2.6 | 2.8 | 2.0 | 2.6 | 2.4 |
| TiH | 4 | 2.6 | 2.6 | 1.9 | 2.3 | 2.2 |
| VH | 3 | 2.0 | 2.2 | | | |
| | 5 | 2.7 | 2.5 | 1.8 | 2.3 | 2.0 |
| CrH | 2 | 2.5 | 2.9 | | | |
| | 4 | 1.8 | 2.6 | | | |
| | 6 | 3.1 | 2.9 | 4.3 | 3.8 | 3.8 |
| MnH | 5 | 1.4 | 2.1 | | | |
| | 7 | 1.1 | 0.8 | 1.3 | 1.2 | 1.2 |
| FeH | 4 | 2.6 | 2.6 | 4.1 | 1.3 | 2.9 |
| CoH | 3 | 2.5 | 2.6 | 3.9 | 1.4 | 2.7 |
| NiH | 2 | 3.2 | 2.3 | 3.7 | 1.8 | 2.6 |
| CuH | 1 | 3.0 | 2.5 | 3.9 | 2.7 | 3.0 |

(a)-Ref 23

Table 3.7 Alpha and beta bonding and non-bonding orbital hybridization coefficients obtained from NBO analysis for the metal hydrides cations calculated with BMK.

| Systems | M | Alpha (M) | | | | | | | | | | Beta (M) | | | | | | | | | |
|------------|---|-------------|----------|---|----|-----------------|-------|-------|-------|------|---|-------------|----------|---|----|-----------------|-------|-------|-------|---|--|
| | | Spin-Charge | Bond (%) | | | Non-bonding (%) | | | | | | Spin-Charge | Bond (%) | | | Non-bonding (%) | | | | | |
| | | | s | p | d | 1 | 2 | 3 | 4 | 5 | 6 | | s | p | d | 1 | 2 | 3 | 4 | 5 | |
| ScH | 2 | 0.22 | 33 | 1 | 66 | d 99 | | | | | | 1.26 | 36 | 2 | 62 | | | | | | |
| TiH | 3 | -0.33 | 33 | 1 | 66 | d 100 | d 100 | | | | | 1.73 | 32 | 1 | 66 | | | | | | |
| VH | 4 | -0.89 | 30 | 1 | 69 | d 100 | d 100 | d 100 | | | | 2.22 | 31 | 1 | 68 | | | | | | |
| CrH | 5 | -1.50 | 16 | 1 | 83 | d 100 | d 100 | d 100 | d 100 | | | 2.75 | 30 | 1 | 69 | | | | | | |
| MnH | 6 | -1.92 | 90 | 2 | 8 | d 100 | d 100 | d 100 | d 100 | d 92 | | 3.14 | 29 | 1 | 70 | | | | | | |
| FeH | 5 | -1.34 | 93 | 2 | 5 | d 100 | d 100 | d 100 | d 100 | d 95 | | 2.52 | 18 | 1 | 81 | d 100 | | | | | |
| CoH | 4 | -0.88 | 95 | 2 | 3 | d 100 | d 100 | d 100 | d 100 | d 97 | | 2.11 | 38 | 1 | 60 | d 100 | d 100 | | | | |
| NiH | 3 | -0.33 | 94 | 2 | 4 | d 100 | d 100 | d 100 | d 100 | d 96 | | 1.42 | 17 | 1 | 83 | d 100 | d 100 | d 100 | | | |
| CuH | 2 | 0.26 | 94 | 3 | 3 | d 100 | d 100 | d 100 | d 100 | d 97 | | 0.77 | 8 | 0 | 92 | d 100 | d 100 | d 100 | d 100 | | |

Table 3.8 Adiabatic ionization potential (IP) of neutral metal hydrides and their errors in comparison to experimental values.

| System | n-mult | c-mult | Exp. ^a | IP (eV) | | IP (eV) | | IP (eV) | | error | | |
|------------|--------|--------|-------------------|-----------|----------|-----------|----------|-----------|--------|--------|----------------------|--|
| | | | Adiabatic | Adiabatic | Vertical | Adiabatic | Vertical | Adiabatic | BMK | TPSS | SA-TPSS ^b | |
| ScH | 1 | 2 | 6.209 | 6.090 | 6.371 | 6.165 | 6.169 | | -0.119 | -0.044 | | |
| TiH | 4 | 3 | 6.600 | 6.523 | 6.555 | 6.618 | 6.649 | 5.960 | -0.077 | 0.018 | -0.640 | |
| VH | 5 | 4 | 6.363 | 6.116 | 6.330 | 6.224 | 6.266 | | -0.247 | -0.139 | | |
| CrH | 6 | 5 | 7.668 | 7.707 | 6.451 | 6.416 | 6.430 | | 0.039 | -1.252 | | |
| MnH | 7 | 6 | 6.635 | 6.898 | 6.970 | 6.866 | 6.939 | 6.510 | 0.263 | 0.231 | -0.125 | |
| FeH | 4 | 5 | 7.374 | 7.467 | 7.479 | 7.677 | 7.905 | | 0.093 | 0.303 | | |
| CoH | 3 | 4 | 7.871 | 7.877 | 8.002 | 8.140 | 8.152 | 7.150 | 0.006 | 0.269 | -0.721 | |
| NiH | 2 | 3 | 8.531 | 8.195 | 8.206 | 8.635 | 8.653 | 7.490 | -0.336 | 0.104 | -1.041 | |
| CuH | 1 | 2 | 9.447 | 9.359 | 9.361 | 9.387 | 9.408 | | -0.088 | -0.060 | | |

(a)-From NIST database and Ref 225, (b)-Ref 32

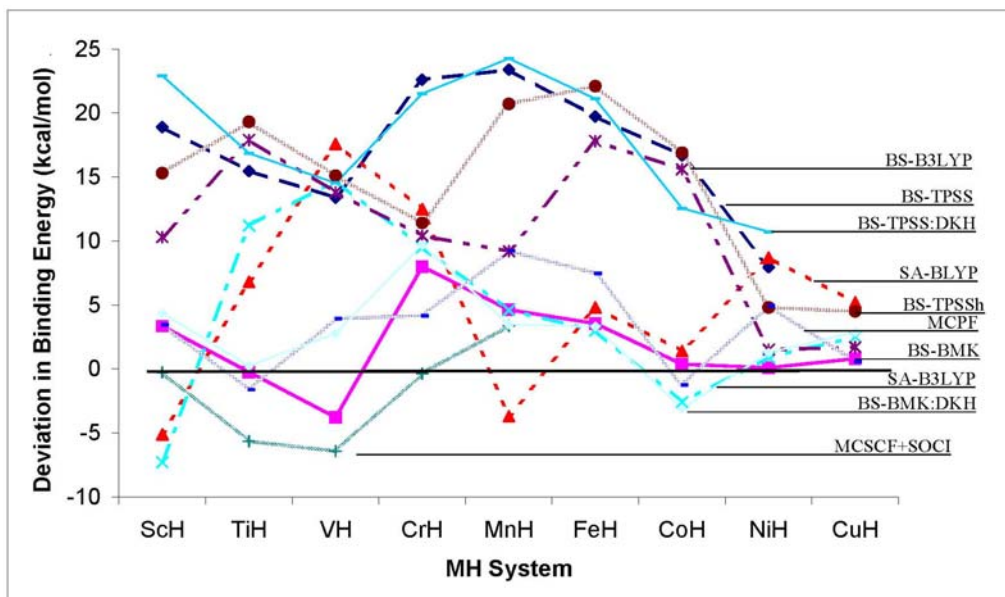


Figure 3.1 Deviations in Binding Energies from experimental data (Set III in Table 3.1.1) for neutral TMH with various DFT and WFT methods.

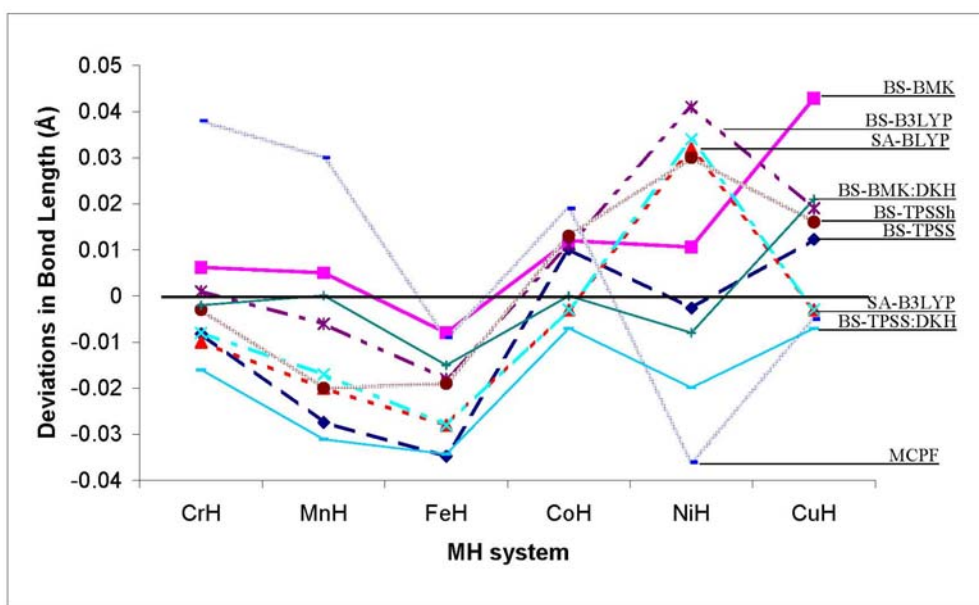


Figure 3.2 Deviations in Bond Lengths from experimental data for neutral TMH with various DFT and WFT methods.

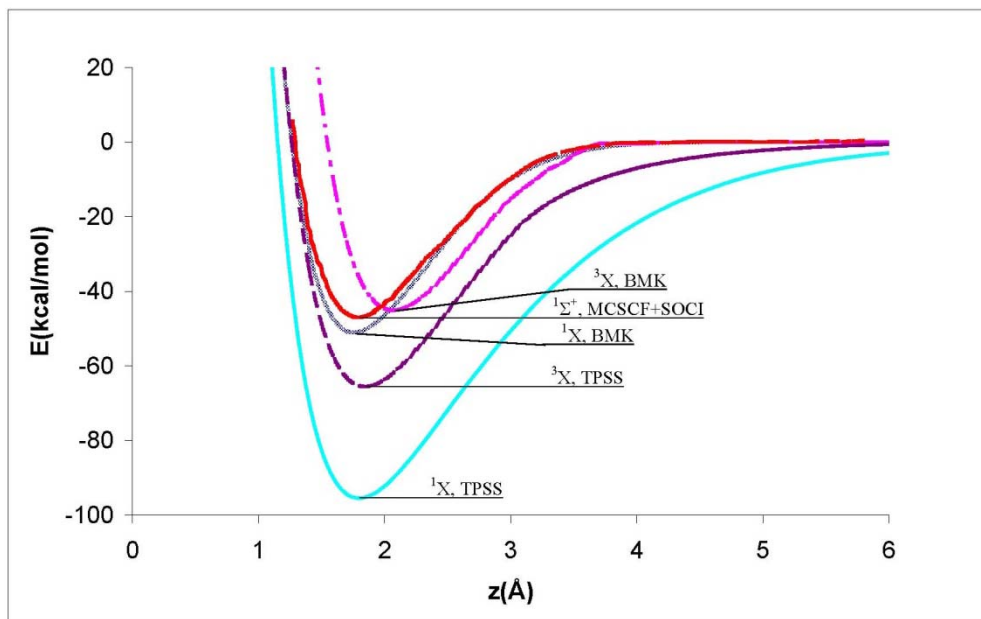


Figure 3.3 Potential Energy Curves of ScH with multiplicity 1 and 3, calculated by non-relativistic TPSS, BMK, and WFT (21) methods.

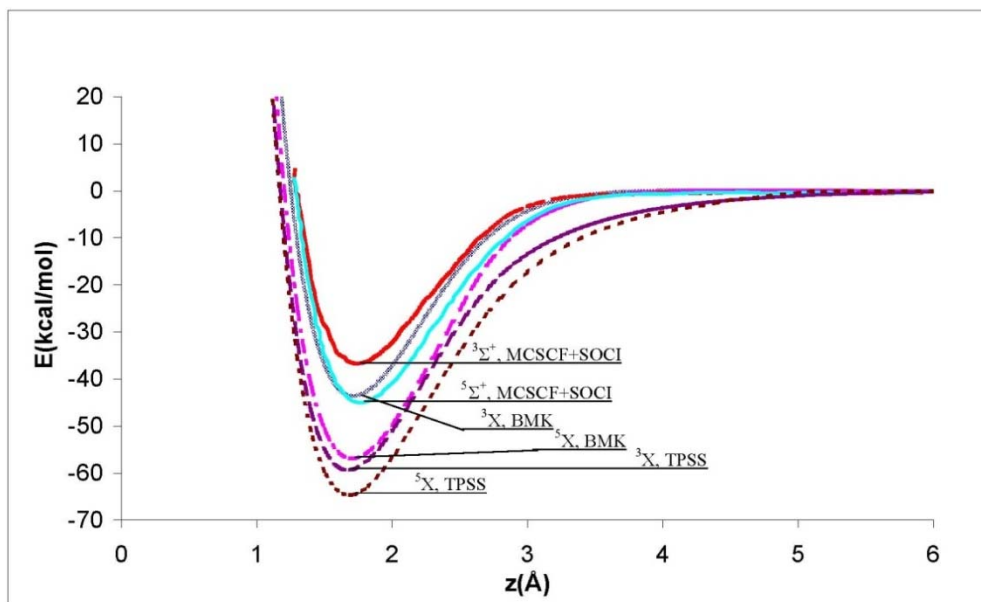


Figure 3.4 Potential Energy Curves of VH with multiplicity 3 and 5, calculated by non-relativistic TPSS, BMK, and WFT (20) methods.

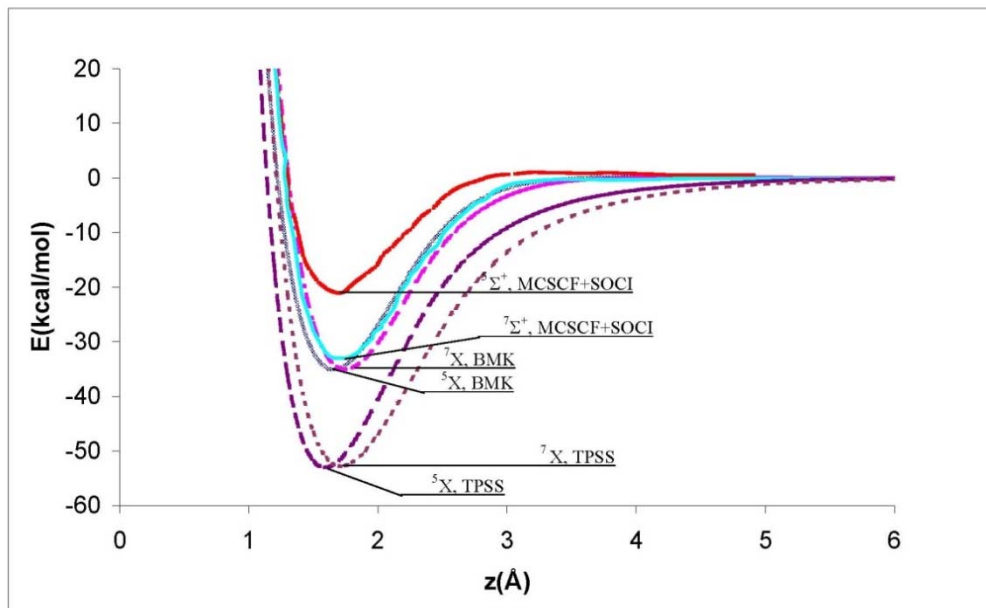


Figure 3.5 Potential Energy Curves of MnH with multiplicity 5 and 7, calculated by non-relativistic TPSS, BMK, and WFT (19) methods.

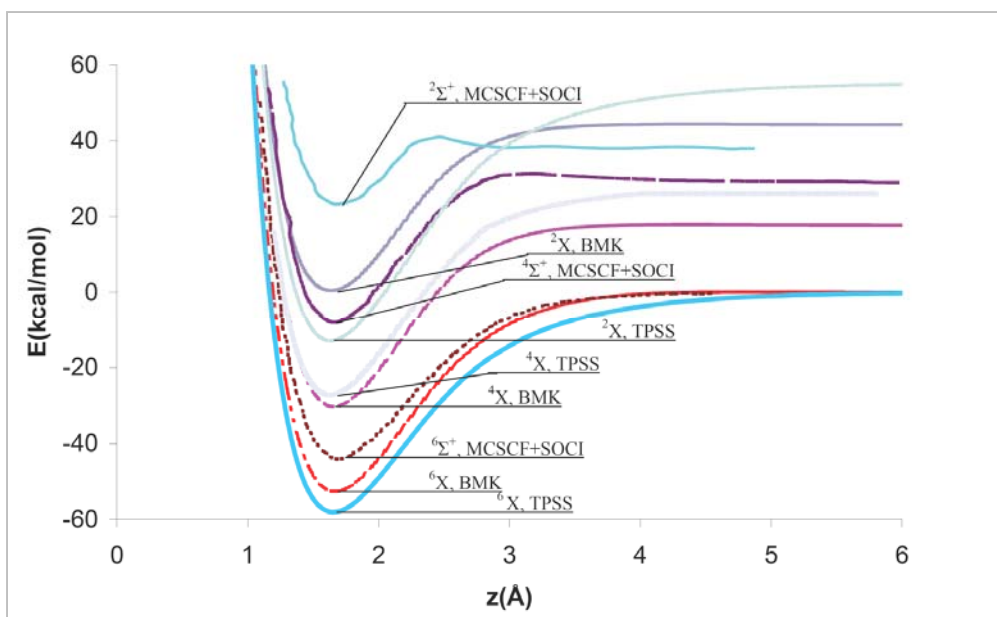


Figure 3.6 Potential Energy Curves of CrH with multiplicity 2, 4 and 6, calculated by non relativistic TPSS, BMK, and WFT (19) methods.

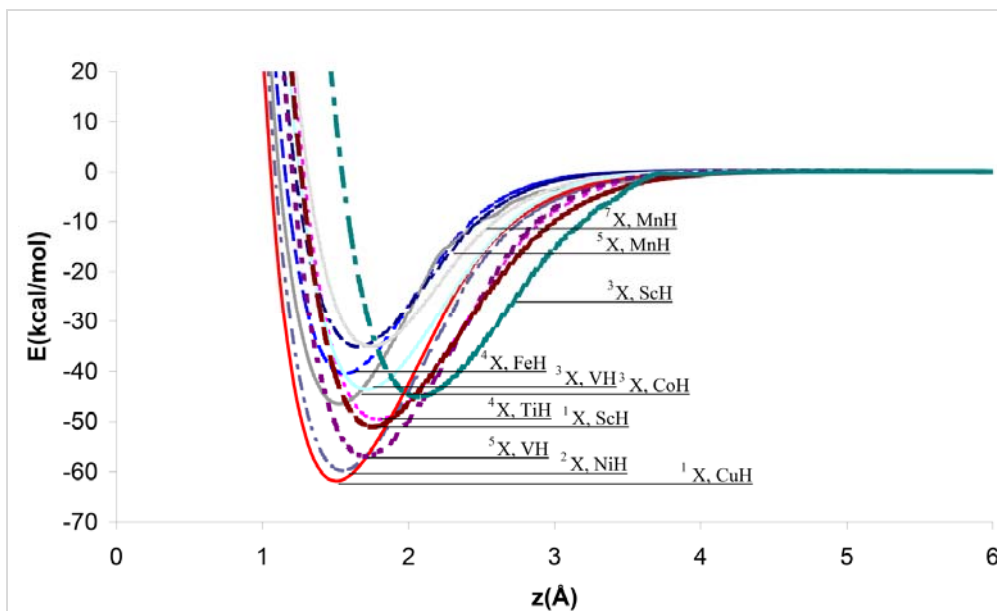


Figure 3.7 Potential Energy Curves of neutral TMH calculated by non-relativistic BMK.

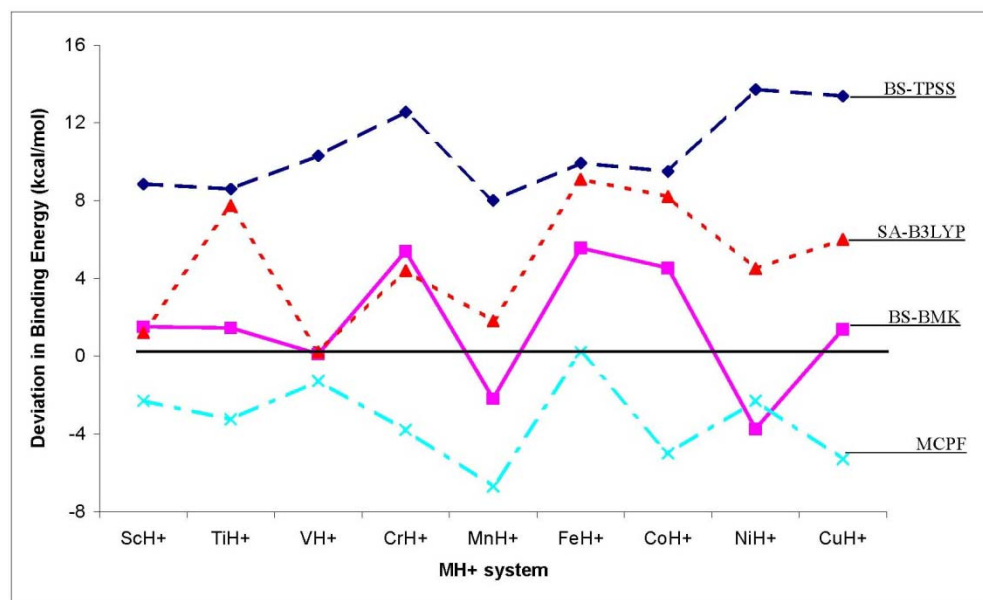


Figure 3.8 Deviations in Binding Energies from experimental data (Set II in Table 3.4.1) for TMH cations with various DFT and WFT methods.

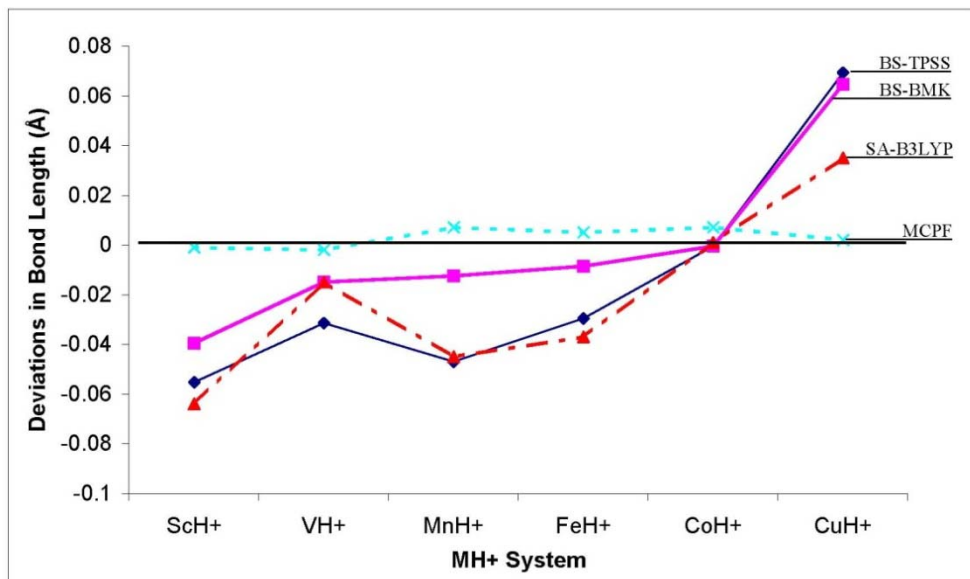


Figure 3.9 Deviations in Bond Lengths from experimental data for TMH cations with various DFT and WFT methods.

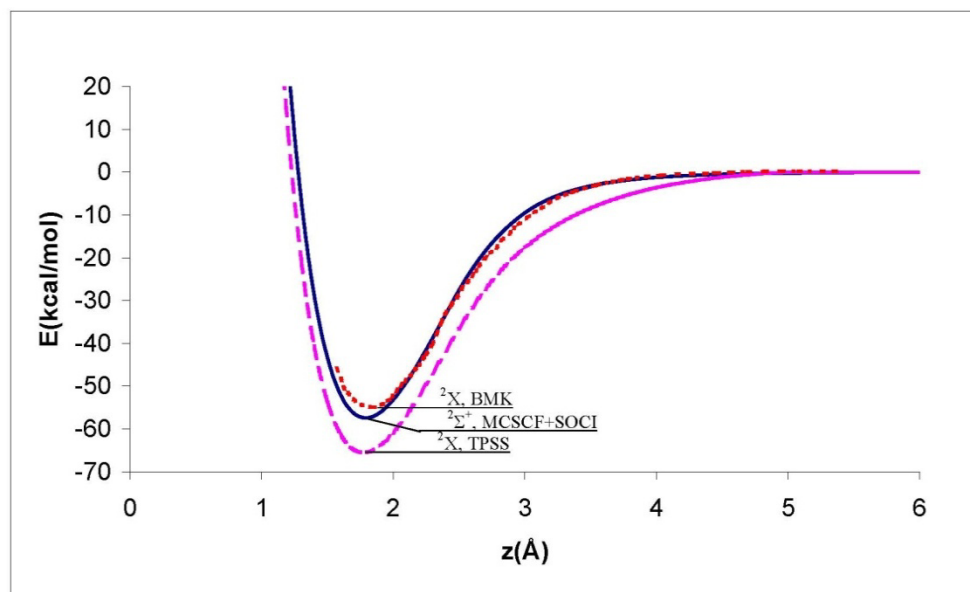


Figure 3.10 Potential Energy Curves of ScH+ with multiplicity 2, calculated by non-relativistic TPSS, BMK, and WFT (230) methods.

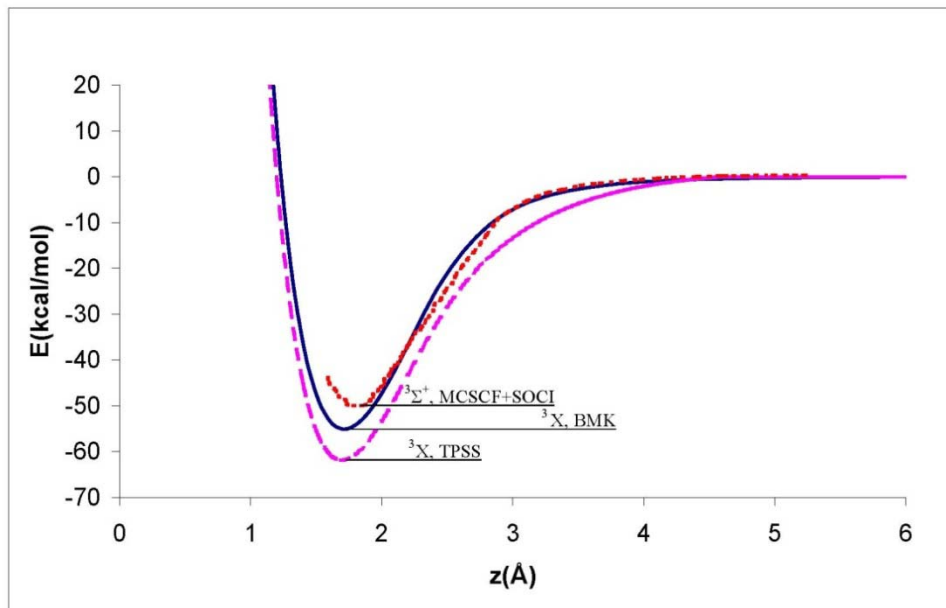


Figure 3.11 Potential Energy Curves of TiH^+ with multiplicity 3, calculated by non relativistic TPSS, BMK, and WFT (28) methods.

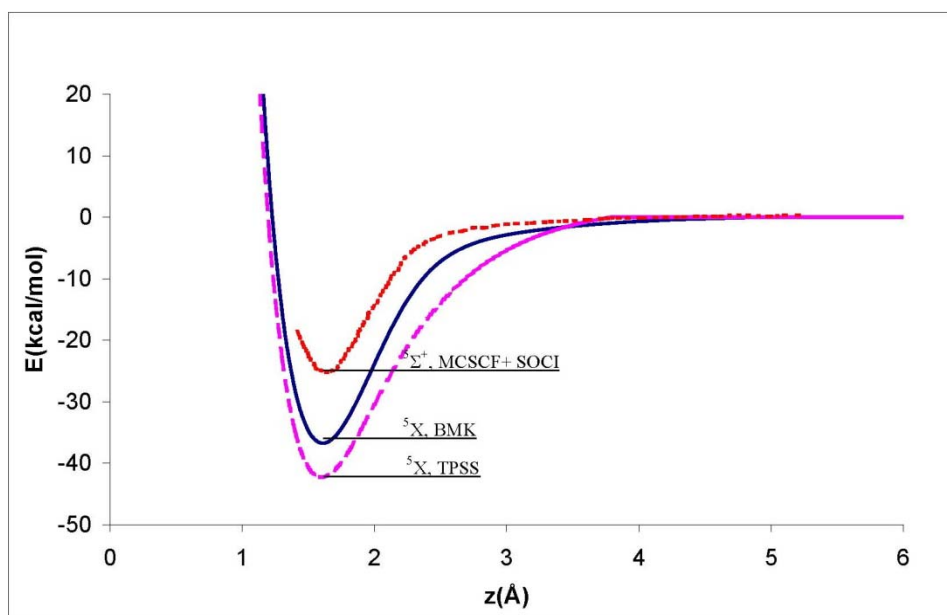


Figure 3.12 Potential Energy Curves of CrH^+ with multiplicity 5, calculated by non relativistic TPSS, BMK, and WFT (240) methods.

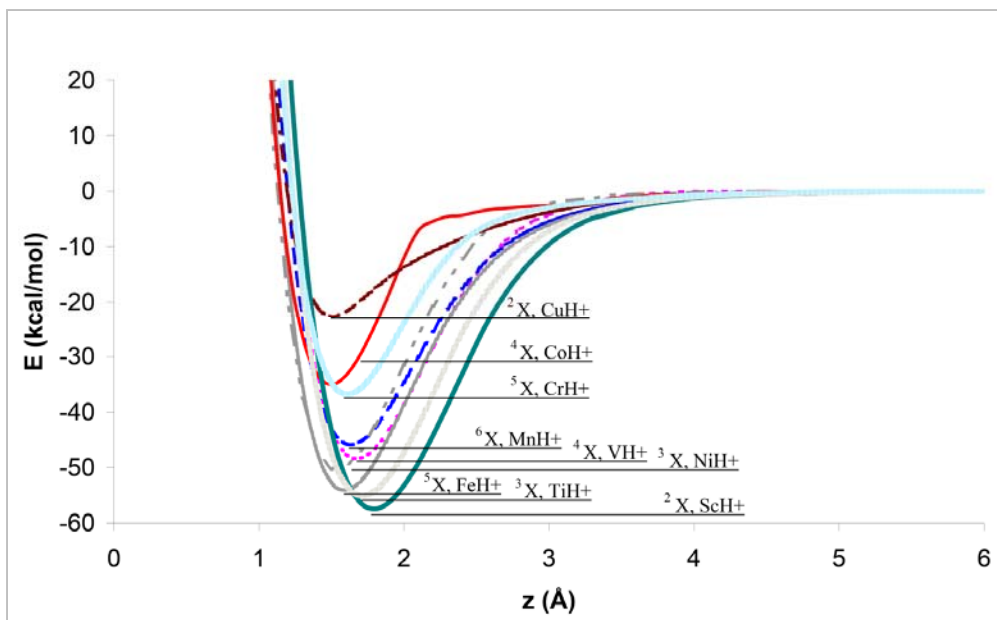


Figure 3.13 Potential Energy Curves of TMH cations calculated by non-relativistic BMK.

CHAPTER 4: TRANSITION METAL CARBIDES (TMC) AND SMALL NICKEL CLUSTERS

To further understand the bonding pattern of the *3d*-transition metals we have investigated their monocarbides, and small nickel clusters. In this chapter we report dissociation curves for MC and equilibrium geometries for Ni_x (x=2-5) in various spin states and compare them with experimental data where available.

To provide the insight into bond breaking and forming, important for catalytic application of the transition methods we focus here on Transition Metal Carbides (TMC). We examined several lowest states of different spin multiplicities, and analyzed variations in bond energies and bond lengths. Potential energy curves for all spin states were compared with PES curves obtained with WFT. In this study we included two new hybrid meta-GGA functionals M05 and M05-2x in addition to TPSS and BMK functionals to compare their performance with WFT methods and experimental data, where available.

4.1 TMC Binding Energies

Dissociation energies for neutral *3d*-transition metal carbides in equilibrium geometry, calculated in this work are reported in Table 4.1. WFT and experimental data are also shown for comparison. This study describes more than one spin multiplicity of these diatomic transition metal systems, where possible. Lack of experimental data on these diatomics we used wave function theory (WFT) results for all spin states for benchmarking. Besides reporting available experimental data for few systems, Table 4.1 also includes other DFT predictions made by Gutsev et. al.³⁶ and WFT literature data.^{37-40, 42-46, 48-52, 54, 221-224}

As we established in Chapter three BMK is accurate in predicting geometry and energetics of 3d transition metal systems due to high fraction of HF exchange compared to

more conventional hybrid DFT functionals like (such as B3LYP). Here we have performed an exhaustive study of TMC with two additional DFT functionals from Truhlar's group:²²⁵ M05 and M05-2x, as well as TPSS and BMK. As one can see from the Table 4.1, M05-2x predictions are much closer to MRCI values for binding energies, except for three cases ^4ScC , ^1TiC and ^3NiC , which merits further investigation. One can also see from Table 4.1 that binding energies of ^3TiC , ^2VC , ^5CrC , ^4CuC as predicted by M05-2x are within 2-3 kcal/mol of MRCI predictions, where as BMK, M05 (this study) and B3LYP (Gutsev et. al.)³⁶ shows large energy variations for these systems. For other systems including ^2ScC , ^7CrC , ^5FeC , ^2CoC , ^1NiC , M05-2x also performs better in comparison to all other functionals tested. Pure DFT functionals such as TPSS (this work) and BLYP (from Gutsev et. al.) overestimate binding energies and not suitable to study energetics of transition metal carbides. The same conclusion was made regarding hydrides in Chapter 3. In the past, relativistic corrections were reported to be important in the systems involving $3d$ transition metals.^{33, 198, 199} We studied scalar relativistic effects on the dissociation energies with Douglas-Kroll¹³⁴ approximations as shown in Table 4.1 and found that relativistic correction does change our predictions, in a sharp contrast to the hydrides. We observe significant corrections in some cases with the use of relativistic calculations in TMC considered here. For first three carbides in the series (ScC , TiC and VC) the relativistic corrections decreases the binding energy and for rest of the systems it increases the energy. In most cases the correction improves M05-2x results as compared to MRCI. However, quantitative conclusion is not possible in the absence of experimental data.

4.2 TMC Bond Lengths

Equilibrium bond lengths for TMC are reported in Table 4.2. From this Table one can see that BMK functional performs better than M05-2x (in contrast to the binding energies). The pure and GGA functionals BLYP and TPSS predict the geometry closest to that of WFT methods. However, they fail to reproduce right trends in energetics.

After relativistic correction is applied BMK calculated bond lengths also show significant change. In contrast to the trends observed in binding energies, bond lengths increased for ScC, TiC and VC and decreased for rest of the carbides. We can conclude that geometry calculations are less sensitive to percentage of HF exchange, which played major role in energetics. Further studies of transition metal systems call for careful selection of DFT functional.

4.3 TMC Potential Energy Curves

Similar to TMH, the potential energy scan was performed along the inter-atomic distances in TMC up to the 6.0 Å to ensure of lowest SCF solution was found. We report these Potential Energy Curves (PEC) in Figures 4.1 to 4.9 obtained with four DFT functionals considered. Available in literature MRCI curves were also plotted for comparison. In addition, each spin state of TMC was separately plotted for clarity.

We observe that M05-2x correctly predicts the main valance resonance structure on an average as per the naïve description ${}^+M \equiv C:^-$ of chemical bond. The curves can serve as a source of data for parameterization of empirical reaction force fields, such as REBO.³⁴ It is quite challenging to predict the ground spin state for transition metal carbides due to the presence of degenerate states very close in energy. Assuming the resonance valance bond (VB) structure ${}^+M \equiv C:^-$ and weak crystal field splitting, one would predict the spin state of

MC to have the same ground state multiplicity as M^{+4} cations. Several studies done in past are reporting more than one spin state as the ground state depending on the theoretical treatment. As pointed out by Tomonari and Tanaka⁵¹ TMC are very sensitive to theory level chosen and one need to be very careful to get the right description. Our results indicate doublet to be the ground state multiplicity of ScC with M05-2x, which is well in agreement with available *ab-initio* results.⁴⁶ There is no consensus on the ground state spin state of TiC in ab-initio calculation done in the past. On one hand Hack et. al.³⁹ reports triplet the lowest and singlet lying close in energy, on the other hand Tomonari and Tanaka⁵¹ found singlet to be the ground state. Our findings, with all DFT functionals used, display singlet to be the lowest spin state, which is in agreement with the DFT findings of Gutsev et.al.³⁶ and with simple VB description.

Several studied found the doublet to be the ground state of VC,^{39,42,52} while quartet is close in energy. Our results with various hybrid functional also vary, M05-2x favored quartet and BMK favored doublet, whereas Gutsev et. al. reported doublet to be the ground spin state in agreement with higher *ab-initio* calculations. Although CrC contains more than two low lying states, triplet is reported as the ground spin state in agreement with our BMK results. We faced convergence problems for triplet state with M05-2x for CrC, FeC and quartet for MnC. For MnC there is only one spin state reported in the literature (quartet), which is also predicted from VB arguments. Our BMK results for FeC shows quintet as the ground spin state, which is not in agreement with other studies. There is experimental data available for CoC and NiC, which states doublet and singlet to be the ground spin states of CoC and NiC respectively. M05-2x finds doublet to be the ground spin state for CoC in agreement with other *ab-initio* data, but gives triplet ground spin state for NiC, which may be due to the presence of low lying states as predicted by Mavridis et. al.⁵⁰ and Shim et. al.³⁸

Finally, the last system in $3d$ -TMC CuC found to possess quartet as ground spin state, similar to MnC with other states lie high in energy.

4.4 Small Nickel Cluster geometries and orbitals

To extend our study of transition metal diatomics described in chapter two and three, we explored geometrical and magnetic structure of small Nickel metal clusters $\text{Ni}_2 - \text{Ni}_5$. Here we report calculations for different spin multiplicities (singlet, triplet, quintet, septet, nonet, undectet and tridectet) of Ni_2 , Ni_3 , Ni_5 and several isomers of Ni_4 . We analyzed variations in geometry and binding energy as a function of spin state. BMK exchange-correlation functional is used throughout. It was validated on TMH and TMC diatomics in chapter three and four respectively.

The optimized geometries of small nickel clusters from Ni_2 - Ni_5 are reported in Table 4.3 This Table includes all possible spin multiplicity of small nickel clusters starting from the lowest on top to the highest, for Ni_2 on the left through Ni_5 on the right. We have investigated four lowest energy isomers of Ni_4 to analyze the structural changes and binding energy variation.

Ni diatomic:

One can see from Table 4.3 the bond length varies in Ni_2 from singlet through septet, where septet is found an unstable with respect to dissociation. We determined the ground electronic state for Ni_2 to be a Boltzman mixture of $^1\text{Ni}_2$ and $^3\text{Ni}_2$ with binding energies 1.99 eV and 1.98 eV respectively, where singlet is more stable by 0.01 eV over triplet, is in agreement with earlier experimental studies.^{12, 58-62} Our bond lengths for $^1\text{Ni}_2$ and $^3\text{Ni}_2$ (2.303 Å and 2.316 Å resp.) is longer than experimentally determined value⁶¹ of 2.155 Å and binding energies (1.99 eV and 1.98 eV resp.) are in fairly good agreement with

experimental value of 2.1 eV. There are several DFT studies done in past with LDA and GGA functionals^{63-68, 126} reported to produce better geometry, but not good energetics, on the other hand our calculations with hybrid functional BMK are suitable for investigating both geometry and energetics. One can notice the increase in bond length and decrease in binding energies with increase in multiplicity of the system, which forbids higher states due to easy bond breaking.

Ni triatomic:

We have determined the structure of Ni₃ in singlet, triplet, quintet, septet and nonet states in Table 4.3 We obtained different geometry for various multiplicities, where triplet and quintet have triangular geometry with three different sides, while septet and nonet are isosceles. Singlet converge to a bent geometry with one angle larger than 120°. We found two stable states triplet and septet to be similar in energy (3.01 eV and 3.09 eV resp) stronger than singlet, quintet and nonet. Structural studies of Ni₃ were always considered significant due to the existing controversy between theory and experiment. On one hand C_{2v} symmetry was found experimentally⁶⁸ with an apex angle more than 60°, while tight binding potential based MD⁶⁹ and EAM⁷⁰ simulations predicted it to be D_{3h} (equilateral triangle) symmetry. LDA studies⁶⁸ gave isosceles triangle type geometry. Arvizu et. al.⁶³ reported triplet to be the ground state for Ni₃ with isosceles geometry in their DFT study of five spin states for Ni₃. Although they have used different initial structures for Ni₃, their optimized geometry remains isosceles with all angles less than 90°, which is in agreement with our findings.

Ni tetraatomic:

We investigated various low lying isomers of Ni₄ in several spin states as reported in Table 4.3. There is not much experimental work done on small nickel clusters and we did not find any experimental data for Ni₄ to compare our results for ground state structure and

multiplicity. We performed full geometry optimization followed by stability analysis of different initial geometries (square planar, tetrahedral1, tetrahedral2 and rhombic) for Ni₄ in several spin states (singlet, triplet, quintet, septet, nonet, undectet and tridectet). We represent these structures with letter in bracket, Ni₄(s) is for square planar, Ni₄(t1) is for tetrahedral, Ni₄(t2) is for distorted tetrahedral and Ni₄(r) is for rhombic. We determined that rhombic (planar) structure is favored in the case of Ni₄ in all but one nonet state, where Ni₄(t1) and Ni₄(t2) are equally stable. We also found many of our other initial geometries (square planar ⁵Ni₄(s) and three dimensional tetrahedral ⁵Ni₄(t2)) converging to the stable rhombic (planar) type structure Ni₄(r). Our results differ from the one reported by Arvizu et. al.⁶³ and Petkov et. al.⁶⁷ in their DFT prediction of quintet Ni₄(t1) as the ground state structure. In another study done in past by Reuse et al.⁶⁵ the authors point out the importance of John-Teller distortion in predicting the right structure. They argued that for Ni configuration of d^8s^1 , One can ignore *d*- electrons and consider *s*- only contribution. The square with 4 valent electrons will undergo distortion into the rhombus structure observed in our study. Nygren et. al.⁷¹ also found planar D_{2h} to be the lowest energy isomer of all five isomers they tested. One can see from Table 4.3 that higher spin states are unstable for Ni₄ isomers and undectet is very loosely bound with binding energy 4 times smaller than the lower spin states.

Nipentatomic:

We investigated only one lowest energy isomer of Ni₅, reported in earlier studies (both experimental and theoretical^{60, 63-66}) to have bipyramidal geometry. Several spin states (reported in Table 4.3) on optimization leads to a symmetric conformation (D_{3h}) in all cases except in case of undectet where we found no convergence. We determined ⁷Ni₅ as the

ground state structure, whereas $^1\text{Ni}_5$ and $^5\text{Ni}_5$ lie very close in energy, which is common in transition metal clusters. The primary factor contributing to this multitude character of states is participation of both s - and d - orbitals in bonding. Michelini et. al. reported existence of two stable quasi-degenerate isomers; septet (C_{4v} symmetry) and quintet (D_{3h} symmetry) for Ni_5 . Their study is supported by the recent⁶³ investigations of five different topologies of Ni_5 cluster obtained with VWN (LDA) calculations, all converging to three dimensional structures, quintet state of bipyramidal being the lowest followed by the pyramidal structure with septet spin state. They found inversion of states with GGA functionals, where pyramidal structure in septet state is the ground state. None of our Ni_5 spin state converged to pyramidal geometry, which is probably the result caused by the limited number of initial geometry tested.

Table 4.4 displays the molecular orbitals of all the spin states (singlet, triplet, quintet, septet and nonet) of Ni_5 as studied here. One can see from the orbitals they are distributed as antibonding (p orbitals) on top as unoccupied, non-bonding (lone pairs, d orbitals) largely distributed and goes until very near to the core followed by bonding s type orbital present next to the core. Table 4.4 also shows the geometry of relative spin state on the top of the table along with their binding energy. Only one out of nearly degenerate set of orbitals remains unoccupied in the singlet state, which explains why triplet state of Ni_5 is most stable multiplicity in agreement with the observed energetics.

4.5 Conclusions

We investigated two new hybrid meta-GGA functionals M05 and M05-2x besides using TPSS and BMK to compare their performance with WFT methods and experimental data, where available, to study carbides formed by $3d$ -transition metals (Sc-Cu). We have

described the energetics and geometry of various spin states of these metal carbides. We found M05-2x performance (dissociation energies and bond lengths) to be the best of all four DFT functionals used, confirming our conclusion of chapter 3, (more the HF exchange better the performance) in case of systems involving *3d*-transition metals. We found significant change in dissociation energies and bond lengths, when Scalar relativistic effects are taken into account with Douglas-Kroll approximation,¹³⁴ but the lack of experimental data limited our discussion here. We determine the VB description of electronic structure is followed in our description of metal carbides as predicted by M05-2x correctly.

Comparing our studies of metal hydrides (chapter3) and metal carbides here we found BMK to be a satisfactory DFT functional to study the transition metal systems. We determined the energetics and geometry of small Ni clusters with BMK to extend our work to larger systems. We found agreement in description of ground states for small clusters Ni₂, Ni₃, Ni₅ and several isomers of Ni₄, in all possible spin states, compared to experimental and WFT results.

Table 4.1 Dissociation energies (kcal/mol) of neutral carbides (TMC) with various DFT functionals compared with ab-initio results and experimental data (where available).

| | ScC | | TiC | | VC | | CrC | | | MnC | | FeC | | | CoC | | | NiC | | CuC |
|--------------------------|-------------------|-------------------|-------------------|-------------------|-------------------|-------|-------------------|-------------------|-------------------|-------------------|-------------------|--------------------|-------------------|-------------------|-------------------|-------------------|-------------------|------|-------------------|-----|
| Multiplicity | 2 | 4 | 1 | 3 | 2 | 4 | 3 | 5 | 7 | 4 | 3 | 5 | 2 | 4 | 6 | 1 | 3 | 4 | | |
| BMK | 59.3 | | 114.5 | 88.6 | 82.6 | 58.7 | 75.6 | 80.0 | 51.0 | 57.9 | | 50.1 | 32.5 | 37.4 | 42.1 | | | | 42.9 | |
| M05 | 78.8 | 72.4 | 125.1 | 96.7 | 123.5 | 85.5 | 81.4 | 60.3 | 47.4 | 62.0 | 78.8 | 91.1 | 85.9 | 82.0 | 63.9 | 95.6 | 72.6 | | 47.2 | |
| M05-2x | 66.1 | 29.0 | 150.2 | 60.9 | 69.9 | 103.3 | | 49.8 | 48.8 | | | 72.5 | 57.0 | | 44.4 | 64.7 | 83.3 | | 39.2 | |
| TPSS | 86.8 | 88.1 | 119.4 | 104.5 | | 99.3 | | 73.5 | 54.8 | 100.0 | 112.8 | 103.1 | 101.8 | | | | | 96.5 | | |
| BMK:DKH | 56.9 | 64.2 | 112.2 | 148.9 | 81.6 | 81.4 | 76.8 | 53.8 | | 56.6 | | 48.8 | | 41.6 | 36.0 | 129.0 | | | 47.0 | |
| M05:DKH | 76.2 | 71.2 | 121.3 | 93.4 | 126.2 | 88.6 | 82.7 | 63.2 | 26.0 | | 79.5 | 94.6 | | 83.7 | 59.6 | 119.8 | 75.5 | | 51.5 | |
| M05-2x:DKH | 63.6 | 26.4 | 146.5 | 57.5 | 102.2 | 105.7 | | 52.0 | 60.6 | | 232.8 | 76.8 | | | 38.9 | 62.9 | 90.7 | | 42.1 | |
| TPSS:DKH | | | 116.9 | 105.2 | | | 204.2 | 322.7 | 173.6 | 98.6 | | 359.4 | | 103.3 | 61.1 | 118.4 | 99.2 | | | |
| B3LYP^a | 69.6 | | 94.5 | | 85.8 | | 64.6 | | | 70.8 | 87.2 | | 71.7 | | | 70.6 | | | 47.0 | |
| BLYP^a | 85.8 | | 106.5 | | 106.1 | | 87.6 | | | 101.0 | 110.7 | | 104.5 | | | 101.7 | | | 59.7 | |
| MRCI^a | 57.2 | | 60.2 | | 66.4 | | 89.0 | | | | 63.9 | | | | | 62.3 | | | | |
| MRCI-Other | 57.1 ^a | 65.5 ^b | 61.3 ^c | 65.0 ^c | 67.3 ^d | | 69.2 ^e | 46.1 ^e | 35.5 ^e | 60.9 ^f | 50.0 ^g | 103.5 ^g | 80.4 ^h | 62.0 ^h | 35.0 ^h | 68.7 ⁱ | 46.4 ⁱ | | 41.0 ^j | |
| Exp | | | | | | | | | | | 89.9 ^k | | | | | 77.0 ^k | | | | |

(a)-Ref 36, (b)-Ref 49, (c)-Ref 54, (d)-Ref 44, (e)-Ref 45, (f)-Ref 46, (g)-Ref 51, (h)-Ref 52, (i)-Ref 53, (j)-Ref 47, (k)-Ref 57

Table 4.2 Equilibrium bond lengths (Å) of neutral carbides (TMC) with various DFT functionals compared with ab-initio results and experimental data (where available).

| | ScC | | TiC | | VC | | CrC | | MnC | | FeC | | CoC | | | NiC | | CuC |
|--------------------------|--------------------|--------------------|--------------------|--------------------|--------------------|-------|--------------------|--------------------|--------------------|--------------------|--------------------|--------------------|--------------------|--------------------|--------------------|--------------------|--------------------|--------------------|
| Multiplicity | 2 | 4 | 1 | 3 | 2 | 4 | 3 | 5 | 7 | 4 | 3 | 5 | 2 | 4 | 6 | 1 | 3 | 4 |
| BMK | 1.743 | 1.868 | 1.639 | 1.655 | 1.538 | 1.656 | 1.720 | 1.715 | 1.951 | 1.826 | | 1.722 | 1.495 | 1.697 | 1.896 | 1.603 | | 1.870 |
| M05 | 1.744 | 1.866 | 1.580 | 1.680 | 1.535 | 1.636 | 1.677 | 1.682 | 1.935 | 1.720 | 1.701 | 1.621 | 1.521 | 1.626 | 1.762 | 1.626 | 1.673 | 1.856 |
| M05-2x | 1.724 | 1.935 | 1.558 | 1.665 | 1.517 | 1.668 | | 1.816 | 2.007 | | 1.825 | 1.613 | 1.586 | | 1.799 | 1.597 | 1.625 | 1.937 |
| TPSS | 1.765 | 1.884 | 1.648 | 1.681 | 1.604 | 1.654 | 1.601 | 1.663 | 1.897 | 1.617 | 1.568 | 1.640 | 1.538 | 1.626 | 1.811 | 1.628 | 1.632 | 1.819 |
| BMK:DKH | 1.746 | 1.868 | 1.630 | 1.655 | 1.539 | 1.657 | 1.708 | 1.699 | | 1.818 | 1.771 | 1.715 | | 1.681 | 1.858 | 1.586 | | 1.839 |
| M05:DKH | 1.749 | 1.866 | 1.585 | 1.683 | 1.536 | 1.634 | 1.671 | 1.670 | 1.861 | 1.715 | 1.690 | 1.614 | | 1.616 | 1.744 | 1.610 | 1.655 | 1.827 |
| M05-2x:DKH | 1.728 | 1.936 | 1.560 | 1.668 | 1.518 | 1.657 | | 1.793 | 1.919 | | 1.804 | 1.600 | | | 1.771 | 1.574 | 1.605 | 1.899 |
| TPSS:DKH | 1.767 | 1.883 | 1.656 | 1.676 | 1.606 | 1.652 | 1.601 | 1.657 | 1.883 | 1.615 | 1.564 | 1.633 | | 1.616 | 1.789 | 1.613 | 1.619 | 1.791 |
| B3LYP^a | 1.753 | | 1.609 | 1.668 | 1.587 | | 1.636 | | | 1.699 | 1.621 | | 1.527 | | | 1.621 | | 1.843 |
| BLYP^a | 1.779 | | 1.651 | | 1.612 | | 1.602 | | | 1.608 | 1.574 | | 1.552 | | | 1.640 | | 1.811 |
| MRCI^a | 1.823 | | 1.790 | | 1.645 | | 1.676 | | | | 1.585 | | | | | 1.631 | | |
| MRCI-Other | 1.823 ^a | 1.889 ^b | 1.790 ^c | 1.733 ^c | 1.645 ^d | | 1.676 ^e | 1.756 ^e | 1.958 ^e | 1.702 ^f | 1.659 ^g | 1.618 ^g | 1.548 ^h | 1.641 ^h | 1.953 ^h | 1.627 ⁱ | 1.620 ⁱ | 1.848 ⁱ |
| Exp | | | | | | | | | | | 1.596 ^k | | 1.561 ^k | | | 1.631 ^k | | |

(a)-Ref 36, (b)-Ref 49, (c)-Ref 54, (d)-Ref 44, (e)-Ref 45, (f)-Ref 46, (g)-Ref 51, (h)-Ref 52, (i)-Ref 53, (j)-Ref 47, (k)-Ref 57

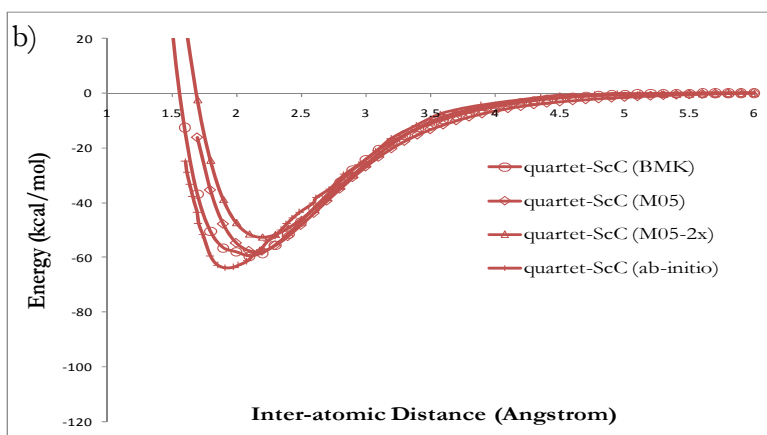
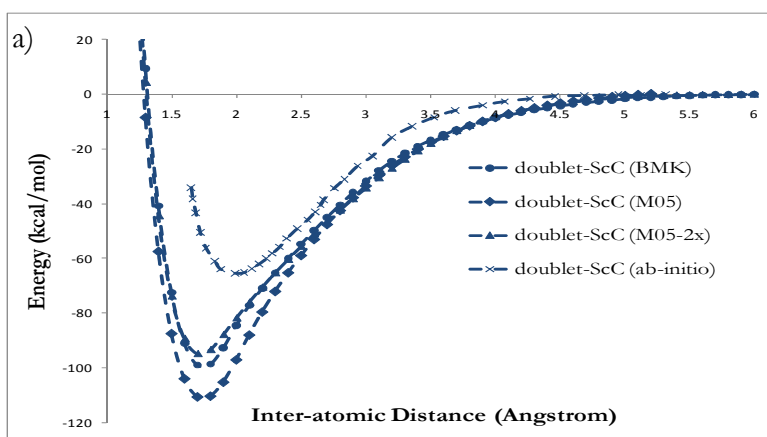
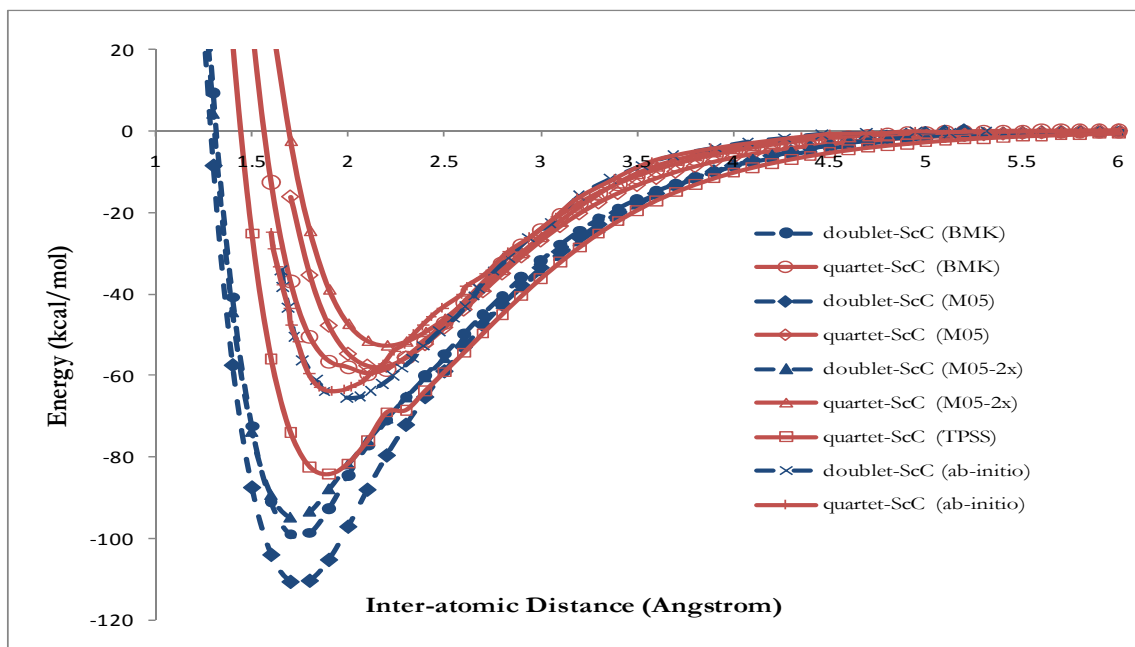


Figure 4.1 Potential Energy Curves of ScC in doublet and quartet spin state, calculated by non-relativistic TPSS, BMK, M05, M05-2x and WFT methods. a) ^2ScC plot with all methods, b) ^4ScC plot with all methods.

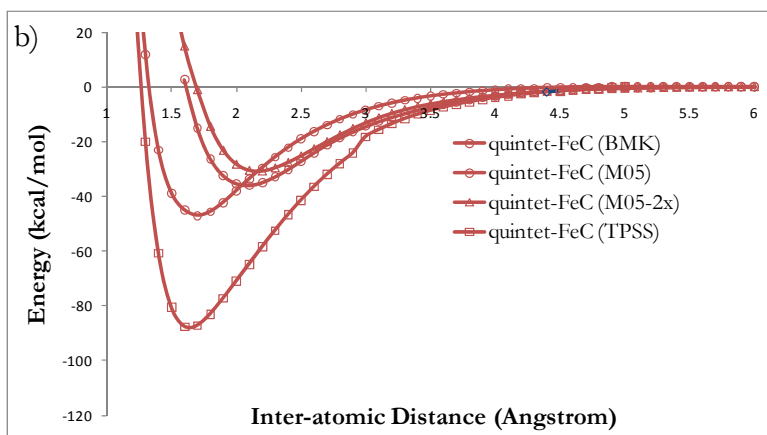
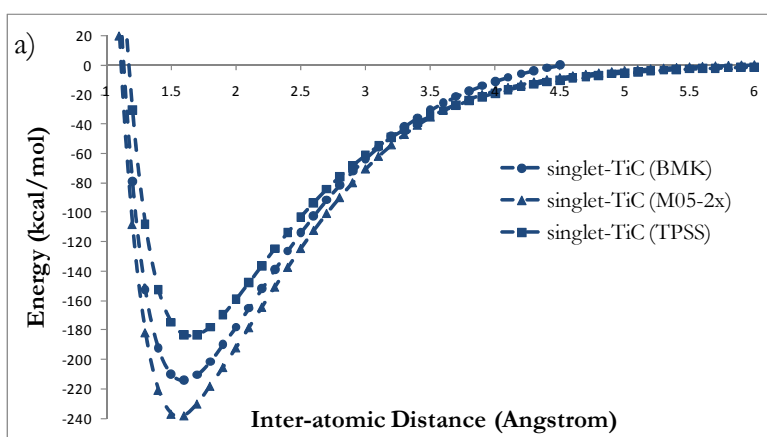
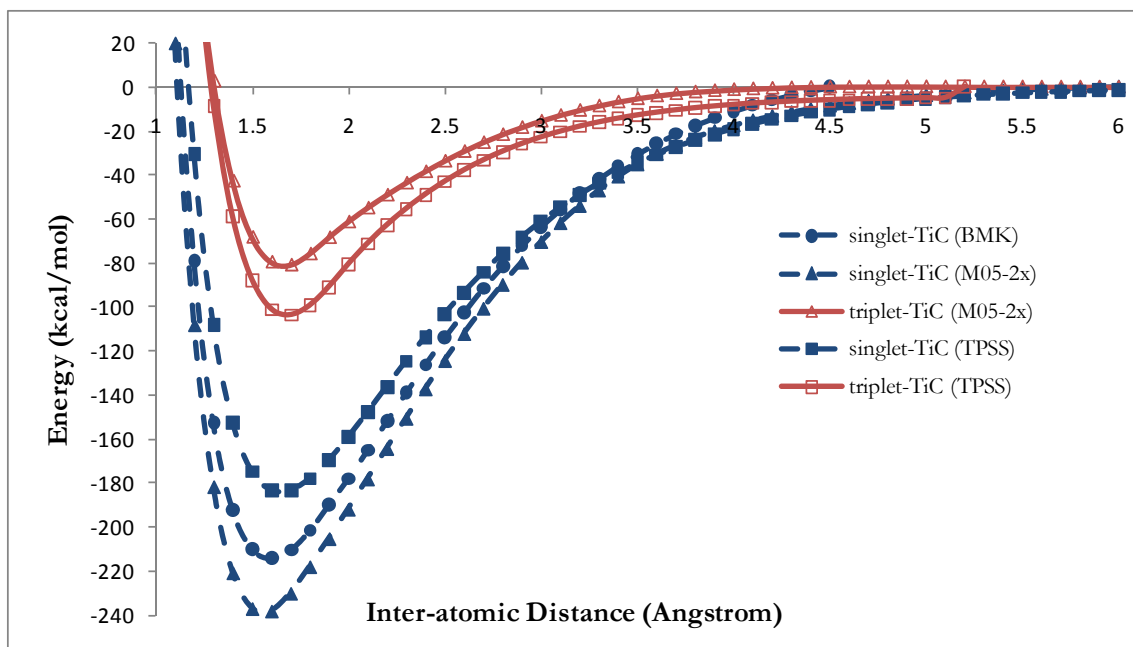


Figure 4.2 Potential Energy Curves of TiC in singlet and triplet spin state, calculated by non-relativistic TPSS, BMK and M05-2x methods. a) ^1TiC plot with all methods, b) ^3TiC plot with all methods.

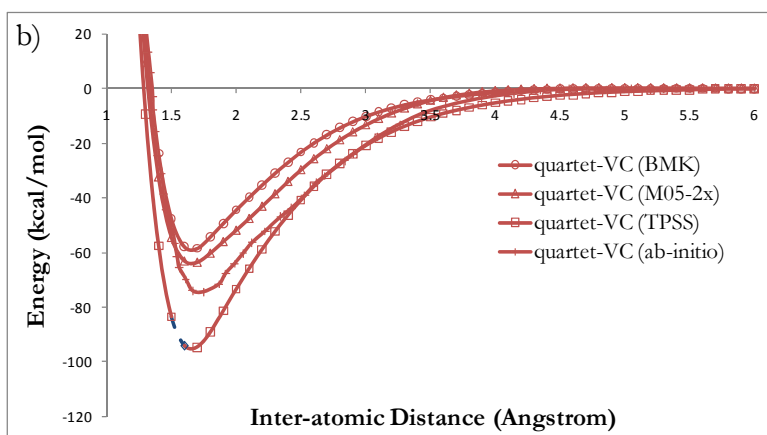
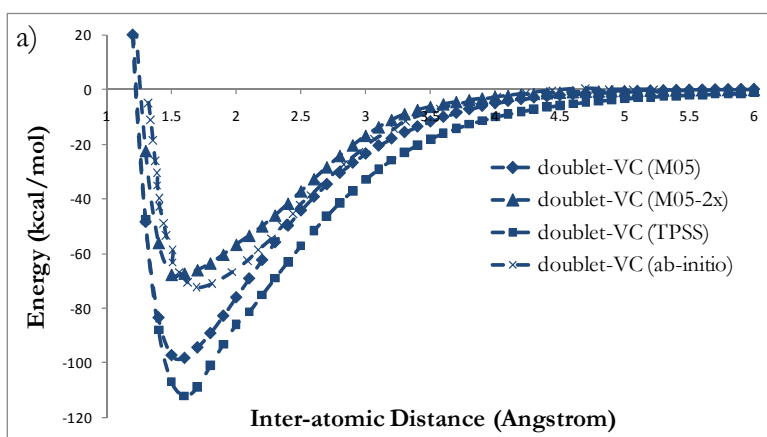
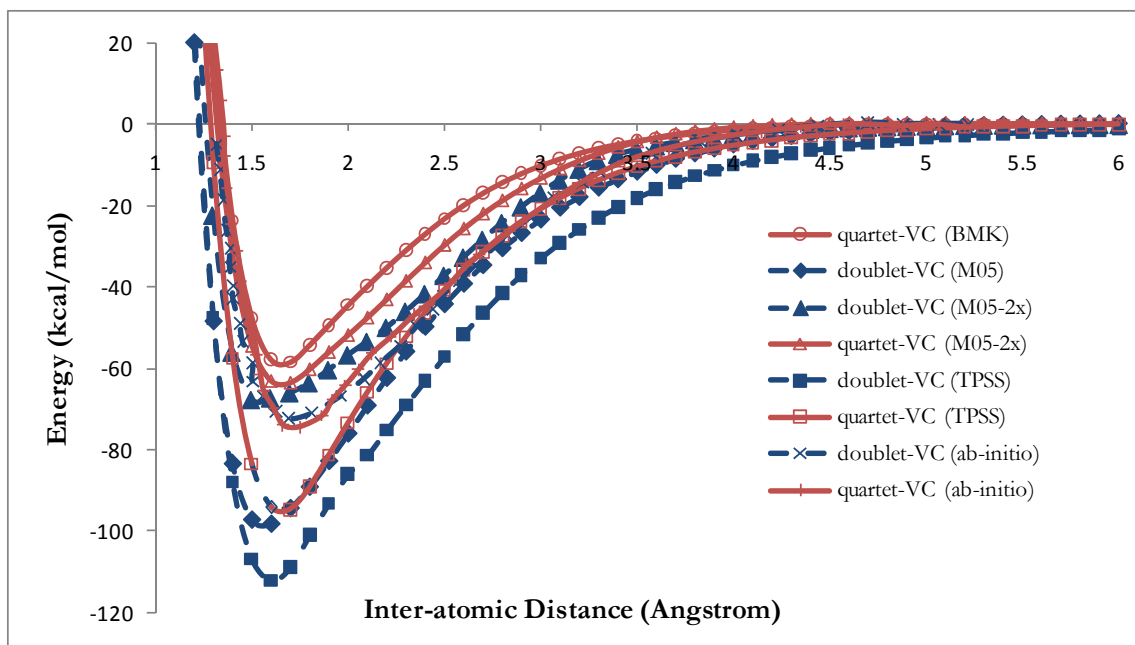


Figure 4.3 Potential Energy Curves of VC in doublet and quartet spin state, calculated by non-relativistic TPSS, BMK, M05, M05-2x and WFT methods. a) ^2VC plot with all methods, b) ^4VC plot with all methods.

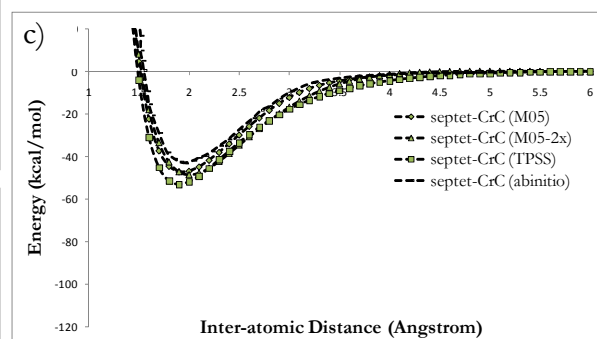
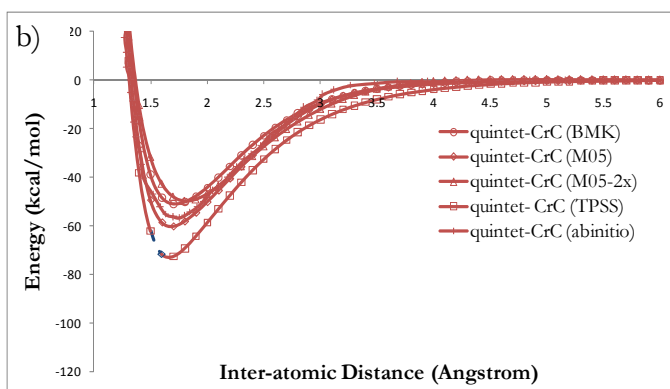
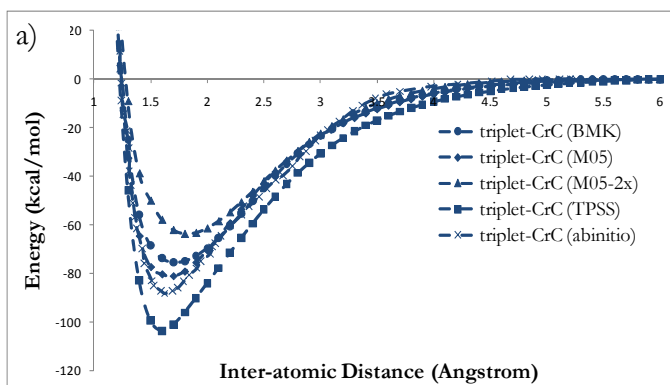
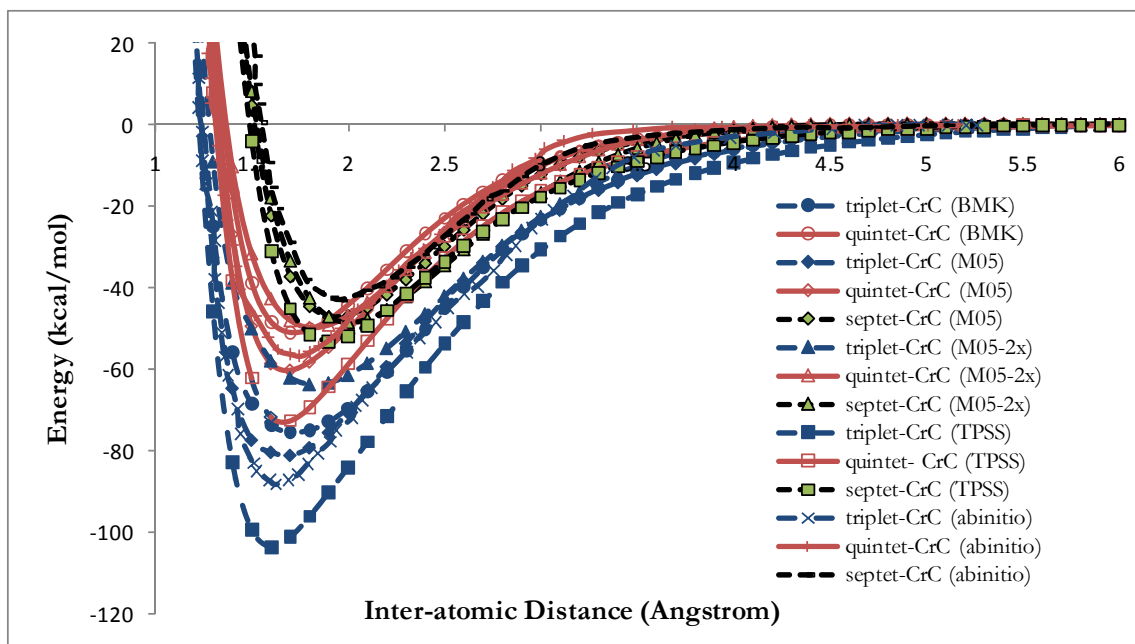


Figure 4.4 Potential Energy Curves of CrC in singlet, quintet and septet spin state, calculated by non-relativistic TPSS, BMK, M05, M05-2x and WFT methods. a) ^3CrC plot with all methods, b) ^5CrC plot with all methods, c) ^7CrC plot with all methods.

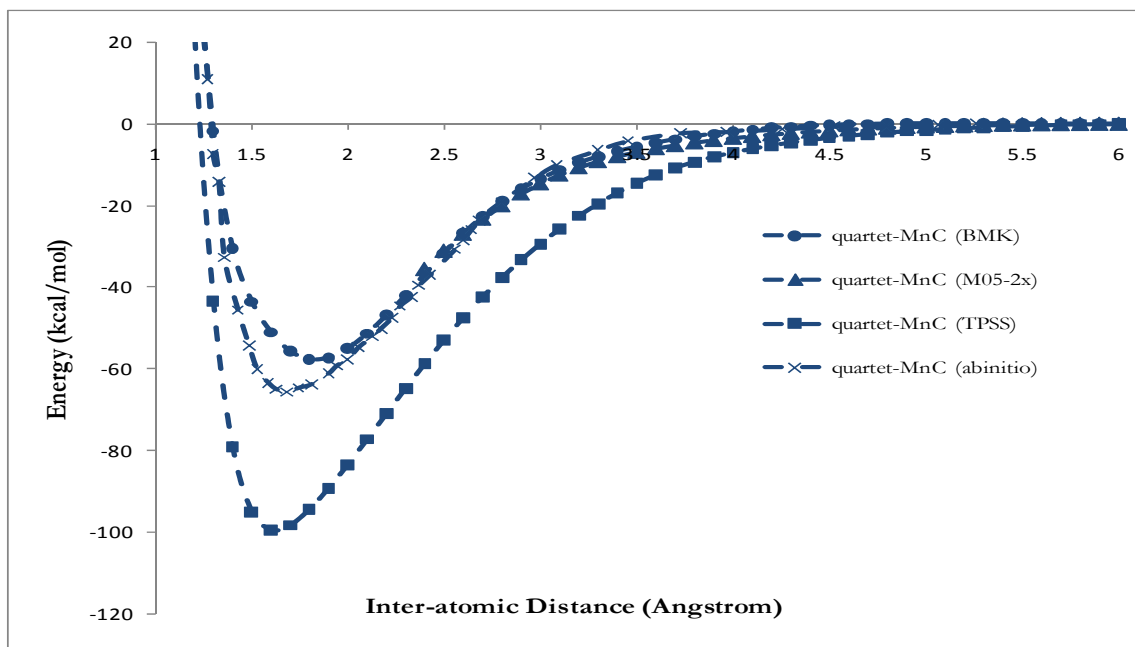


Figure 4.5 Potential Energy Curves of MnC in quartet spin state, calculated by non-relativistic TPSS, BMK, M05-2x and WFT methods.

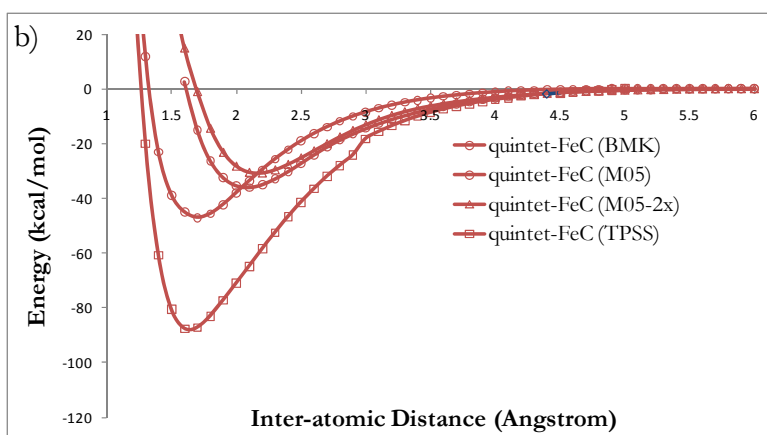
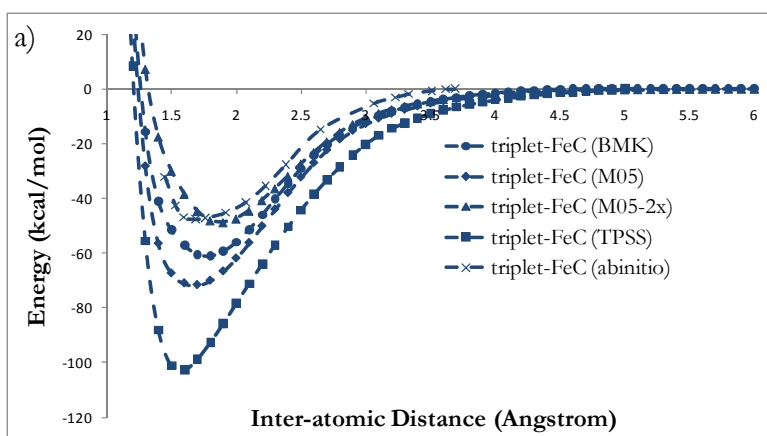
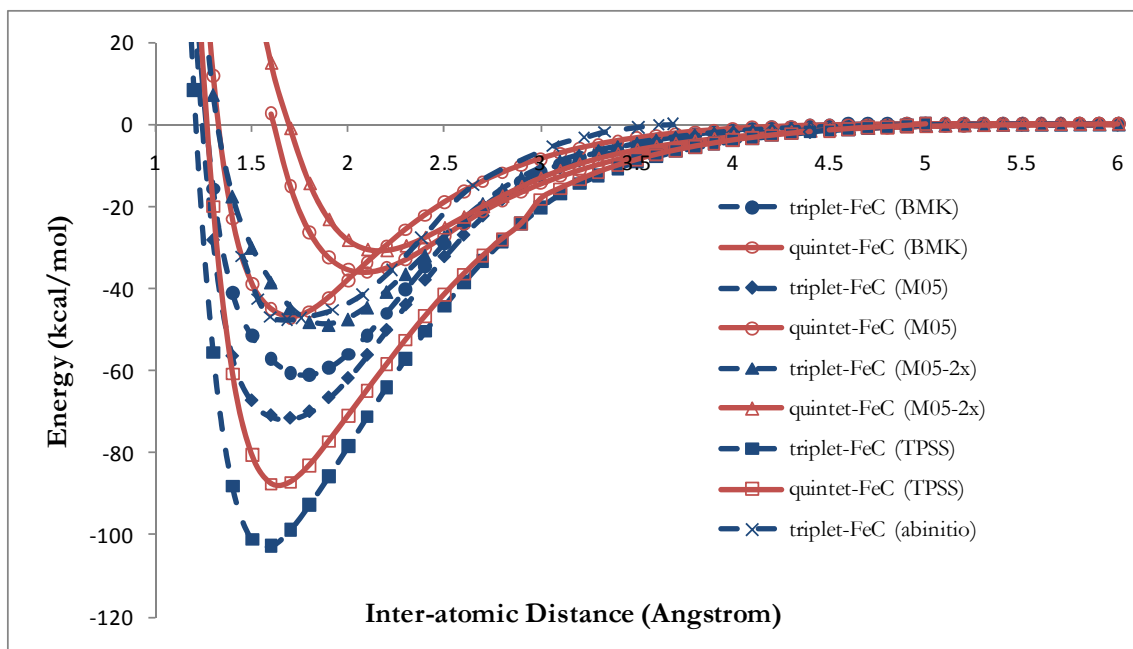


Figure 4.6 Potential Energy Curves of FeC in triplet and quintet spin state, calculated by non-relativistic TPSS, BMK, M05, M05-2x and WFT methods. a) ^3FeC plot with all methods, b) ^5FeC plot with all methods.

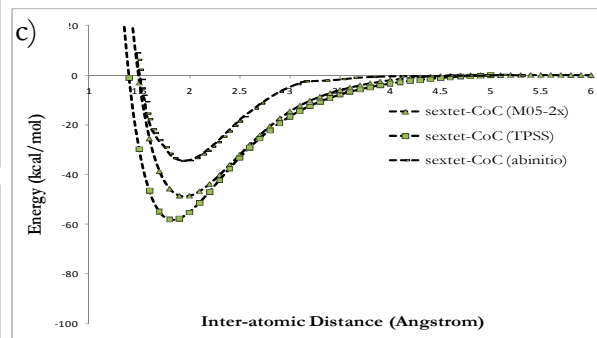
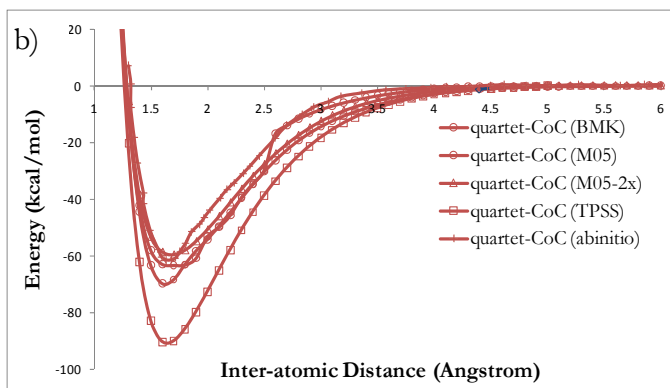
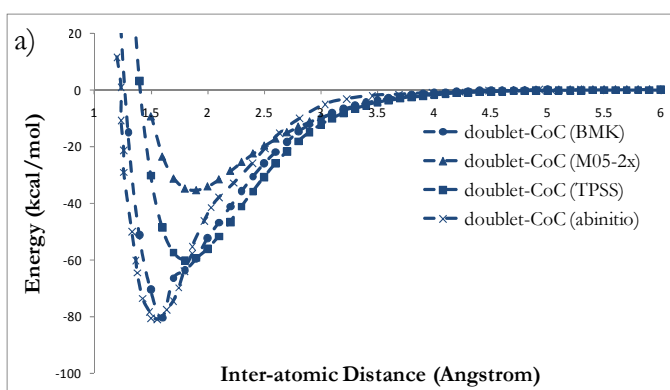
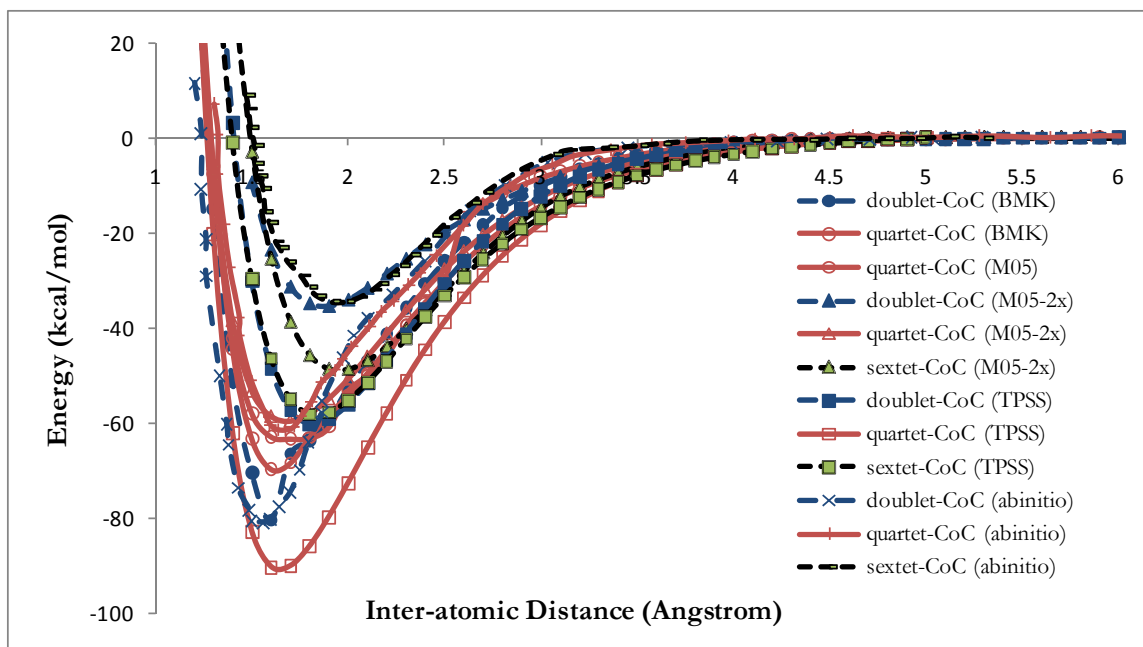


Figure 4.7 Potential Energy Curves of CoC in doublet, quartet and sextet spin state, calculated by non-relativistic TPSS, BMK, M05, M05-2x and WFT methods. a) ^2CoC plot with all methods, b) ^4CoC plot with all methods, c) ^6CoC plot with all methods.

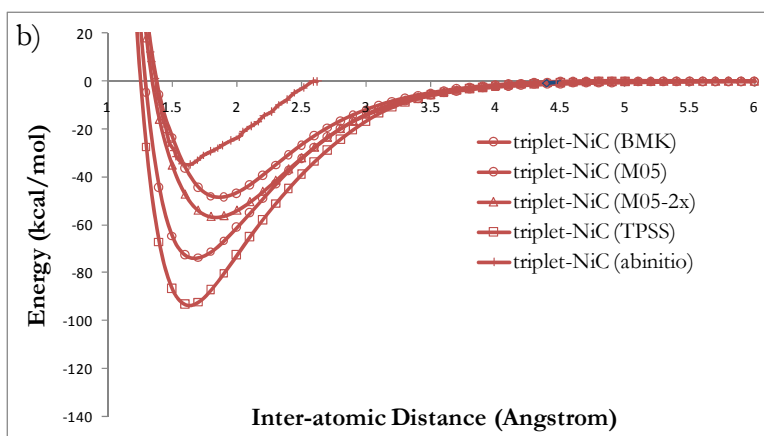
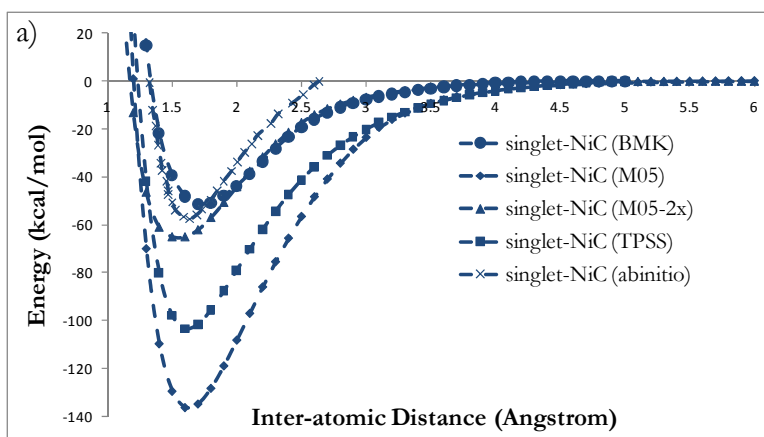
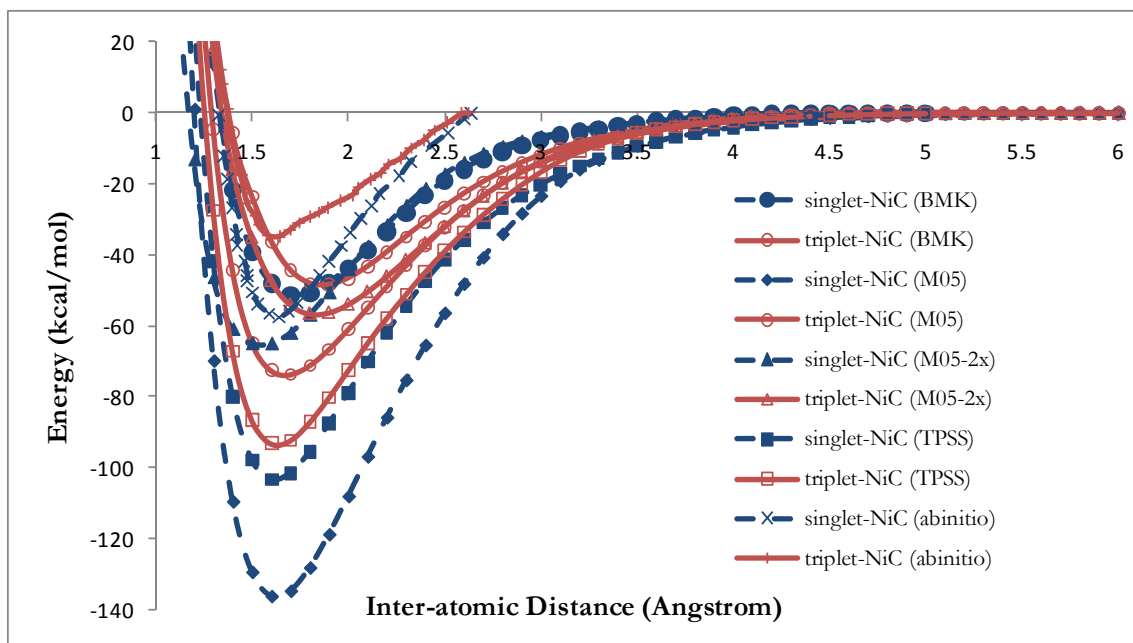


Figure 4.8 Potential Energy Curves of NiC in singlet, triplet spin state, calculated by non-relativistic TPSS, BMK, M05, M05-2x and WFT methods. a) ^1NiC plot with all methods, b) ^3NiC plot with all methods.

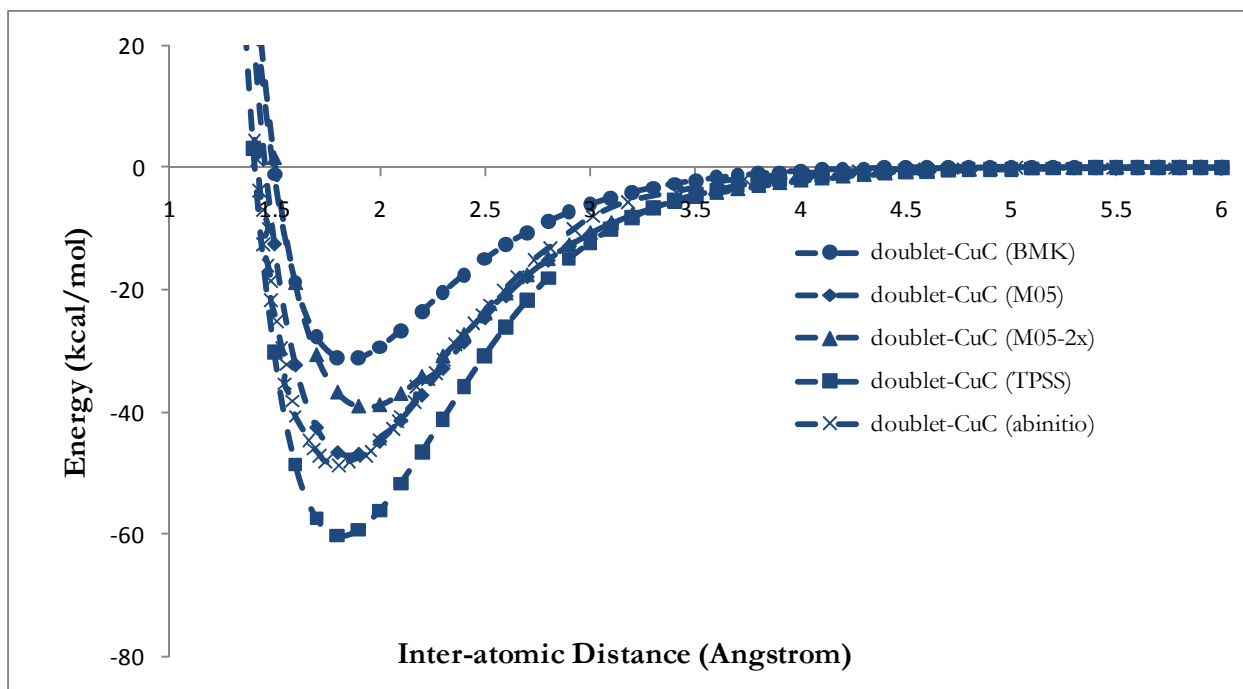



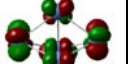
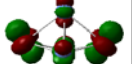
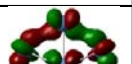
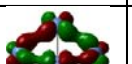
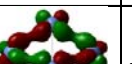

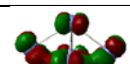
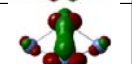
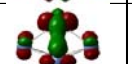
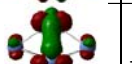
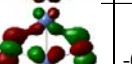





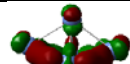




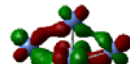
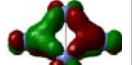

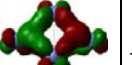


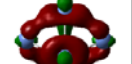



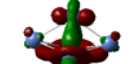


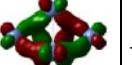
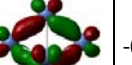
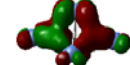




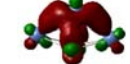

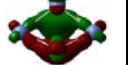




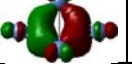
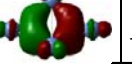
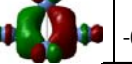
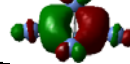
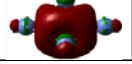
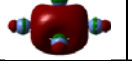
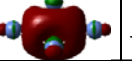
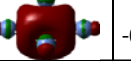
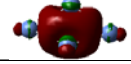
Figure 4.9 Potential Energy Curves of CuC in quartet, calculated by non-relativistic TPSS, BMK, M05, M05-2x and WFT methods.

Table 4.3 Geometries of Ni₂, Ni₃, Ni₅ and four isomers of Ni₄ with several spin states (singlet, triplet, quintet, septet, nonet, undectet, duodectet and tridectet) with their bondlengths (Å) and binding energy (kcal/mol) displayed on each structure.

| M | Ni ₂ | Ni ₃ | Ni ₄ (d) | Ni ₄ (T1) | Ni ₄ (T2) | Ni ₄ | Ni ₅ |
|----|-----------------|-----------------|---------------------|----------------------|----------------------|-----------------|-----------------|
| 1 | 1.99 | 2.92 | 0.21 | 4.48 | 4.50 | 5.42 | 7.17 |
| 3 | 1.98 | 3.01 | 4.37 | 4.48 | 4.49 | 5.43 | 6.37 |
| 5 | 0.95 | 2.56 | 5.43 | 4.57 | 4.61 | 4.76 | 7.17 |
| 7 | -1.72 | 3.09 | 4.53 | 4.59 | 4.61 | 4.84 | 7.25 |
| 9 | | 2.31 | 2.84 | 3.80 | 3.80 | 3.05 | 6.74 |
| 11 | | | | 0.95 | 1.02 | 1.02 | 6.74 |
| 13 | | | | -1.77 | -1.39 | -1.39 | |

Table 4.4 Molecular orbitals of all stable spin states (singlet, triplet, quintet, septet and nonet) of Ni₅ tabulated as per their distribution antibonding (*p* orbitals) on top as unoccupied, non-bonding (lone pairs, *d* orbitals) and bonding *s* orbitals the last.

| Ni ₅ _09 7.17 | | Ni ₅ _07 6.37 | | Ni ₅ _05 7.17 | | Ni ₅ _03 7.25 | | Ni ₅ _01 6.74 | |
|-----------------------------|--|-----------------------------|---|-----------------------------|---|-----------------------------|---|-----------------------------|---|
| | | | | | | | | | |
| L+4/79 -0.060 | | - | - | - | - | - | - | - | - |
| L+3/78 -0.077 | | L+4/78 -0.075 | | - | - | - | - | - | - |
| L+2/77 -0.085 | | L+3/77 -0.088 | | L+4/77 -0.085 | | - | - | - | - |
| L+1/76 -0.087 | | L+2/76 -0.088 | | L+3/76 -0.085 | | L+4/76 -0.087 | | - | - |
| L/75 -0.116 | | L+1/75 -0.117 | | L+2/75 -0.119 | | L+3/75 -0.112 | | L+4/75 -0.118 | |
| S/74 -0.176 | | L/74 -0.170 | | L+1/74 -0.172 | | L+2/74 -0.181 | | L+3/74 -0.171 | |
| S-1/73 -0.183 | | S/73 -0.187 | | L/73 -0.183 | | L+1/73 -0.183 | | L+2/73 -0.185 | |
| S-2/72 -0.215 | | S-1/72 -0.215 | | S/72 -0.218 | | L/72 -0.210 | | L+1/72 -0.216 | |
| S-3/71 -0.250 | | S-2/71 -0.248 | | S-1/71 -0.249 | | S/71 -0.252 | | L/71 -0.248 | |
| S-4/70 -0.252 | | S-3/70 -0.250 | | S-2/70 -0.250 | | S-1/70 -0.252 | | H/70 -0.250 | |
| S-5/69 -0.255 | | S-4/69 -0.253 | | S-3/69 -0.255 | | H/69 -0.252 | | H-1/69 -0.253 | |
| S-6/68 -0.255 | | S-5/68 -0.255 | | H/68 -0.255 | | H-1/68 -0.253 | | H-2/68 -0.255 | |
| S-7/67 -0.255 | | H/67 -0.258 | | H-1/67 -0.257 | | H-2/67 -0.259 | | H-3/67 -0.257 | |
| H/66 -0.258 | | H-1/66 -0.259 | | H-2/66 -0.260 | | H-3/66 -0.261 | | - | - |
| H-1/65 -0.261 | | H-2/65 -0.261 | | H-3/65 -0.262 | | - | - | - | - |

| | | | | | | | | | |
|------------------|---|------------------|---|--------------|---|--------------|---|--------------|---|
| H-2/64 -0.264 |  | H-3/64 -0.262 |  | - | - | - | - | - | - |
| H-3/63 -0.266 |  | - | - | - | - | - | - | - | - |
| - | - | - | - | - | - | - | - | - | - |
| - | - | - | - | - | - | - | - | - | - |
| 56 -0.289 |  | 56 -0.285 |  | 56 -0.284 |  | 56 -0.288 |  | 56 -0.285 |  |
| 55 -0.294 |  | 55 -0.289 |  | 55 -0.293 |  | 55 -0.289 |  | 55 -0.290 |  |
| 54 -0.298 |  | 54 -0.300 |  | 54 -0.302 |  | 54 -0.301 |  | 54 -0.300 |  |
| 53 -0.308 |  | 53 -0.300 |  | 53 -0.304 |  | 53 -0.302 |  | 53 -0.301 |  |
| 52 -0.310 |  | 52 -0.304 |  | 52 -0.304 |  | 52 -0.309 |  | 52 -0.304 |  |
| 51 -0.314 |  | 51 -0.310 |  | 51 -0.314 |  | 51 -0.313 |  | 51 -0.310 |  |
| 50 -0.314 |  | 50 -0.316 |  | 50 -0.316 |  | 50 -0.314 |  | 50 -0.315 |  |
| 49 -0.324 |  | 49 -0.319 |  | 49 -0.321 |  | 49 -0.325 |  | 49 -0.319 |  |
| 48 -0.330 |  | 48 -0.334 |  | 48 -0.333 |  | 48 -0.326 |  | 48 -0.333 |  |
| 47 -0.357 |  | 47 -0.355 |  | 47 -0.360 |  | 47 -0.347 |  | 47 -0.356 |  |
| 46 -0.436 |  | 46 -0.431 |  | 46 -0.436 |  | 46 -0.434 |  | 46 -0.432 |  |

CHAPTER 5: SMALL GOLD CLUSTERS WITH AND WITHOUT LIGANDS

We carried a systematic study of ligand binding in small gold clusters with and without solvent. We considered several low energy isomers of four gold clusters (Au_2 , Au_4 , Au_6 and Au_8) and phosphine ligand to describe the ligand effect on geometry and energetics of these clusters. For the practical purposes, an acceptable model quantum chemistry should provide reasonable accuracy to infer significant physical trends and to enable comparison of computational results with experimental data; at the same time, the related numerical cost should be low to allow scaling to larger systems. Thus, we performed a benchmark study to explore the effect of different basis sets and DFT functionals on the geometries and electronic properties of small gold clusters (Au_2 and Au_4) in the presence of several ligands (NH_3 , NMe_3 , PH_3 , and PMe_3). Analysis of results from different methodologies leads to understanding of the underlying physical phenomena defining cluster geometry and chemical stability, and allows singling out low-cost computational approaches applicable to larger systems. We choose LANL2DZ ECP basis set to describe the effect of one-by-one attachment of phosphine ligand on geometry and energetic of small gold nanoclusters (Au_2 , Au_4 , Au_6 and Au_8), due to its low computational cost and ability to produce trends in same type of ligand, while testing five different generations of DFT functionals.

In this chapter we study the importance of these factors for realistic simulations, and resolve dilemma about 2D \rightarrow 3D geometry transition in the lowest energy isomers of small gold clusters. The only study¹⁰⁴ considering the effect of anions on binding energy of small gold clusters including one of the isomer of Au_6 establish that binding energy doesn't vary much beyond Au_2 for clusters $\leq \text{Au}_{20}$. In the contrast, we observed significant variation in the binding energy of small clusters when we go from Au_2 to Au_8 . Analysis of results from

different gold chemistry is strongly influenced by relativistic effects arising due to its tendency to form close metal-metal interaction. These effects play major role in gold binding as compared to other atoms in the same group.¹⁰⁰ We have considered both scalar relativistic effects (including ZORA), and Spin-Orbit coupling and found negligible effect on small gold clusters energetics.

5.1 Benchmark study of Au₂ and Au₄ in presence of different ligands with several basis sets and DFT functionals

Representative geometries of ligated Au₂ and Au₄ clusters are shown in Figure 5.1. We consider butterfly (rhombus) geometry of the Au₄ cluster, previously found to be the lowest energy isomer.²²⁶ Four types of ligand molecules (NH₃, NMe₃, PH₃, and PMe₃) model ligands used in an experiment, have been employed to construct three types of ligated clusters (12 molecules total): Au₂L₂ (e.g., Figure 5.1a), Au₄L₂ (e.g., Figure 5.1b), and Au₄L₄ (e.g., Figure 5.1c).

We start the discussion of computational results with ligand binding energy which is a critical quantity showing ligand ability to stabilize a metal cluster. The magnitude of the binding energy has been determined as a difference between energies of optimal structures of bound compound and its respective components that is free ligand molecules and a bare gold cluster, normalized by the number of ligands in the ligated cluster. Figure 5.2 shows dependence of the ligand binding energy on the DFT model calculated using TZVP basis set. Despite the different origin of five DFT functionals used in our study, the results produced by four of these functionals (with the exception of LSDA) are consistent and in a close agreement between each other. Particularly, the binding energies calculated with three functionals (GGA, meta-GGA and LC-hybrid) are within 2-3 kcal/mol for all clusters

(Figure 5.2). As expected, the LSDA model consistently overestimated the binding energies by about 15 kcal/mol (50-70%) compared to all other models. This is a typical case for many molecular systems, when more advanced exchange-correlation functional models (such as GGA or meta-GGA) produce much more accurate results when compared with experimental data.²²⁷ For reference, Table 5.1 provides comparison of the bond lengths and dissociation energies of the bare Au₂ dimer using various functionals. Indeed, the LSDA produces the best match to the experimental⁵⁷ bond length of Au₂ (2.47Å), but significantly overestimates the dimer's binding energy. From Figure 5.2 we also observe that B3LYP slightly underestimates the metal-ligand binding energies by ~4-5 kcal/mol in all molecules. Overall we conclude that the ligand binding energy is not overly sensitive to the choice of functional, and the modern DFT models proven reliable for other molecular systems^{125, 228}, are able to provide stable and consistent trends in all clusters considered.

Figure 5.3 shows dependence of the ligand binding energy on the basis set size calculated using TPSS functional. It is apparent that the basis set plays a key role in determining correct energetic trends for ligand binding energies, regardless of the cluster type. Large basis sets (TZVP and QZVP) result in essentially identical ligand binding energies (within 1.5 kcal/mol in all cases). Subsequently, TZVP and QZVP basis sets can be used as reference methods for evaluation of the other three basis sets. We notice that the relative binding strength of amines versus phosphines changes significantly with the change in the basis set flexibility. From all three sets of data in Figure 5.3, it appears that the lack of polarization in the basis set artificially increases the bonding strength of amine ligands and weakens the bonding of phosphines. The lack of adequate description of polarization effects leads to the underestimation of phosphorous nucleophilicity, thereby lowering the strength of its interaction with gold. At the same time, it leads to artificially high energy of $\sigma^*(\text{Au-N})$

antibond, it's lower occupancy and, consequently, increased bonding of amines with gold. As a result, the least expensive LANL2DZ basis set lacking polarization functions fails to reproduce the relative binding strength of amines versus phosphines. Even adding a single polarization function for each element (LANL2DZ-P) allows to correct the trend. Notably, all small basis sets (including LANL2DZ) reproduce well the changes in bonding energies for the same family of ligands (NH_3 vs. NMe_3) or (PH_3 vs. PMe_3) well.

The above analysis allows us to select TPSS/TZVP methodology to be adequate to analyze effects of ligand binding to small gold clusters. We further notice, that for all three types of ligated clusters, there is an expected increase in binding energies in the following order of ligands: $\text{NMe}_3 \approx \text{NH}_3 < \text{PH}_3 < \text{PMe}_3$. The similar binding energies of NH_3 and NMe_3 are expected due to high electronegativity of nitrogen that dampens the effect of extra electron density from donating CH_3 groups. The observed similarity is consistent with close values of gas-phase proton affinities of NH_3 and NMe_3 (196 and 216 kcal/mol, respectively).¹⁸⁴ In contrast to amines, the presence of donating groups on phosphorous significantly increases its nucleophilicity, which manifests in stronger binding energies of PMe_3 when compared to PH_3 . Finally, the radial extent and polarizability of the amine lone pair is smaller than that of the phosphine, which in turn leads to weaker binding of amines to gold compared to phosphines. For all ligands we observe increase in ligand binding energies in the order $\text{Au}_4\text{L}_4 < \text{Au}_2\text{L}_2 < \text{Au}_4\text{L}_2$. The increase in ligand binding from Au_4L_4 to Au_2L_2 most likely comes from increasing nucleophilicity of ligands as their number decreases around the cluster, and the strongest binding of ligands in Au_4L_2 is a result of extra electron density delocalization over four gold atoms compared to only two in Au_2L_2 . It is noteworthy that the results produced in the presence of solvent are consistent with above order of binding strengths, but there is an observed increase in binding energies of nitrogen based

ligands by 2kcal/mol for Au_2L_2 and Au_4L_4 whereas there is no such change observed for Au_4L_2 .

Table 5.2 presents variations of Au-Au and Au-L bond lengths for three geometries of the gold clusters we considered determined with different basis sets. Analysis of bare and ligated Au_2 and Au_4 gold cluster geometries indicates that both TZVP and QZVP basis sets can be considered flexible enough to give rise to converged values of both Au-Au and Au-L bond lengths, since the unsigned average difference between Au-L and Au-Au bond lengths in TZVP and QZVP cluster geometries are 0.005Å and 0.008Å, respectively. Consequently, either of the two basis sets can be considered as reference in our study. The performance of the other three, smaller basis sets is evaluated in comparison to TZVP or QZVP, since the use of the former is more desirable for lower computational cost when larger ligated gold clusters are studied. The LANL2DZ basis set justifiably can be considered the least flexible, as it lacks any polarization functions on either atom. The lack of polarization mostly affects Au-P bonds, causing them to be on average 0.19Å longer when compared to QZVP geometries. Au-N bonds are only slightly elongated (ca. 0.01Å) in LANL2DZ geometries. As expected, the trend for Au-Au bonding would be reversed, and in LANL2DZ geometries of phosphine-ligated clusters the average Au-Au bond is 0.02Å longer and twice as much in the *amine-passivated* ones, compared to reference geometries. The augmentation of LANL2DZ with a single polarization function added to every atom in LANL2DZ-P affects Au-P bonds the most, causing them to shrink by ca. 0.11Å, in contrast to Au-N bonds that slightly *expand* by 0.01Å. The Au-Au bonding follows the opposite trend and with polarization the metal-metal bonding increases by 0.01Å in phosphine-ligated clusters and shrinks by 0.02Å in amine-ligated ones. The use of the split-valence SVP basis set further causes slight shortening of Au-P bonds by 0.017Å and elongation of Au-N bonds by the same amount

with Au-Au bonds are being practically unaffected. Since LANL2DZ-P is somewhat less costly than SVP and its use fixes most shortcomings of parental LANL2DZ basis, we believe that LANL2DZ-P may be preferred over SVP in ligated gold cluster geometry optimizations.

The ligation of bare Au₂ dimer with NH₃ and PH₃ leads to the increase of the Au-Au metal bond in case of PH₃ (by 0.05Å) and does not affect the metal-metal separation in case of the bonding with NH₃. We believe that the interplay of two effects is responsible for the observed opposing trends in metal-metal bonding. The NBO electronic configuration of gold changes from $6s^{0.99}5d^{9.97}6p^{0.03}$ to $6s^{1.16}5d^{9.83}6p^{0.08}$ and $6s^{1.16}5d^{9.84}6p^{0.14}$ upon coordination of NH₃ and PH₃, respectively. As such, the promotion of electron density from 5d to 6s orbital should lead to the shortening of Au-Au distance, as 6s orbitals are less spatially extended than 5d. On the other hand, electropositive phosphorous populates significantly the $\sigma^*(\text{Au-Au})$ NBO antibonding orbital of the gold dimer, thereby causing the elongation of the Au-Au bond, in contrast to the electronegative nitrogen ($\sigma^*(\text{Au-Au})$ population of 0.003e in Au₂ increases to 0.146e and 0.268e in Au₂(NH₃)₂ and Au₂(PH₃)₂, respectively).

The coordination of two NH₃ or PH₃ molecules to Au₄ cluster causes the shortening of the central Au-Au bond by 0.04Å or elongation by 0.08Å, respectively, and elongation of four peripheral Au-Au bonds by 0.01Å and 0.03Å, respectively, if compared to bare Au₄ geometry. It is important to note that geometry optimizations usually take many steps to converge since the multidimensional potential energy surfaces are very shallow in all clusters, particularly in Au₄L₄ case. Consequently, we would expect large conformational freedom in the ligated clusters caused by solvent and thermal bath fluctuations. A representative case is the coordination of four ligands to Au₄: we observe that the amine ligand attachment causes an asymmetric shift of the peripheral gold atoms toward one of the central gold atoms

(Figure 5.1d) compared to the symmetric structure in the case of phosphine ligands (Figure 5.1c). This symmetry breaking leads to a significant elongation ($\sim 0.15 \text{ \AA}$) and weakening of two Au-Au bonds. Even though this conformational change is large, gain in energy due to this symmetry breaking is minimal: the energies of optimal symmetric (when artificial symmetry constraints are imposed) and asymmetric structures are different by 0.4 kcal/mol which is smaller than the room temperature thermal quantum $kT \sim 0.6 \text{ kcal/mol}$. Moreover, the introduction of solvent causes Au_4L_4 geometries to appear similar to Figure 5.1d structure in a presence of any ligand considered. As such, we expect large conformational space will be sampled by the ensemble of ligated clusters in solvent

5.2 Geometry and energetics of small gold clusters

Our benchmark study of ligated Au_2 and Au_4 finds weak dependence of geometries and ligand binding energies on DFT functionals used in calculations (except LSDA), while underscores the importance of polarization functions being present in the basis sets. Our results demonstrated that though TPSS/TZVP level of theory (if affordable) would be the method of choice for geometry optimization and chemical energy computations of ligated clusters. LANL2DZ ECP basis set can be employed to predict the geometry of ligated gold clusters in case only one type of ligands (belonging to same family) are used, considering their easy extendability to larger systems of interest. We obtain $\text{NMe}_3 \approx \text{NH}_3 < \text{PH}_3 < \text{PMe}_3$ order of ligand binding energies for Au_2 and Au_4 clusters. Ligand binding energies also increase in the order $\text{Au}_4\text{L}_4 < \text{Au}_2\text{L}_2 < \text{Au}_4\text{L}_2$ for all ligands.

5.2.1 Bare gold clusters

Geometries of bare gold clusters have been extensively studied in recent years with numerous computational methods. Figure 5.3 presents the geometries of ten isomers of Au₂, Au₄, Au₆ and Au₈ clusters. The index used to distinguish different isomers of the same nuclearity is shown in parentheses next to the isomer's formula. Multiple studies have discussed the relative stabilities of various isomers of these clusters based on DFT^{41, 63, 85, 88, 90, 97, 229} and *ab-initio*^{79, 87, 92, 96, 98, 226} levels of theory. Our results are consistent with previous findings that DFT treatment of gold clusters tends to stabilize planar isomers and not the 3D ones.²³⁰ Table 5.3 shows comparison of ground state energies for all the isomers of bare clusters considered. The energy of the lowest energy is taken as zero and relative energies of other isomers are given in kcal/mol.

Au₂: It is the simplest cluster with two atoms and widely studied to gauge the performance of different computational approaches.²³⁰⁻²³⁴ Relatively inexpensive TPSS/TPSS/LANL2DZ level of theory used in our calculations produced Au₂ dimer's bond length of 2.54 Å and bonding energy of 2.19 eV that compares very well with similar DFT calculations available from previous studies²²⁹ and even high-level *ab initio* results. For example, the use of LANL2DZ basis set in conjunction with high-level QCISD *ab initio* method⁷⁹ seems produce relatively poor agreement with the experimental values. The Au-Au distance was calculated to be 2.66 Å with the bond energy of only 1.90eV. On the other hand, B3LYP calculations using modified WTBS full-electron basis set, gave rise to²³⁴ closer to experimental value of 2.507 Å for Au₂ dimer bond length, but significantly overestimated its bonding energy as 2.57 eV. The same work reports bond length in Au₂ to be 2.488 Å and bonding energy of 2.19 eV when CCSD(T) method was used instead of DFT approach.

Au₄: Two isomers (Au₄(b) and Au₄(t)) were analyzed in this work with Au₄(b) found to be of the lowest energy, but with the second isomer only 0.8 kcal/mol higher in energy (Table 5.3) at TPSS/LANL2DZ level. Previously found energy difference between these two isomers was 1.8 kcal/mol (PW91PW91/CRENBL level)⁸⁶, 3.18 kcal/mol (BLYP/DNP level)²²⁹ or 6.02 kcal/mol (MP4/LANL2DZ level).⁷⁹ The average Au-Au peripheral bond length for Au₄(b) is 2.72 Å as found in our study, which agrees well with MP2/MP4 value of 2.77 Å calculated by Bravo-Pérez et. al.⁷⁹ and the value of 2.69 Å obtained by means of POLCI/MRSDCI by Balasuramanian et. al.²²⁶ The other isomer Au₄(t) is planar ‘Y’-shaped structure with average Au-Au bond length of 2.73 Å for the triangular part and 2.55 Å for the dimeric “tail”. Our obtained values of Au-Au bond length for Au₄(t) isomer are also consistent with Bravo-Pérez et. al.⁷⁹ predictions of 2.79 Å and 2.63 Å for triangular and dimeric part respectively. The obtained small energy difference between Au₄(b) and Au₄(t) isomers is likely to give rise to their rapid interconvertibility or coexistence.

Au₆: We have investigated four isomers of Au₆ Au₆(t), Au₆(p), Au₆(3d) and Au₆(dt) in this study. Au₆(t) is the lowest energy planar isomer is compared with other non-planar higher energy isomers, Au₆(p), Au₆(3d), and Au₆(dt) in Table 5.3. There is a remarkable difference of more than 20 kcal/mol in relative energy of non-planar isomers as shown in Table 5.3. Our finding about the bare Au₆(t) being the most stable structure is in agreement with other studies.^{63, 79, 229} Our results shows the peripheral Au-Au bond length of Au₆(t) is 2.66 Å and central Au-Au bond length is 2.82 Å.

Au₈: We consider three isomers of Au₈ to compare their energetics. The lowest energy isomer Au₈(s) being planar (in our study) is most debated.^{63, 85} We found the other two isomers Au₈(h) (planar) and Au₈(3d) (non-planar) are more than 5 kcal/mol higher in energy as shown in Table 5.3. The peripheral and central Au-Au bond length for Au₈(s) is

determined as 2.66 Å and 2.78 Å respectively. Detailed bond length comparison for all the isomers considered in this study is given in Figure 5.4.

5.2.2 Ligands and solvent effect

5.2.2.1 Relative stability of isomers

To investigate the ligand induced stability one can look at Table 5.3 and Figure 5.5. Table 5.3 gives the relative energies of bare clusters, while considering lowest energy structure zero; Figure 5.5 compares the stability of these clusters upon ligation. We have determined that geometry plays a crucial role in ligand attachment to these clusters. Different isomers of same clusters gets saturated (fully ligated) with different number of ligands based on their geometry. In the plots shown in Figure 5.5. we have compared these isomers with same number of ligands starting from the fully ligated isomer with least number of ligands attached. With one exception of Au₈ isomers, we have kept the reference isomer same as in bare clusters in Table 5.3. In case of Au₈ cluster the Au₈(s) (most stable isomer in bare form) gets fully saturated with 4 ligands whereas Au₈(t) and Au₈(3d) can take upto 7 ligands, which makes it less preferable to be a reference structure for comparison in our plots of Figure 5.5.

Top pair of plots in Figure 5.5 shows the effect of ligand attachment in case of Au₄ isomers with PH₃ ligands. In bare form Au₄(b) is the lowest energy isomer as discussed above, which is in agreement with previous studies. Also the energy difference between two isomers Au₄(b) and Au₄(t) is very small, which raised the question of coexistence in past. We observed the reversal of stability when these clusters get ligated. From the topmost plot in Figure 5.5, one can observe Au₄(b) is more stable than Au₄(t) in bare form, but stability reverses in the presence of three surrounding ligands, where Au₄(t) becomes more stable

than $\text{Au}_4(\text{b})$ and their energy difference is close to 2 kcal/mol. This leads us to a conclusion that the effect of ligands is not only important to compliment the experimental observations; it can also contribute to the debate on lowest stable isomer of small gold clusters.

Middle pair of the plots in Figure 5.5 gives energy difference between isomers of Au_6 cluster in bare form and towards full ligation. Taking the trend forward observed incase of Au_4 isomers, we observed ligation induced stability in case of Au_6 as well, where fully ligated clusters are determined to be most stable form as compared to partial ligated ones. $\text{Au}_6(\text{dt})$ fully ligated geometry when compared with the our reference $\text{Au}_6(\text{t})$ geometry with four surrounding ligands is notably an order of magnitude lower in energy in comparison to their bare form. Another isomer $\text{Au}_6(\text{p})$, which can take upto the maximum of five ligands to get saturated is observed to be more stable when compared with $\text{Au}_6(\text{t})$ surrounding by equal number of ligands. One can attribute this trend of stability alternation with ligation to the saturation of isomers with different number of ligands as seen in the case of $\text{Au}_6(\text{dt})$ and $\text{Au}_6(\text{p})$ against $\text{Au}_6(\text{t})$. $\text{Au}_6(\text{t})$ geometry is observed to form bond with six surrounding ligands and can be better compared with $\text{Au}_6(3\text{d})$ isomer, which also observed to form bonds with equal number of ligands. Although, there is a small energy barrier between two fully ligated isomers which can lead to switching between two conformations, but it is most likely restricted due to ligands positioning. We determine that ligation induced effect not only makes the $\text{Au}_6(3\text{d})$ lower in energy than $\text{Au}_6(\text{t})$, it also raises the possibility of 2D to 3D transition happening as low as Au_6 for small gold clusters.

The last plot at the bottom in Figure 5.5 displays the energy variation in different isomers of Au_8 upon ligation. Similar to the trends observed with smaller gold clusters discussed above, $\text{Au}_8(\text{s})$ isomer which forms bond with 4 surrounding ligands is found lower in energy as compared to other two isomers in bare as well as ligated form. The other two

isomers planar $\text{Au}_8(\text{h})$ and non-planar $\text{Au}_8(3\text{d})$ gets saturated with seven surrounding ligands. We observe that fully ligated $\text{Au}_8(3\text{d})$ is lower in energy as compared to $\text{Au}_8(\text{h})$, although the energy difference is less than 1 kcal/mol in the presence of PH_3 ligand. One can attribute this small energy difference may have been caused by flipping of the geometry (planar to non-planar) in case of $\text{Au}_8(\text{h})$.

5.2.2.2 Effect on cluster geometries

Figures 5.6, 5.7 and 5.8 shows the structural changes observed with one-by-one attachment of phosphine to the isomers of Au_4 , Au_6 , and Au_8 respectively. We observe no change in geometry of either $\text{Au}_4(\text{b})$ (left) or $\text{Au}_4(\text{t})$ (right) in 5.6, when surrounded by 1, 2 and 3 ligands. On the contrary, all four isomers of Au_6 are observed to go through geometrical changes with increase in number of surrounding ligands. Figure 5.7 shows these four isomers of Au_6 , with ability to get saturated with different number of ligands around them, arranged in increasing number of ligands attached (top to bottom). Planar isomer $\text{Au}_6(\text{t})$ first from left in Figure 6 shows distortion in its non-ligated base geometry, when added with 2, 3, 4 and 5 ligands, and retains back its bare geometry on full ligation with 6 surrounding ligands. We observed an interesting trend in case of $\text{Au}_6(\text{p})$ (2nd from the left in Figure 5.7), this non-planar isomer in bare form becomes planar with addition of ligands. $\text{Au}_6(\text{p})$ maintains a lower energy planar form with addition of 1 to 4 ligands before attaining pentagonal shape flat geometry, capped pentagonal in bare form, upon saturation with 5 surrounding ligands. The other two isomers $\text{Au}_6(\text{dt})$ (3rd from the left) and $\text{Au}_6(3\text{d})$ (4th and last from the left) are also determined to attain their central (similar to bare form) gold-gold geometry upon full ligation with 4 and 6 surrounding ligands respectively. One can easily conclude that these small gold clusters would want to occupy all available sites by forming bonds with surrounding ligands.

Figure 5.8 shows the ligand induced structural changes in three isomers of Au_8 . One can see the availability of only four binding sites with the outer gold atoms attached to the inner square in $\text{Au}_8(\text{s})$ allowing adaptation of maximum of four surrounding ligands. Each atom in the inner square of $\text{Au}_8(\text{s})$ geometry found to display bonding with four other gold atoms in this geometry leaving no room for extra electron density from any ligand. The other two geometries $\text{Au}_8(\text{h})$ and $\text{Au}_8(\text{3d})$ both can bind upto 7 ligands with not much of the geometry change upon increase in ligation other than one noticeable 2D to 3D transition incase of $\text{Au}_8(\text{h})$ with 7 surrounding ligands. Thus ligation does affect the initial geometry of small gold clusters as observed in $\text{Au}_6(\text{p})$ and $\text{Au}_8(\text{h})$. This study helps us being conclusive about the dilemma of 2D to 3D transition in small gold clusters. One can summarize that most stable structure in the presence of ligands in case of Au_6 and Au_8 is a 3D structure.

5.2.2.3 Cluster energetics

Plots in Figure 5.9 displays the effect of ligand attachment on the binding energy (per ligand in kcal/mol) of small gold clusters with and without solvent. Both the Figures show expected decrease in binding energy per ligand with the increase in number of ligands attached to the gold cluster core. The trend when compared across the isomers in terms of increasing number of ligands is consistent. Ligand binding takes away the extra electron density available around the gold cluster and tend to saturate the cluster geometry providing stability. Fully ligated clusters are most stable and due to large size have lower binding energy per ligand as expected. Solvent tends to mimic the electrostatic effect of ligands and have significant effect on bare cluster, which gets lower with the increase in number of surrounding ligands. We observe a consistent blue shift in the binding energy per ligand curves in the presence of solvent as shown in Figure 5.9 (plots on the right). One can see the binding energy per ligand vary with change in geometry of the cluster in case of Au_6 and Au_8 .

Though Redel et. al.¹⁰⁴ reports no change in binding energy on increase of cluster size from 2 to 20 atoms, our study reveals that the binding energy per ligand for small gold clusters Au₂, Au₄, Au₆ and Au₈ are not close to each other upon phosphine ligation. We suspect their conclusion was based on study of one isomeric form of small gold clusters.

Figure 5.10 shows variation of Au-Au (bottom) and Au-L (Gold-Ligand) bond lengths with increase in number of surrounding ligands for small gold. We observe an increase in Au-L bond length with increase in surrounding ligands consistently in all the isomers as shown in Figure 5.10 (top). With increase in surrounding ligands electron donation also increases, thus to accommodate new ligand cluster grow in size resulting to longer bond lengths. On the other hand the Au-Au (Bottom plot in Figure 5.10) distance remains unaffected in most of the isomers except three dimensional clusters.

5.3 Conclusions

Our study provides the comprehensive analysis of how ligand and solvation affect the geometry and energetics of ten isomers of four small gold clusters with a systematic one-by-one attachment of surrounding ligand to the optimized bare gold cluster geometry. The search for global minima of small clusters (Au₂, Au₄, Au₆, and Au₈) provides an insight to correct the long standing discrepancy of non-ligated clusters through the ligand induced stability of otherwise less stable isomers. Different isomers of small gold clusters get saturated by different number of surrounding ligands depending upon the available of gold binding sites. Most stable structure of the ligated isomers is the one with full ligation (saturated). We observe decrease in binding energy with increase in number of surrounding ligands when geometry of the gold cage is maintained in all the isomers and noticed the change in trend when base gold geometry distorts. Similarly, average gold-ligand bond length

increases systematically with the increase of surrounding ligands whereas no effect to the gold-gold bond lengths is observed in most of the planar isomers. This study reveals the 2D→3D transition happening at Au₆ which is even lower than much debated size of Au₈ and Au₁₃. To make the direct comparison of this study with the experiments, one need to calculate the optical properties of these ligated small gold clusters.

Finally, we observe shallow potential energy surfaces for considered ligated gold cluster. Consequently, significant conformational freedom in larger clusters with many ligands is expected due to solvent environment and thermal bath. This work provides useful computational guidelines and insights for future theoretical and experimental studies toward using ligands as chemical tools to achieve desirable optical properties in the noble metal clusters.

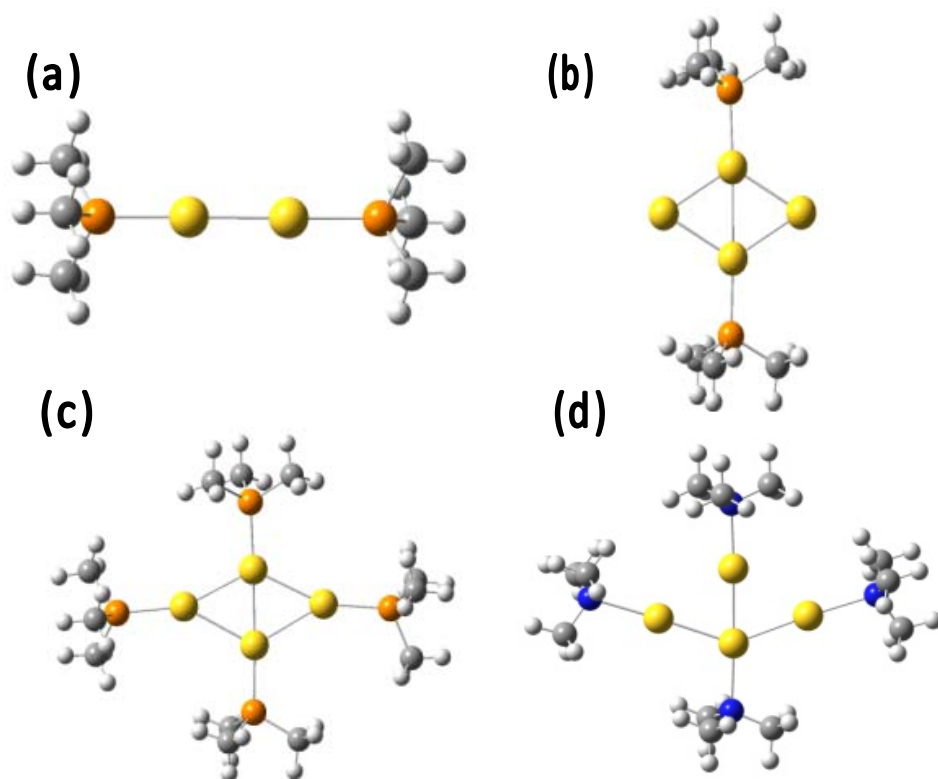


Figure 5.1 Representative geometries of Au_2 and Au_4 cluster with ligand attached as PMe_3 . (a) $\text{Au}_2(\text{PMe}_3)_2$, (b) $\text{Au}_4(\text{PMe}_3)_2$, (c) $\text{Au}_4(\text{PMe}_3)_4$, (d) $\text{Au}_4(\text{NMe}_3)_4$.

Table 5.1 Binding energies and bond length for Au_2 calculated with different DFT functionals and compared with experimental data.

| DFT Functional | Binding Energy (kcal/mol) | Bond Lengths (\AA) |
|---------------------------------|---------------------------|-------------------------------|
| Au_2 | | |
| SVWN5 | 64.138 | 2.491 |
| PBE | 50.031 | 2.549 |
| TPSS | 50.583 | 2.544 |
| B3LYP | 43.200 | 2.573 |
| CAM-B3LYP | 41.619 | 2.551 |
| Exp* | 53.000 | 2.470 |

* Kordis et. al., *Journal of Chemical Physics*, 1974, 61, 5114.

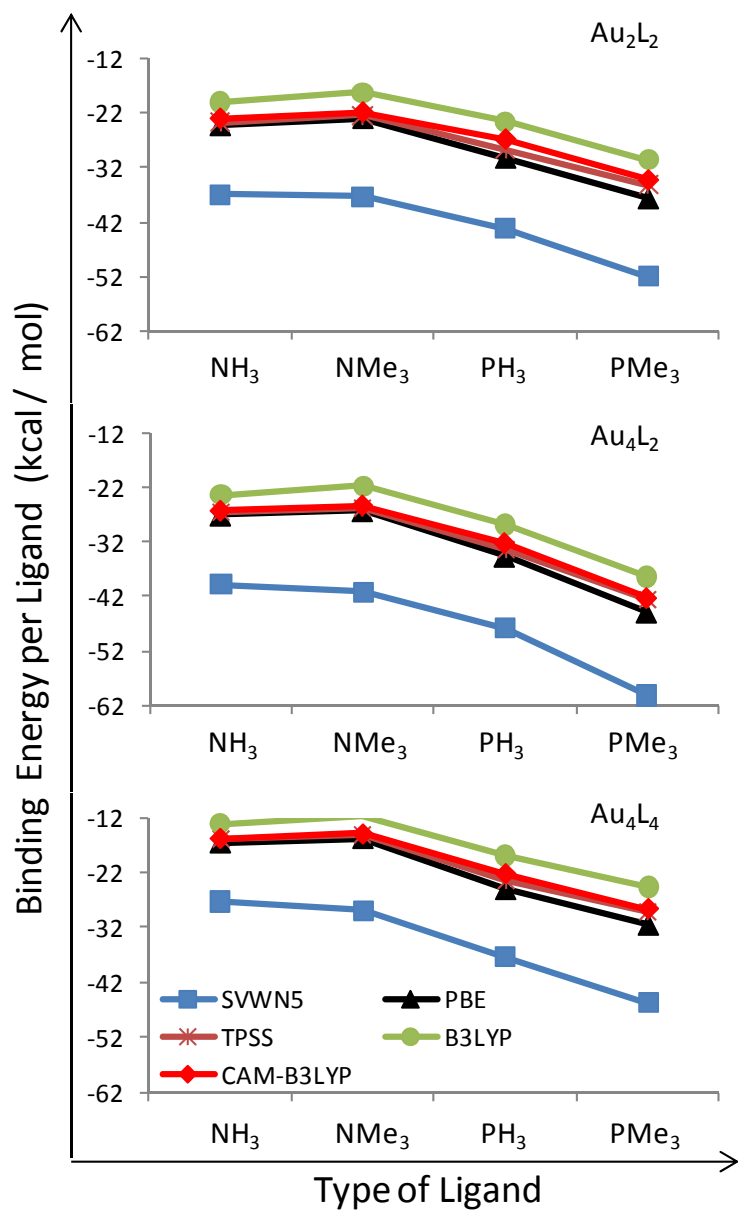


Figure 5.2 Comparison of binding energy per Ligand in kcal/mol for geometries of Au₂ and Au₄ in partial and fully ligated form determined by DFT functional model. TZVP basis set has been used for all calculations.

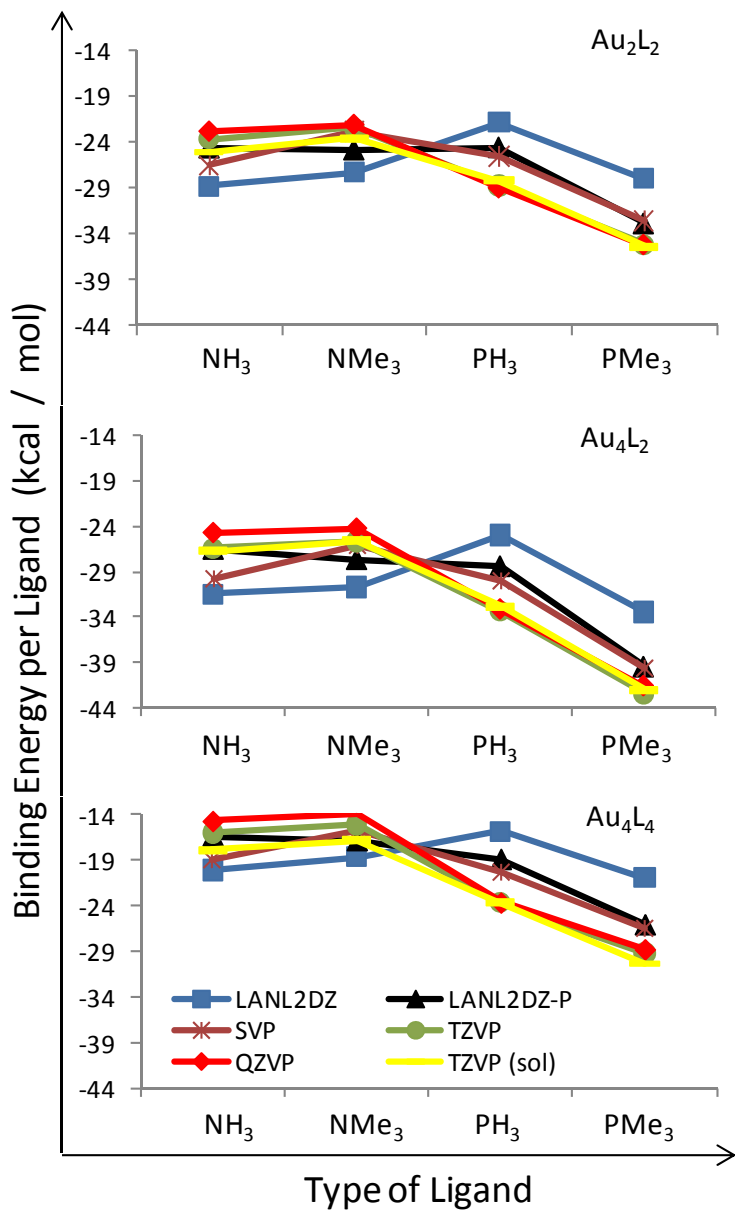


Figure 5.3 Comparison of binding energy per Ligand in kcal/mol for geometries of Au_2 and Au_4 in partial and fully ligated form determined by basis set. TPSS functional has been used for all calculations.

Table 5.2 Au-Au (Peripheral), Au-Au (Base) and Au-Ligand bond lengths for optimized structures of Au₂ and Au₄ clusters with different ligands. TPSS functional has been used for all calculations with different basis set.

| Bond Lengths (Å) | | | | | | | | | | | | | | | | |
|--------------------------------|------------------|-----------|-----------|-----------|-----------|-----------|-----------|-----------|-----------|-----------|-----------|-----------|-----------|-----------|-----------|-----------|
| DFT functional used - TPSS | | | | | | | | | | | | | | | | |
| Cluster | Ligand | LANL2DZ | | | LANL2DZ-P | | | SVP | | | TZVP | | | QZVP | | |
| | | Au-Au (P) | Au-Au (B) | Au-Ligand | Au-Au (P) | Au-Au (B) | Au-Ligand | Au-Au (P) | Au-Au (B) | Au-Ligand | Au-Au (P) | Au-Au (B) | Au-Ligand | Au-Au (P) | Au-Au (B) | Au-Ligand |
| Au ₂ | NH ₃ | 2.530 | - | 2.257 | 2.521 | - | 2.261 | 2.522 | - | 2.274 | 2.512 | - | 2.247 | 2.507 | - | 2.243 |
| | NMe ₃ | 2.535 | - | 2.289 | 2.523 | - | 2.297 | 2.525 | - | 2.315 | 2.515 | - | 2.281 | 2.509 | - | 2.280 |
| | PH ₃ | 2.537 | - | 2.521 | 2.551 | - | 2.412 | 2.564 | - | 2.386 | 2.564 | - | 2.335 | 2.559 | - | 2.327 |
| | PMe ₃ | 2.552 | - | 2.514 | 2.567 | - | 2.411 | 2.577 | - | 2.399 | 2.574 | - | 2.355 | 2.570 | - | 2.348 |
| Au ₄ L ₂ | NH ₃ | 2.750 | 2.604 | 2.224 | 2.739 | 2.590 | 2.228 | 2.740 | 2.595 | 2.238 | 2.719 | 2.580 | 2.218 | 2.706 | 2.572 | 2.218 |
| | NMe ₃ | 2.752 | 2.617 | 2.241 | 2.740 | 2.598 | 2.252 | 2.741 | 2.601 | 2.276 | 2.718 | 2.589 | 2.247 | 2.706 | 2.579 | 2.249 |
| | PH ₃ | 2.736 | 2.645 | 2.465 | 2.724 | 2.678 | 2.365 | 2.724 | 2.699 | 2.346 | 2.702 | 2.700 | 2.300 | 2.690 | 2.693 | 2.292 |
| | PMe ₃ | 2.741 | 2.694 | 2.452 | 2.730 | 2.711 | 2.358 | 2.730 | 2.723 | 2.352 | 2.708 | 2.722 | 2.314 | 2.697 | 2.714 | 2.308 |
| Au ₄ L ₄ | NH ₃ | 2.867 | 2.530 | 2.321 | 2.826 | 2.526 | 2.345 | 2.825 | 2.529 | 2.354 | 2.805 | 2.517 | 2.326 | 2.790 | 2.510 | 2.321 |
| | NMe ₃ | 2.849 | 2.543 | 2.364 | 2.816 | 2.534 | 2.392 | 2.803 | 2.542 | 2.425 | 2.790 | 2.527 | 2.384 | 2.782 | 2.519 | 2.388 |
| | PH ₃ | 2.774 | 2.571 | 2.558 | 2.780 | 2.581 | 2.429 | 2.788 | 2.593 | 2.398 | 2.780 | 2.579 | 2.332 | 2.771 | 2.572 | 2.322 |
| | PMe ₃ | 2.755 | 2.577 | 2.540 | 2.802 | 2.585 | 2.411 | 2.806 | 2.594 | 2.400 | 2.796 | 2.583 | 2.344 | 2.786 | 2.574 | 2.335 |
| Au ₂ | 2.47-Exp | 2.537 | - | - | 2.527 | - | - | 2.535 | - | - | 2.520 | - | - | 2.509 | - | - |
| Au ₄ | | 2.706 | 2.641 | - | 2.713 | 2.629 | - | 2.714 | 2.642 | - | 2.691 | 2.620 | - | 2.675 | 2.611 | - |

*Au-Au (P) - Peripheral, Au-Au (B) - Base

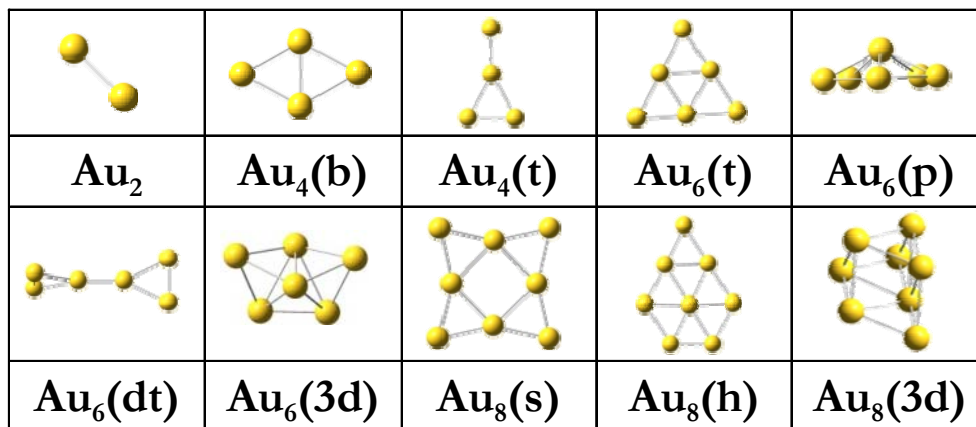


Figure 5.4 Lowest energy isomers (10) of small gold clusters (Au₂, Au₄, Au₆ and Au₈).

Table 5.3 Relative energies for different isomers of bare gold clusters. The lowest energy isomer is taken as reference structure (zero energy) for comparison. ‘NC- no convergence’

| Functional | Au ₄ (b) | Au ₄ (t) | Au ₆ (t) | Au ₆ (p) | Au ₆ (3d) | Au ₆ (dt) | Au ₈ (s) | Au ₈ (h) | Au ₈ (3d) |
|------------|---------------------|---------------------|---------------------|---------------------|----------------------|----------------------|---------------------|---------------------|----------------------|
| SVWN5 | 0.0 | 3.7 | 0.0 | 20.9 | 25.0 | 53.8 | 0.0 | 5.5 | -3.9 |
| PBEPBE | 0.0 | 0.3 | 0.0 | 20.8 | 29.7 | 42.6 | 0.0 | 9.1 | 9.2 |
| TPSSTPSS | 0.0 | 0.8 | 0.0 | 21.1 | 28.1 | 44.8 | 0.0 | 8.4 | 5.3 |
| B3LYP | 0.0 | NC | 0.0 | 21.3 | 34.3 | 38.3 | 0.0 | 12.5 | 17.2 |
| CAM-B3LYP | 0.0 | 0.0 | 0.0 | 23.0 | 35.4 | 42.1 | 0.0 | 14.5 | 17.4 |

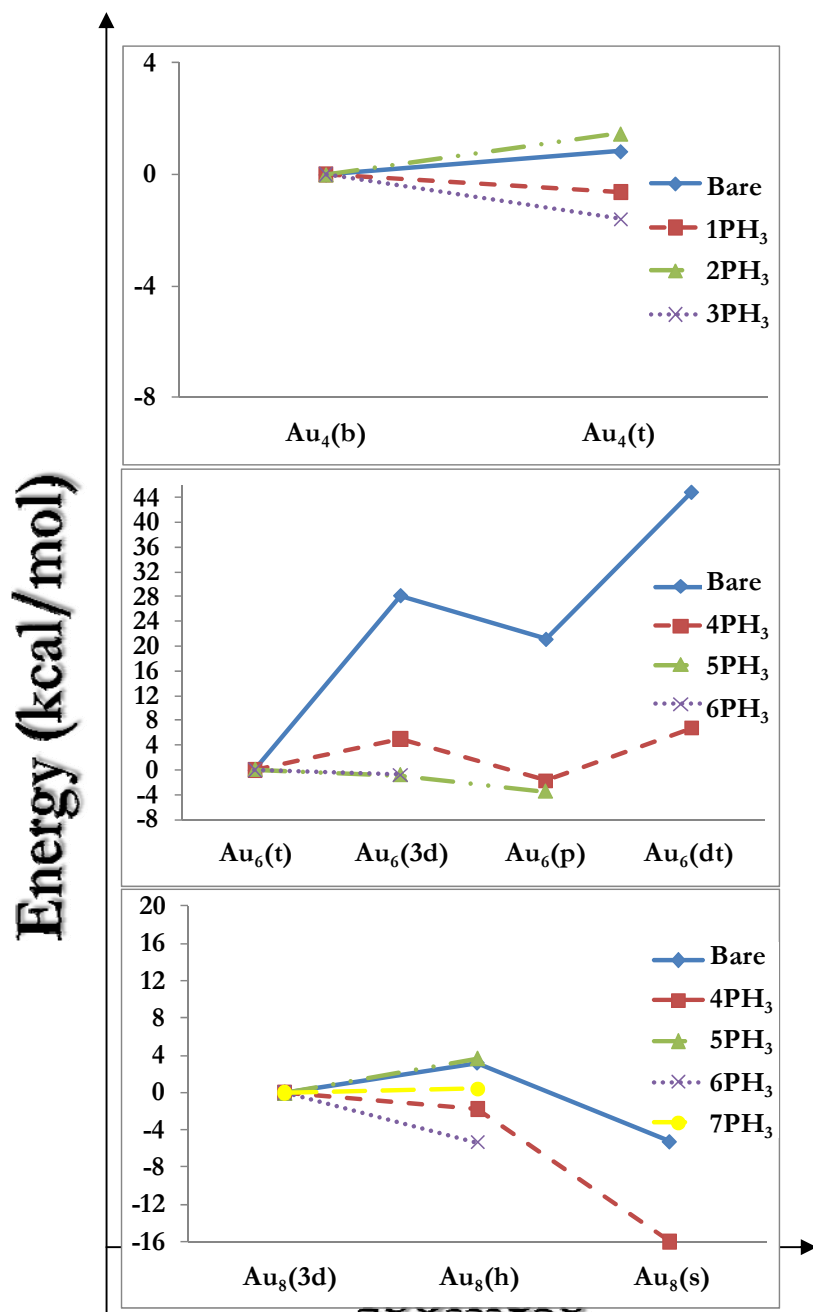


Figure 5.5 Relative energies for different isomers of small gold clusters with ligands. Comparison displays variations starting from saturated isomer with least number of ligands to the saturated isomer with most number of ligands. The lowest energy isomer is taken as reference structure (zero energy) for comparison.

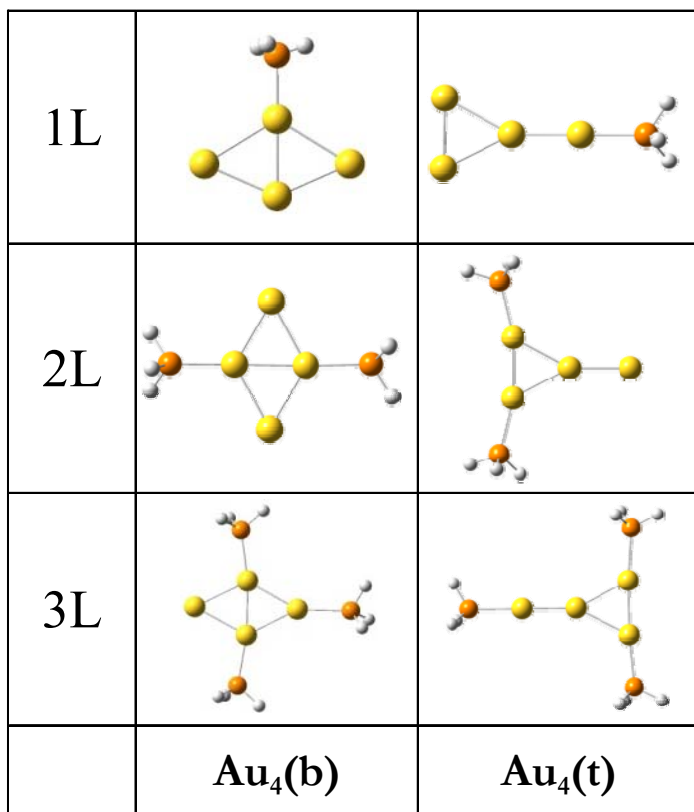


Figure 5.6 Geometries of two isomers of Au₄ with ligand attachment from one (top) to full ligation (saturation, bottom).

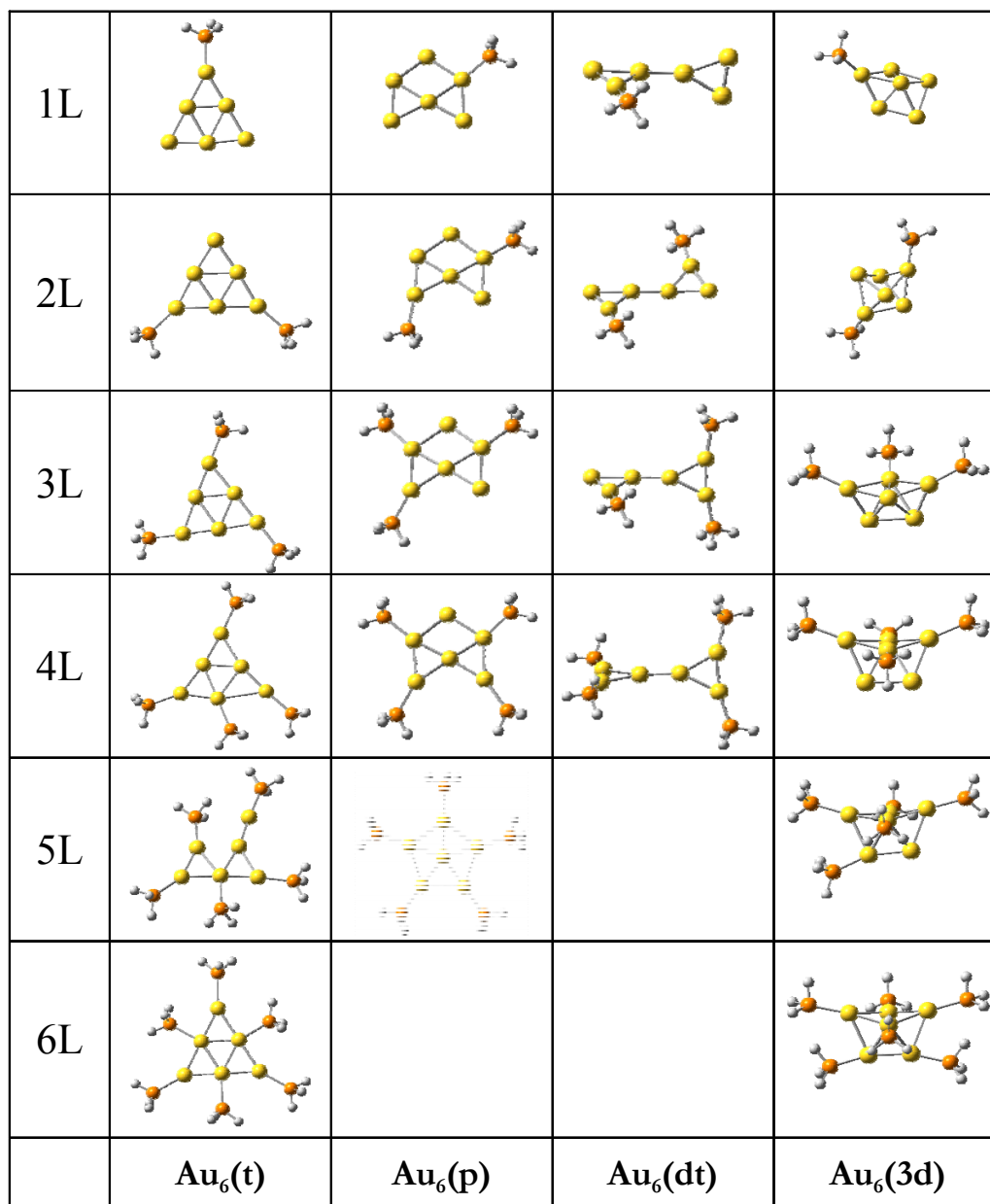


Figure 5.7 Geometries of four isomers of Au₆ with ligand attachment from one (top) to full ligation (Last geometry in respective columns).

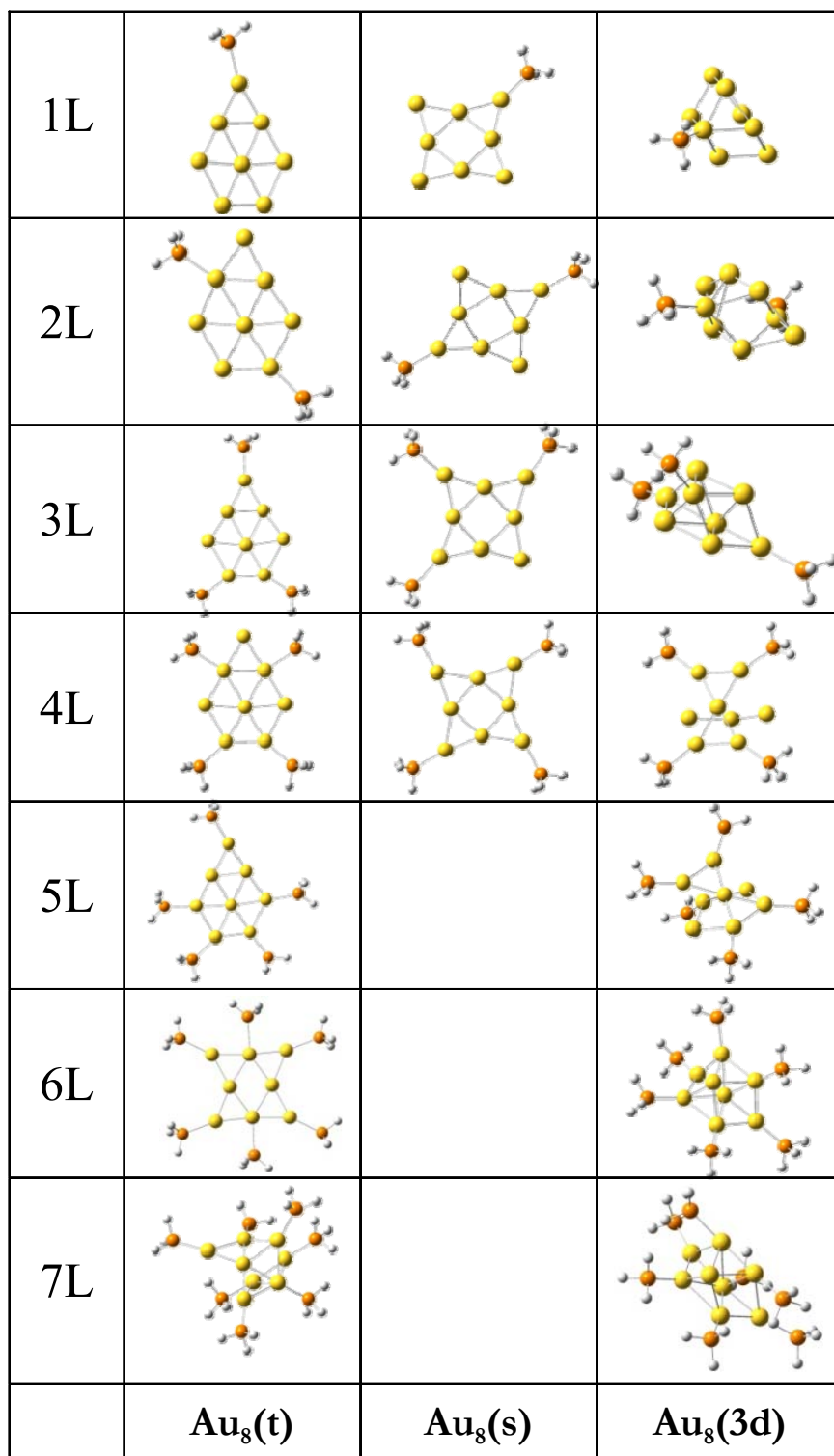


Figure 5.8 Geometries of four isomers of Au₈ with ligand attachment from one (top) to full ligation (Last in respective columns, saturation).

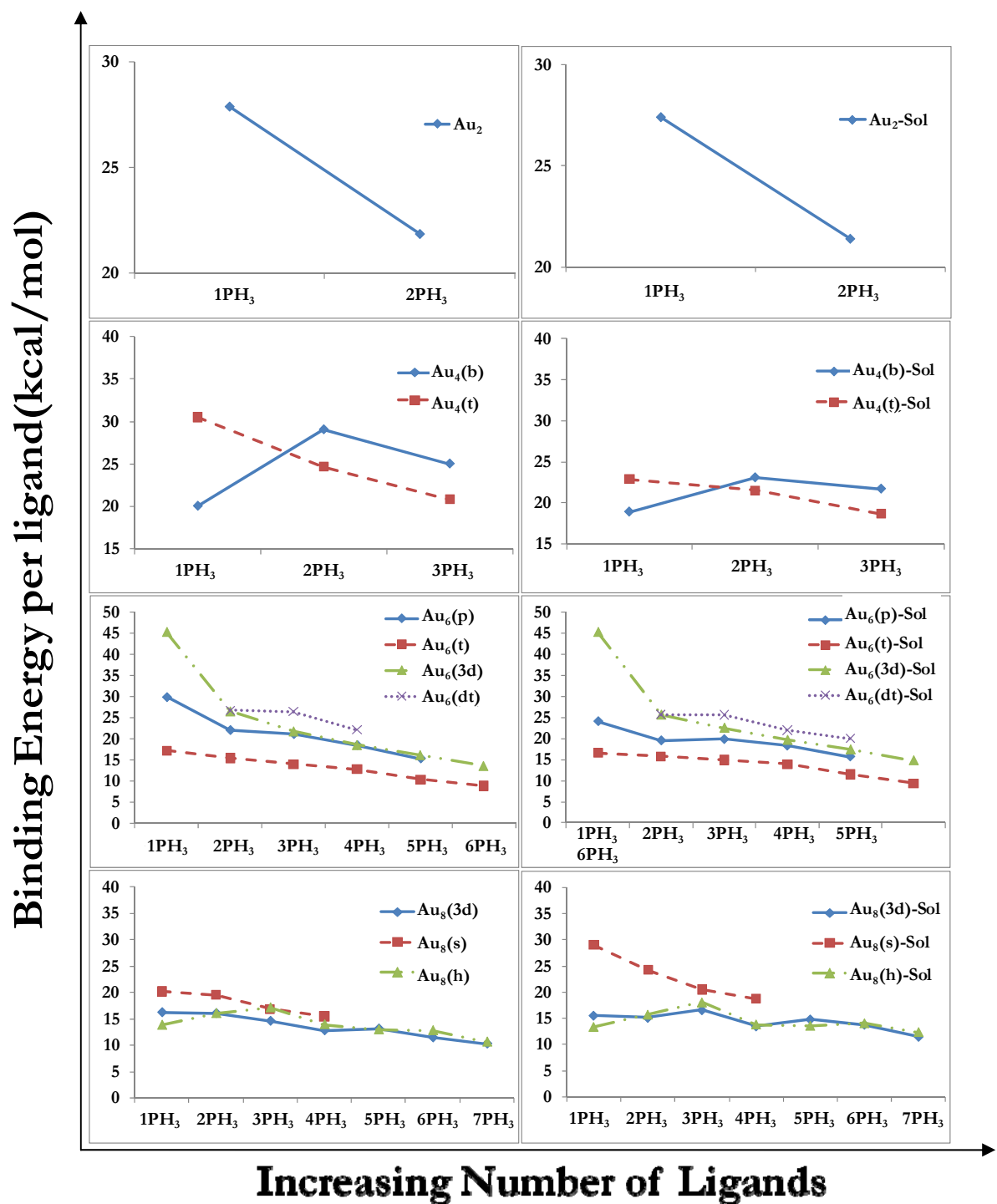


Figure 5.9 Binding energies per ligand (kcal/mol) of different isomers of small gold cluster (Au₂, Au₄, Au₆, Au₈) geometries with increase in number of ligands (PH₃) with (right) and without (left) solvent.

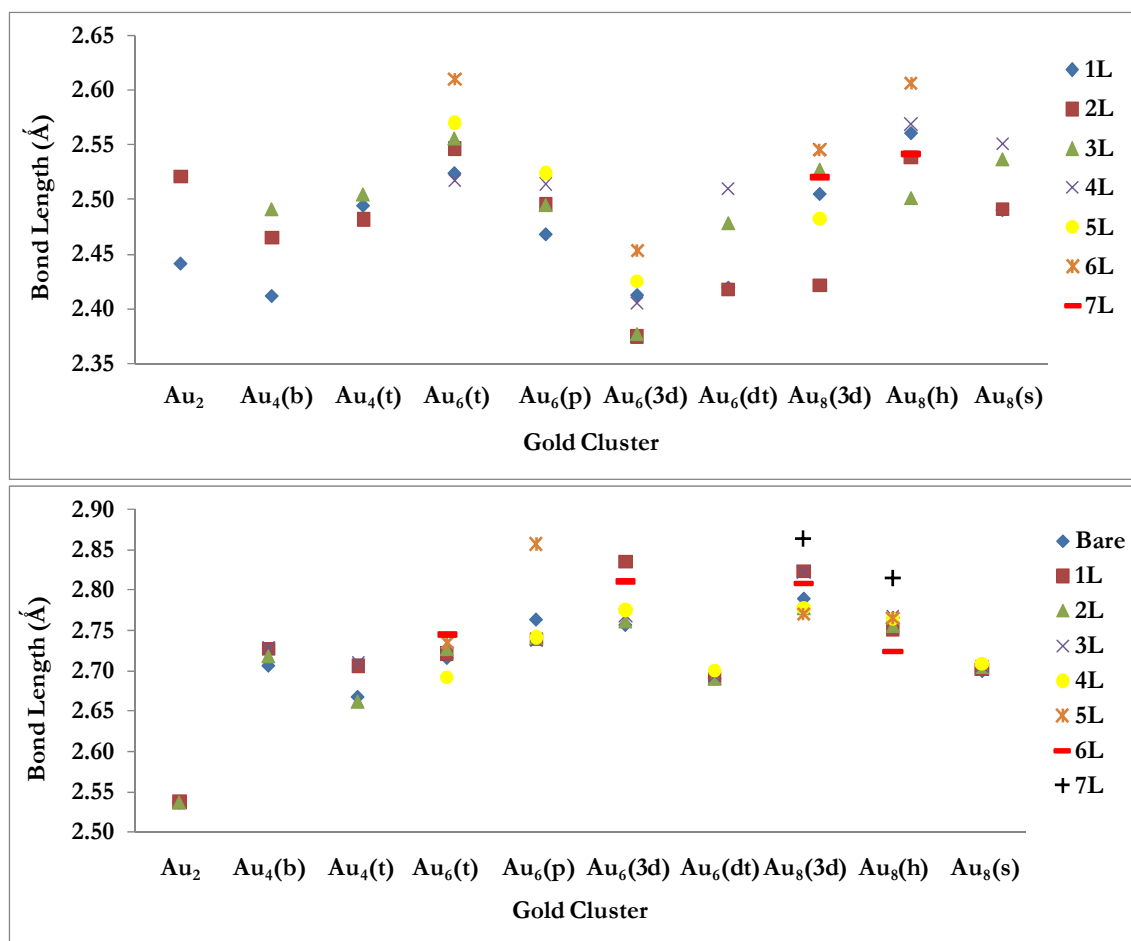


Figure 5.10 Bond length variation between gold-gold and gold-ligand bonds in different isomers of small gold clusters, when ligands are attached starting from one to full ligation (Saturation).

SUMMARY AND OUTLOOK

Our work here primarily focused on *3d*-transition metal systems (hydride and carbide diatomics and small Nickel clusters) and small gold clusters. We investigated the geometry and energetics of these small molecules and nanoclusters using DFT theory approach. Our motivation to study transition metal clusters is based on their numerous applications, most of which belong to two areas: catalysis and photonics. While atomic and magnetic structures of the nanoclusters are important for catalytic applications, the ability of the transition metals to form and break chemical bonds with atoms of other elements is even more important.

We have successfully described applicability of new exchange-correlation functional to study transition metal systems and also, the alternative theoretical descriptions (spin-contamination correction in broken symmetry DFT and ensemble Kohn-Sham (EKS)). We were able to provide superior DFT results for TM hydrides and carbides as compared to available *ab-initio* data, which might be a new start point for experimentalist to better understand the underlying phenomenon of bond breaking important in catalytic processes. We tested several exchange-correlation functionals including recently introduced long range corrected CAM-B3LYP and Truhlar's functionals M05-2x and M05 along with conventional LDA, GGA and hybrid functionals. Our test included functionals with explicit dependence on kinetic energy density (τ -functionals) for the description of hydrides (both neutral and cationic) and carbides formed by *3d*-transition metals. We found M05-2x and BMK dissociation energies were in better agreement with experiment (where available) than those obtained with high level wavefunction theory methods, published previously. This agreement with experiment deteriorated quickly for other functionals when the fraction of the Hartree-Fock exchange in DFT functional was decreased. Higher fraction of HF exchange was also essential in EKS formalism, but it did not help when spin-adapted

unrestricted approach was employed. We analyzed the electron spin densities using Natural Bond Orbital population analysis and found that simple description of $3d$ electrons as non-bonding in character is rarely correct.

Qualitatively correct description of the bond dissociation was ensured by allowing the spatial and spin symmetry to break. Our unrestricted formalism treatment to get better results gave appreciable spin-contamination for some of the systems at equilibrium, which lead us to propose a new scheme in order to correct the spin contamination effect on the energies. We have shown to get significant correction on one of the transition metal system with more than 10% spin contamination, after validating our approach on a simple H_2 system. In another attempt to correct DFT limitations to study strongly correlated systems with conventional one determinant approach, we presented Ensemble KS formalism to investigate the dissociation of C_2 molecule. We found that high fraction of HF exchange was essential to reproduce the results of EKS treatment with exact exchange-correlation functional.

For TM hydrides, our study reported that the average unsigned error for ionization potentials is much lower (0.14 and 0.27 eV for BMK and TPSS respectively) that previously reported owing to the careful SCF protocol employed. However, the spin gaps for the systems with multiple spin states considered is in disagreement with the wavefunction data available even after the spin-contamination correction. We found M05-2x performance (dissociation energies and bond lengths) to be the best of all four DFT functionals used in case of TMC following BMK performance in TMH. We concluded that in case of systems involving $3d$ -transition metals, more the percentage of HF exchange better is the performance. Our scalar relativistic corrections gave us mixed results for TMH and TMC, while the correction was not significant in TMH energetics, it was found to play role in TMC

energetics but we were limited on discussion due to the lack of experimental data. We found that the VB description of electronic structure is followed in our description of metal carbides as predicted by M05-2x correctly.

Comparing our studies of metal hydrides and metal carbides we employed BMK to study the small Nickel clusters. We found agreement in description of ground states for small clusters Ni_2 , Ni_3 , Ni_5 and several isomers of Ni_4 , in all possible spin states, compared to experimental and WFT results. Further we extended the scope of diatomics and small clusters to include effect of solvent and ligation on our investigations of small gold clusters. We described how ligand and solvation affect the geometry and energetics of ten isomers of four small gold clusters with a systematic one-by-one attachment of surrounding ligand to the optimized bare gold cluster geometry. The search for global minima of small clusters (Au_2 , Au_4 , Au_6 , and Au_8) provided an insight to correct the long standing discrepancy of non-ligated clusters through the ligand induced stability of otherwise less stable isomers. This study revealed the 2D \rightarrow 3D transition happening at Au_6 which was even lower than much debated size of Au_8 and Au_{13} . To make the direct comparison of this study with the experiments, one needed to calculate the optical properties of these ligated small gold clusters. Finally, we observed shallow potential energy surfaces for considered ligated gold cluster. Consequently, significant conformational freedom in larger clusters with many ligands was expected due to solvent environment and thermal bath. This work provides useful computational guidelines and insights for future theoretical and experimental studies toward using ligands as chemical tools to achieve desirable optical properties in the noble metal clusters.

REFERENCES

1. Furche, F.; Perdew, J. P., The performance of semilocal and hybrid density functionals in 3d transition-metal chemistry. *Journal of Chemical Physics* **2006**, 124, (4), 044103-044129.
2. Harrison, J. G., Density functional calculations for atoms in the 1st transition series. *Journal of Chemical Physics* **1983**, 79, (5), 2265-2269.
3. Jensen, K. P.; Roos, B. O.; Ryde, U., Performance of density functionals for first row transition metal systems. *Journal of Chemical Physics* **2007**, 126, (1), 014103-014116.
4. Zheng, J.; Petty, J. T.; Dickson, R. M., High quantum yield blue emission from water-soluble Au₈ nanodots. *Journal of the American Chemical Society* **2003**, 125, (26), 7780-7781.
5. Simoes, J. A. M.; Beauchamp, J. L., Transition-Metal hydrogen and metal-carbon bond strengths - the keys to catalysis. *Chemical Reviews* **1990**, 90, (4), 629-688.
6. Walker, J. H.; Walker, T. E. H.; Kelly, H. P., Ground and Low-Lying Excited Electronic States of FeH. *Journal of Chemical Physics* **1972**, 57, (5), 2094-2098.
7. Tanaka, K.; Sekiya, M.; Yoshimine, M., Ab initio study of the lower few states of FeH: Application of the multireference coupled pair approximation. *Journal of Chemical Physics* **2001**, 115, (10), 4558-4564.
8. Sodupe, M.; Lluch, J. M.; Oliva, A.; Illas, F.; Rubio, J., Abinitio study of the ground and low-lying states of FeH. *Journal of Chemical Physics* **1990**, 92, (4), 2478-2480.
9. Bagus, P. S.; Bjorkman, C., Electronic-structure of transition-metal hydrides - NiH and PdH. *Physical Review A* **1981**, 23, (2), 461-472.
10. Blomberg, M. R. A.; Siegbahn, P. E. M.; Roos, B. O., A Theoretical-Study of NiH - Optical-Spectrum and Potential Curves. *Molecular Physics* **1982**, 47, (1), 127-143.
11. Marian, C. M.; Blomberg, M. R. A.; Siegbahn, P. E. M., Multireference and relativistic effects in NiH. *Journal of Chemical Physics* **1989**, 91, (6), 3589-3595.
12. Pouamerigo, R.; Merchan, M.; Nebotgil, I.; Malmqvist, P. A.; Roos, B. O., The chemical-bonds in CuH, Cu⁻², NiH, and Ni⁻² studied with multiconfigurational 2nd-order perturbation-theory. *Journal of Chemical Physics* **1994**, 101, (6), 4893-4902.
13. Anglada, J.; Bruna, P. J.; Grein, F., Theoretical-study of low-lying electronic states of CoH⁺. *Journal of Chemical Physics* **1990**, 92, (11), 6732-6741.
14. Bauschlicher, C. W., Full Configuration-Interaction Benchmark Calculations for TiH. *Journal of Physical Chemistry* **1988**, 92, (11), 3020-3023.

15. Dai, D. G.; Balasubramanian, K., Spectroscopic properties and potential-energy curves for 21 electronic states of CrH. *Journal of Molecular Spectroscopy* **1993**, 161, (2), 455-465.
16. Freindorf, M.; Marian, C. M.; Hess, B. A., Theoretical-study of the electronic-spectrum of the CoH molecule. *Journal of Chemical Physics* **1993**, 99, (2), 1215-1223.
17. Raghavachari, K.; Sunil, K. K.; Jordan, K. D., Theoretical-study of the bonding in CuH and Cu₂. *Journal of Chemical Physics* **1985**, 83, (9), 4633-4640.
18. Walch, S. P.; Bauschlicher, C. W., CASSCF/CI calculations for first row transition metal hydrides: The TiH□(⁴Φ), VH□(⁵Δ), CrH□(⁶Σ⁺), MnH□(⁷Σ⁺), FeH□(^{4,6}Δ), and NiH□(²Δ) states. *Journal of Chemical Physics* **1983**, 78, (7), 4597-4605.
19. Kunz, A. B.; Guse, M. P.; Blint, R. J., Potential-energy curves for ScH. *Journal of Physics B-Atomic Molecular and Optical Physics* **1975**, 8, (14), L358-L361.
20. Koseki, S.; Matsushita, T.; Gordon, M. S., Dissociation potential curves of low-lying states in transition metal hydrides. 3. Hydrides of groups 6 and 7. *Journal of Physical Chemistry A* **2006**, 110, (7), 2560-2570.
21. Koseki, S.; Ishihara, Y.; Fedorov, D. G.; Umeda, H.; Schmidt, M. W.; Gordon, M. S., Dissociation potential curves of low-lying states in transition metal hydrides. 2. Hydrides of groups 3 and 5. *Journal of Physical Chemistry A* **2004**, 108, (21), 4707-4719.
22. Koseki, S.; Ishihara, Y.; Umeda, H.; Fedorov, D. G.; Gordon, M. S., Dissociation potential curves of low-lying states in transition metal hydrides. I. Hydrides of Group 4. *Journal of Physical Chemistry A* **2002**, 106, (5), 785-794.
23. Meunier, B., Metalloporphyrins as versatile catalysts for oxidation reactions and oxidative DNA cleavage. *Chemical Reviews* **1992**, 92, (6), 1411-1456.
24. Chong, D. P.; Langhoff, S. R.; Bauschlicher, C. W.; Walch, S. P., Theoretical dipole-moments for the 1st-row transition-metal hydrides. *Journal of Chemical Physics* **1986**, 85, (5), 2850-2860.
25. Ohanessian, G.; Goddard, W. A., Valence-bond concepts in transition-metals - metal hydride diatomic cations. *Accounts of Chemical Research* **1990**, 23, (11), 386-392.
26. Sodupe, M.; Lluch, J. M.; Oliva, A.; Illas, F.; Rubio, J., Ground and low-lying states of FeH⁺ as derived from abinitio self-consistent field and configuration-interaction calculations. *Journal of Chemical Physics* **1989**, 90, (11), 6436-6442.
27. Alvaradoswaisgood, A. E.; Allison, J.; Harrison, J. F., Electronic and geometric structures of the chromium cations CrH⁺, CrCH³⁺, CrCH²⁺, and CrCH⁺. *Journal of Physical Chemistry* **1985**, 89, (12), 2517-2525.

28. Mavridis, A.; Harrison, J. R., Electronic and geometric structure of the titanium hydrides, TiH^+ and TiH^{+2} . *Journal of the Chemical Society-Faraday Transactions Ii* **1989**, 85, 1391-1399.
29. Ziegler, T.; Li, J., Bond-Energies for cationic bare metal-hydrides of the first transition series - a challenge to density-functional theory. *Canadian Journal of Chemistry-Revue Canadienne De Chimie* **1994**, 72, (3), 783-789.
30. Barone, V.; Adamo, C.; Mele, F., Comparison of conventional and hybrid density functional approaches. Cationic hydrides of first-row transition metals as a case study. *Chemical Physics Letters* **1996**, 249, (3-4), 290-296.
31. Baker, J.; Pulay, P., Assessment of the OLYP and O3LYP density functionals for first-row transition metals. *Journal of Computational Chemistry* **2003**, 24, (10), 1184-1191.
32. Riley, K. E.; Merz, K. M., Assessment of density functional theory methods for the computation of heats of formation and ionization potentials of systems containing third row transition metals. *Journal of Physical Chemistry A* **2007**, 111, (27), 6044-6053.
33. Schultz, N. E.; Zhao, Y.; Truhlar, D. G., Density functionals for inorganometallic and organometallic chemistry. *Journal of Physical Chemistry A* **2005**, 109, (49), 11127-11143.
34. Diaconu, C. V.; Cho, A. E.; Doll, J. D.; Freeman, D. L., Broken-symmetry unrestricted hybrid density functional calculations on nickel dimer and nickel hydride. *Journal of Chemical Physics* **2004**, 121, (20), 10026-10040.
35. Barone, V.; Adamo, C., First-row transition-metal hydrides: A challenging playground for new theoretical approaches. *International Journal of Quantum Chemistry* **1997**, 61, (3), 443-451.
36. Gutsev, G. L.; Andrews, L.; Bauschlicher, C. W., Similarities and differences in the structure of 3d-metal monocarbides and monoxides. *Theoretical Chemistry Accounts* **2003**, 109, (6), 298-308.
37. Shim, I.; Gingerich, K. A., Electronic states and nature of the chemical-bond in the molecule CrC by all-electron abinitio calculations. *International Journal of Quantum Chemistry* **1992**, 42, (2), 349-363.
38. Shim, I.; Gingerich, K. A., All electron ab initio investigations of the electronic states of the FeC molecule. *European Physical Journal D* **1999**, 7, (2), 163-172.
39. Hack, M. D.; Maclagan, R.; Scuseria, G. E.; Gordon, M. S., An ab initio study of TiC: A comparison of different levels of theory including density functional methods. *Journal of Chemical Physics* **1996**, 104, (17), 6628-6630.
40. Maclagan, R.; Scuseria, G. E., An ab initio study of CrC: A comparison of different levels of theory including density functional methods. *Journal of Chemical Physics* **1997**, 106, (4), 1491-1494.

41. Borin, A. C.; Gobbo, J. P., The lowest quartet electronic states of MnC. *Chemical Physics Letters* **2006**, 417, (4-6), 334-340.
42. Kalemos, A.; Dunning, T. H.; Mavridis, A., The electronic structure of vanadium carbide, VC. *Journal of Chemical Physics* **2005**, 123, (1), 014301-014308.
43. Kalemos, A.; Dunning, T. H.; Mavridis, A., Ab initio study of the electronic structure of manganese carbide. *Journal of Chemical Physics* **2006**, 124, (15), 154308-154313.
44. Kalemos, A.; Dunning, T. H.; Mavridis, A., The electronic structure of the two lowest states of CuC. *Journal of Chemical Physics* **2008**, 129, (17), 174306-174309.
45. Kalemos, A.; Mavridis, A., Theoretical investigation of titanium carbide, TiC: X-3 Sigma(+), a(1)Sigma(+), A(3)Delta, and b(1)Delta states. *Journal of Physical Chemistry A* **2002**, 106, (15), 3905-3908.
46. Kalemos, A.; Mavridis, A.; Harrison, J. F., Theoretical investigation of scandium carbide, ScC. *Journal of Physical Chemistry A* **2001**, 105, (4), 755-759.
47. Kerkines, I. S. K.; Mavridis, A., Electronic structure of scandium and titanium carbide cations, ScC+ and TiC+. Ground and low-lying states. *Journal of Physical Chemistry A* **2000**, 104, (50), 11777-11785.
48. Tzeli, D.; Mavridis, A., Theoretical investigation of iron carbide, FeC. *Journal of Chemical Physics* **2002**, 116, (12), 4901-4921.
49. Tzeli, D.; Mavridis, A., Electronic structure of cobalt carbide, CoC. *Journal of Physical Chemistry A* **2006**, 110, (28), 8952-8962.
50. Tzeli, D.; Mavridis, A., Theoretical investigation of the ground and low-lying excited states of nickel carbide, NiC. *Journal of Chemical Physics* **2007**, 126, (19), 194304-194315.
51. Tomonari, M.; Tanaka, K., Theoretical study of the TiC molecule: clarification of the ground state. *Molecular Physics* **2003**, 101, (1-2), 111-116.
52. Majumdar, D.; Balasubramanian, K., A theoretical study of potential energy curves and spectroscopic constants of VC. *Molecular Physics* **2003**, 101, (9), 1369-1376.
53. Balfour, W. J.; Cao, J. Y.; Prasad, C. V. V.; Qian, C. X. W., Electronic spectroscopy of jet-cooled iron monocarbide. The ${}^3\Delta_1 \leftarrow {}^3\Delta_1$ transition near 493 nm. *Journal of Chemical Physics* **1995**, 103, (10), 4046-4051.
54. Itono, S. S.; Taketsugu, T.; Hirano, T.; Nagashima, U., Ab initio study of the ground and two low-lying electronic excited states of FeC. *Journal of Chemical Physics* **2001**, 115, (24), 11213-11220.

55. Adam, A. G.; Peers, J. R. D., A rotational and hyperfine analysis of the $[14.0]^2\Sigma^+ - X^2\Sigma^+$ band system of cobalt monocarbide. *Journal of Molecular Spectroscopy* **1997**, 181, (1), 24-32.
56. Brewster, M. A.; Ziurys, L. M., The millimeter-wave spectrum of NiC ($X^1\Sigma^+$) and CoC ($X^2\Sigma^+$) *Astrophysical Journal* **2001**, 559, (2), L163-L166.
57. Brugh, D. J.; Morse, M. D., Resonant two-photon ionization spectroscopy of NiC. *Journal of Chemical Physics* **2002**, 117, (23), 10703-10714.
58. Kant, A., Dissociation energies of diatomic molecules of the transition elements. I. Nickel. *The Journal of Chemical Physics* **1964**, 41, (6), 1872-1876.
59. Moskovits, M.; Hulse, J. E., Ultraviolet-visible spectra of diatomic, triatomic, and higher nickel clusters. *Journal of Chemical Physics* **1977**, 66, (9), 3988-3994.
60. Parks, E. K.; Zhu, L.; Ho, J.; Riley, S. J., The structure of small nickel clusters. Ni₃-Ni₁₅. *Journal of Chemical Physics* **1994**, 100, (10), 7206-7222.
61. Pinegar, J. C.; Langenberg, J. D.; Arrington, C. A.; Spain, E. M.; Morse, M. D., Ni-2 Revisited-reassignment of the ground electronic state. *Journal of Chemical Physics* **1995**, 102, (2), 666-674.
62. Wang, H. M.; Haouari, H.; Craig, R.; Lombardi, J. R.; Lindsay, D. M., Raman spectra of mass-selected nickel dimers in argon matrices. *Journal of Chemical Physics* **1996**, 104, (10), 3420-3422.
63. Arvizu, G. L.; Calaminici, P., Assessment of density functional theory optimized basis sets for gradient corrected functionals to transition metal systems: The case of small Ni_n (n ≤ 5) clusters. *Journal of Chemical Physics* **2007**, 126, (19), 194102-194111.
64. Reuse, F. A.; Khanna, S. N., Geometry, electronic structure, and magnetism of small Ni_N (N=2-6, 8, 13) clusters. *Chemical Physics Letters* **1995**, 234, (1-3), 77-81.
65. Reuse, F. A.; Khanna, S. N., Photoabsorption spectrum of small Ni-n (n = 2-6, 13) clusters. *European Physical Journal D* **1999**, 6, (1), 77-81.
66. Michelini, M. C.; Diez, R. P.; Jubert, A. H., Density functional study of the ionization potentials and electron affinities of small Ni-n clusters with n=2-6 and 8. *Computational Materials Science* **2004**, 31, (3-4), 292-298.
67. St Petkov, P.; Vayssilov, G. N.; Kruger, S.; Rosch, N., Structure, stability, electronic and magnetic properties of Ni-4 clusters containing impurity atoms. *Physical Chemistry Chemical Physics* **2006**, 8, (11), 1282-1291.
68. Xie, Z.; Ma, Q. M.; Liu, Y.; Li, Y. C., First-principles study of the stability and Jahn-Teller distortion of nickel clusters. *Physics Letters A* **2005**, 342, (5-6), 459-467.

69. Luo, C. L., The structure of small nickel clusters: Ni-2-Ni-19. *Modelling and Simulation in Materials Science and Engineering* **2000**, 8, (2), 95-101.
70. Grigoryan, V. G.; Springborg, M., Structural and energetic properties of nickel clusters: $2 \leq N \leq 150$. *Physical Review B* **2004**, 70, (20), 205415-205419.
71. Nygren, M. A.; Siegbahn, P. E. M.; Wahlgren, U.; Akeby, H., Theoretical ionization energies and geometries for Ni_N ($N \leq 4$ to $N \leq 9$). *Journal of Physical Chemistry* **1992**, 96, (9), 3633-3640.
72. Zheng, J.; Zhang, C.; Dickson, R. M., Highly fluorescent, water-soluble, size-tunable gold quantum dots. *Physical Review Letters* **2004**, 93, (7), 077402-077405.
73. Zheng, J.; Nicovich, P. R.; Dickson, R. M., Highly fluorescent noble-metal quantum dots. *Annual Review of Physical Chemistry* **2007**, 58, (1), 409-431.
74. Charles W. Bauschlicher, Jr.; Stephen, R. L.; Harry, P., Theoretical study of the structures and electron affinities of the dimers and trimers of the group IB metals (Cu, Ag, and Au). *The Journal of chemical physics* **1989**, 91, (4), 2412-2419.
75. Balasubramanian, K.; Liao, M. Z., Electronic states and potential energy surfaces of gold and silver trimers. *Chem, Phys* **1988**, 127, (1-3), 313-324.
76. Balasubramanian, K.; Dai-Wei, L., Is Au₆ a circular ring? *The Journal of chemical physics* **1991**, 94, (7), 5233-5236.
77. Oliver, D. H.; Sai-Cheong, C.; Mauro, S.; Notker, R., From clusters to bulk: A relativistic density functional investigation on a series of gold clusters Au[_n], $n = 6, \dots, 147$. *The Journal of chemical physics* **1997**, 106, (12), 5189-5201.
78. Michaelian, K.; Rendón, N.; Garzón, I. L., Structure and energetics of Ni, Ag, and Au nanoclusters. *Physical Review B* **1999**, 60, (3), 2000-2010.
79. Bravo-Pérez, G.; Garzón, I. L.; Novaro, O., Ab initio study of small gold clusters. *Journal of Molecular Structure: THEOCHEM* **1999**, 493, (1-3), 225-231.
80. Wang, J.; Wang, G.; Zhao, J., Density-functional study of Au_n ($n=2-20$) clusters: Lowest-energy structures and electronic properties. *Physical Review B* **2002**, 66, (3), 035418-035423.
81. Zhao, J.; Yang, J.; Hou, J. G., Theoretical study of small two-dimensional gold clusters. *Physical Review B* **2003**, 67, (8), 085404-085409.
82. Abrams, M. L.; Sherrill, C. D., Full configuration interaction potential energy curves for the X ¹Σg⁺, B ¹Δg, and B' ¹Σg⁺ states of C₂: A challenge for approximate methods. *Journal of Chemical Physics* **2004**, 121, (19), 9211-9219.
83. Fernández, E. M.; Soler, J. M.; Garzón, I. L.; Balbás, L. C., Trends in the structure and bonding of noble metal clusters. *Physical Review B* **2004**, 70, (16), 165403.

84. Remacle, F.; Kryachko, E. S., Structure and energetics of two- and three-dimensional neutral, cationic, and anionic gold clusters $Au_{5 \leq n \leq 9}^Z$ ($Z=0, \pm 1$). *The Journal of chemical physics* **2005**, 122, (4), 044304-044317.
85. Olson, R. M.; Varganov, S.; Gordon, M. S.; Metiu, H.; Chretien, S.; Piecuch, P.; Kowalski, K.; Kucharski, S. A.; Musial, M., Where Does the Planar-to-Nonplanar Turnover Occur in Small Gold Clusters? *Journal of the American Chemical Society* **2004**, 127, (3), 1049-1052.
86. Walker, A. V., Structure and energetics of small gold nanoclusters and their positive ions. *The Journal of chemical physics* **2005**, 122, (9), 094310-094321.
87. Olson, R. M.; Gordon, M. S., Isomers of Au_8 . *The Journal of chemical physics* **2007**, 126, (21), 214310-214315.
88. Häkkinen, H.; Landman, U., Gold clusters (Au_N , $2 \leq N \leq 10$) and their anions. *Physical Review B* **2000**, 62, (4), 2287-2290.
89. Spivey, K.; Williams, J. I.; Wang, L., Structures of undecagold clusters: Ligand effect. *Chemical Physics Letters* **2006**, 432, (1-3), 163-166.
90. Assadollahzadeh, B.; Schwerdtfeger, P., A systematic search for minimum structures of small gold clusters Au ($n=2-20$) and their electronic properties. *The Journal of chemical physics* **2009**, 131, 064306.
91. Lee, H. M.; Ge, M.; Sahu, B. R.; Tarakeshwar, P.; Kim, K. S., Geometrical and electronic structures of gold, silver, and gold silver binary clusters: origins of ductility of gold and gold silver alloy formation. *Journal of Physical Chemistry B* **2003**, 107, (37), 9994-10005.
92. Liao, D.; Balasubramanian, K., Electronic structure of Cu_6 , Ag_6 , Au_6 , and their positive ions. *The Journal of Chemical Physics* **1992**, 97, 2548.
93. Periyasamy, G.; Remacle, F., Ligand and solvation effects on the electronic properties of Au_{55} clusters: A density functional theory study. *Nano Letters* **2009**, 9, (8), 3007-3011.
94. Samah, M.; Bouguerra, M.; Guerbous, L.; Berd, M., DFT based study of Au_n (4-7) clusters: new stabilized geometries. *Physica Scripta* **2007**, 75, (4), 411.
95. Xiao, L.; Tollberg, B.; Hu, X.; Wang, L., Structural study of gold clusters. *The Journal of chemical physics* **2006**, 124, 114309-114318.
96. Pyykkö, P., Theoretical chemistry of gold. III. *Chemical Society Reviews* **2008**, 37, (9), 1967-1997.
97. Pyykkö, P., Theoretical chemistry of gold. *Angewandte Chemie (International edition in English)* **2004**, 43, (34), 4412-4456.

98. Pyykkö, P., Theoretical chemistry of gold. II. *Inorganica Chimica Acta* **2005**, 358, (14), 4113-4130.
99. Daniel, M.-C.; Astruc, D., Gold nanoparticles: assembly, supramolecular chemistry, quantum-size-related properties, and applications toward biology, catalysis, and nanotechnology. *Chemical Reviews* **2003**, 104, (1), 293-346.
100. Pyykko, P., Relativity, Gold, closed-shell interactions, and CsAu.NH₃. *Angewandte Chemie International Edition* **2002**, 41, (19), 3573-3578.
101. Shafai, G.; Hong, S.; Bertino, M.; Rahman, T. S., Effect of ligands on the geometric and electronic structure of Au₁₃ clusters. *The Journal of Physical Chemistry C* **2009**, 113, (28), 12072-12078.
102. Garzón, I. L.; Rovira, C.; Michaelian, K.; Beltrán, M. R.; Ordejón, P.; Junquera, J.; Sánchez-Portal, D.; Artacho, E.; Soler, J. M., Do thiols merely passivate gold nanoclusters? *Physical Review Letters* **2000**, 85, (24), 5250-5251.
103. Wilson, N. T.; Johnston, R. L., Passivated clusters: a theoretical investigation of the effect of surface ligation on cluster geometry. *Physical Chemistry Chemical Physics* **2002**, 4, (17), 4168-4171.
104. Redel, E.; Walter, M.; Thomann, R.; Vollmer, C.; Hussein, L.; Scherer, H.; Krüger, M.; Janiak, C., Synthesis, stabilization, functionalization and DFT calculations of Gold nanoparticles in fluoruous phases (PTFE and Ionic Liquids). *Chemistry-A European Journal* **2009**, 15, (39), 10047-10059.
105. Hohenberg, P.; Kohn, W., Inhomogeneous electron gas. *Physical Review* **1964**, 136, (3B), B864 - B871.
106. Kohn, W.; Becke, A. D.; Parr, R. G., Density functional theory of electronic structure. *Journal of Physical Chemistry* **1996**, 100, (31), 12974-12980.
107. Kohn, W.; Sham, L. J., Self-consistent equations including exchange and correlation effects. *Physical Review* **1965**, 140, (4A), 1133-1138.
108. Geerlings, P.; De Proft, F.; Langenaeker, W., Conceptual density functional theory. *Chemical Reviews* **2003**, 103, (5), 1793-1873.
109. Bredow, T.; Geudtner, G.; Jug, K., MSINDO parameterization for third-row transition metals. *Journal of Computational Chemistry* **2001**, 22, (8), 861-887.
110. Porezag, D.; Frauenheim, T.; Kohler, T.; Seifert, G.; Kaschner, R., Construction of tight-binding-like potentials on the basis of density-functional theory - application to carbon. *Physical Review B* **1995**, 51, (19), 12947-12957.
111. Pettersson, L. G. M.; Bauschlicher, C. W.; Langhoff, S. R.; Partridge, H., Positive-Ions of the 1st-Row and 2nd-Row Transition-Metal Hydrides. *Journal of Chemical Physics* **1987**, 87, (1), 481-492.

112. Becke, A. D., Density-functional exchange-energy approximation with correct asymptotic-behavior. *Physical Review A* **1988**, 38, (6), 3098-3100.
113. Becke, A. D., Density-functional thermochemistry .4. A new dynamical correlation functional and implications for exact-exchange mixing. *Journal of Chemical Physics* **1996**, 104, (3), 1040-1046.
114. Frisch, M. J. T., G. W.; Schlegel, H. B.; Scuseria, G. E.; Robb, M. A.; Cheeseman, J. R.; Montgomery, Jr., J. A.; Vreven, T.; Kudin, K. N.; Burant, J. C.; Millam, J. M.; Iyengar, S. S.; Tomasi, J.; Barone, V.; Mennucci, B.; Cossi, M.; Scalmani, G.; Rega, N.; Petersson, G. A.; Nakatsuji, H.; Hada, M.; Ehara, M.; Toyota, K.; Fukuda, R.; Hasegawa, J.; Ishida, M.; Nakajima, T.; Honda, Y.; Kitao, O.; Nakai, H.; Klene, M.; Li, X.; Knox, J. E.; Hratchian, H. P.; Cross, J. B.; Bakken, V.; Adamo, C.; Jaramillo, J.; Gomperts, R.; Stratmann, R. E.; Yazyev, O.; Austin, A. J.; Cammi, R.; Pomelli, C.; Ochterski, J. W.; Ayala, P. Y.; Morokuma, K.; Voth, G. A.; Salvador, P.; Dannenberg, J. J.; Zakrzewski, V. G.; Dapprich, S.; Daniels, A. D.; Strain, M. C.; Farkas, O.; Malick, D. K.; Rabuck, A. D.; Raghavachari, K.; Foresman, J. B.; Ortiz, J. V.; Cui, Q.; Baboul, A. G.; Clifford, S.; Cioslowski, J.; Stefanov, B. B.; Liu, G.; Liashenko, A.; Piskorz, P.; Komaromi, I.; Martin, R. L.; Fox, D. J.; Keith, T.; Al-Laham, M. A.; Peng, C. Y.; Nanayakkara, A.; Challacombe, M.; Gill, P. M. W.; Johnson, B.; Chen, W.; Wong, M. W.; Gonzalez, C.; and Pople, J. A.; *Gaussian 03*, Revision D.01; Gaussian Inc., Wallingford, CT: 1994-2003.
115. Becke, A. D., Density-functional thermochemistry. 3-The role of exact exchange. *Journal of Chemical Physics* **1993**, 98, (7), 5648-5652.
116. Sousa, S. F.; Fernandes, P. A.; Ramos, M. J., General performance of density functionals. *Journal of Physical Chemistry A* **2007**, 111, (42), 10439-10452.
117. Zhao, Y.; Truhlar, D. G., Exploring the limit of accuracy of the global hybrid meta density functional for main-group thermochemistry, kinetics, and noncovalent interactions. *Journal of Chemical Theory and Computation* **2008**, 4, (11), 1849-1868.
118. Jacquemin, D.; Wathelet, V.; Perpète, E. A.; Adamo, C., Extensive TD-DFT benchmark: singlet-excited states of organic molecules. *Journal of Chemical Theory and Computation* **2009**, 5, (9), 2420-2435.
119. Boese, A. D.; Martin, J. M. L., Development of density functionals for thermochemical kinetics. *Journal of Chemical Physics* **2004**, 121, (8), 3405-3416.
120. Quintal, M. M.; Karton, A.; Iron, M. A.; Boese, A. D.; Martin, J. M. L., Benchmark study of DFT functionals for late-transition-metal reactions. *Journal of Physical Chemistry A* **2006**, 110, (2), 709-716.
121. Ruiz, E., Exchange coupling constants using density functional theory: The MOX suite. *Chemical Physics Letters* **2008**, 460, (1-3), 336-338.
122. Casida, M. E., Time-dependent density-functional theory for molecules and molecular solids. *Journal of Molecular Structure-Theochem* **2009**, 914, (1-3), 3-18.

123. Henderson, T. M.; Janesko, B. G.; Scuseria, G. E., Range Separation and Local Hybridization in Density Functional Theory. *Journal of Physical Chemistry A* **2008**, 112, (49), 12530-12542.
124. Chai, J. D.; Head-Gordon, M., Systematic optimization of long-range corrected hybrid density functionals. *Journal of Chemical Physics* **2008**, 128, (8), 15.
125. Yanai, T.; Tew, D. P.; Handy, N. C., A new hybrid exchange-correlation functional using the Coulomb-attenuating method (CAM-B3LYP). *Chemical Physics Letters* **2004**, 393, (1-3), 51-57.
126. Akinaga, Y.; Ten-No, S., Intramolecular charge-transfer excitation energies from range-separated hybrid functionals using the yukawa potential. *International Journal of Quantum Chemistry* **2009**, 109, (9), 1905-1914.
127. Akinaga, Y.; Ten-no, S., Range-separation by the Yukawa potential in long-range corrected density functional theory with Gaussian-type basis functions. *Chemical Physics Letters* **2008**, 462, (4-6), 348-351.
128. Schipper, P. R. T.; Gritsenko, O. V.; Baerends, E. J., One-determinantal pure state versus ensemble Kohn-Sham solutions in the case of strong electron correlation: CH₂ and C₂. *Theoretical Chemistry Accounts* **1998**, 99, (5), 329-343.
129. Wachters, A. J., Gaussian basis set for molecular wavefunctions containing third-row atoms. *Journal of Chemical Physics* **1970**, 52, (3), 1033-1036.
130. Hay, P. J., Gaussian basis sets for molecular calculations - representation of 3d orbitals in transition-metal atoms. *Journal of Chemical Physics* **1977**, 66, (10), 4377-4384.
131. Rabuck, A. D.; Scuseria, G. E., Improving self-consistent field convergence by varying occupation numbers. *Journal of Chemical Physics* **1999**, 110, (2), 695-700.
132. Schaftenaar, G.; Noordik, J. H., Molden: a pre- and post-processing program for molecular and electronic structures. *Journal of Computer-Aided Molecular Design* **2000**, 14, (2), 123-134.
133. Reed, A. E.; Weinhold, F., Natural Bond Orbital analysis of internal-rotation barriers and related phenomena. *Israel Journal of Chemistry* **1991**, 31, (4), 277-285.
134. Douglas, M.; Kroll, N. M., Quantum electrodynamic corrections to fine-structure of helium. *Annals of Physics* **1974**, 82, (1), 89-155.
135. Jansen, G.; Hess, B. A., Revision of the Douglas-Kroll Transformation. *Physical Review A* **1989**, 39, (11), 6016-6017.
136. Frisch, M. J. T., G. W.; Schlegel, H. B.; Scuseria, G. E.; Robb, M. A.; Cheeseman, J. R.; Montgomery, Jr., J. A.; Vreven, T.; Kudin, K. N.; Burant, J. C.; Millam, J. M.; Iyengar, S. S.; Tomasi, J.; Barone, V.; Mennucci, B.; Cossi, M.; Scalmani, G.; Rega, N.; Petersson, G. A.; Nakatsuji, H.; Hada, M.; Ehara, M.; Toyota, K.; Fukuda, R.;

- Hasegawa, J.; Ishida, M.; Nakajima, T.; Honda, Y.; Kitao, O.; Nakai, H.; Klene, M.; Li, X.; Knox, J. E.; Hratchian, H. P.; Cross, J. B.; Bakken, V.; Adamo, C.; Jaramillo, J.; Gomperts, R.; Stratmann, R. E.; Yazyev, O.; Austin, A. J.; Cammi, R.; Pomelli, C.; Ochterski, J. W.; Ayala, P. Y.; Morokuma, K.; Voth, G. A.; Salvador, P.; Dannenberg, J. J.; Zakrzewski, V. G.; Dapprich, S.; Daniels, A. D.; Strain, M. C.; Farkas, O.; Malick, D. K.; Rabuck, A. D.; Raghavachari, K.; Foresman, J. B.; Ortiz, J. V.; Cui, Q.; Baboul, A. G.; Clifford, S.; Cioslowski, J.; Stefanov, B. B.; Liu, G.; Liashenko, A.; Piskorz, P.; Komaromi, I.; Martin, R. L.; Fox, D. J.; Keith, T.; Al-Laham, M. A.; Peng, C. Y.; Nanayakkara, A.; Challacombe, M.; Gill, P. M. W.; Johnson, B.; Chen, W.; Wong, M. W.; Gonzalez, C.; and Pople, J. A.; *Gaussian 09 Revision A-2*, 2009.
137. Hay, P. J.; Wadt, W. R., Ab-initio effective core potentials for molecular calculations - Potentials for K to Au including the outermost core orbitals. *Journal of Chemical Physics* **1985**, 82, (1), 299-310.
138. Check, C. E.; Faust, T. O.; Bailey, J. M.; Wright, B. J.; Gilbert, T. M.; Sunderlin, L. S., Addition of Polarization and Diffuse Functions to the LANL2DZ Basis Set for P-Block Elements. *The Journal of Physical Chemistry A* **2001**, 105, (34), 8111-8116.
139. Schafer, A.; Horn, H.; Ahlrichs, R., Fully optimized contracted gaussian basis sets for atoms like Li to Kr. *Journal of Chemical Physics* **1992**, 97, (4), 2571-2577.
140. Weigend, F.; Ahlrichs, R., Balanced basis sets of split valence, triple zeta valence and quadruple zeta valence quality for H to Rn: Design and assessment of accuracy. *Physical Chemistry Chemical Physics* **2005**, 7, (18), 3297-3305.
141. Weigend, F.; Furche, F.; Ahlrichs, R., Gaussian basis sets of quadruple zeta valence quality for atoms H-Kr. *Journal of Chemical Physics* **2003**, 119, (24), 12753-12762.
142. Barone, V.; Cossi, M., Quantum calculation of molecular energies and energy gradients in solution by a conductor solvent model. *Journal of Physical Chemistry A* **1998**, 102, (11), 1995-2001.
143. Ziegler, T.; Rauk, A.; Baerends, E. J., Calculation of multiplet energies by Hartree-Fock-Slater method. *Theoretica Chimica Acta* **1977**, 43, (3), 261-271.
144. Vonbarth, U., Local-density theory of multiplet structure. *Physical Review A* **1979**, 20, (4), 1693-1703.
145. Lannoo, M.; Baraff, G. A.; Schluter, M., Self-consistent 2nd-order perturbation treatment of multiplet structures using local-density theory. *Physical Review B* **1981**, 24, (2), 943-954.
146. Wood, J. H., Atomic multiplet structures obtained from Hartree-Fock, statistical exchange and local spin-density approximations. *Journal of Physics B-Atomic Molecular and Optical Physics* **1980**, 13, (1), 1-14.

147. Weinert, M.; Watson, R. E.; Fernando, G. W., Density-functional theory and atomic multiplet levels. *Physical Review A* **2002**, 66, (3), 032508-032516.
148. Johnson, E. R.; Dickson, R. M.; Becke, A. D., Density functionals and transition-metal atoms. *Journal of Chemical Physics* **2007**, 126, (18), 184104-184110.
149. Perdew, J. P.; Savin, A.; Burke, K., Escaping the symmetry dilemma through a pair-density interpretation of spin-density functional theory. *Physical Review A* **1995**, 51, (6), 4531-4541.
150. Benard, M., Study of Hartree-Fock instabilities in $\text{Cr}_2(\text{O}_2\text{CH})_4$ and $\text{Mo}_2(\text{O}_2\text{CH})_4$. *Journal of Chemical Physics* **1979**, 71, (6), 2546-2556.
151. Hay, P. J.; Thibeault, J. C.; Hoffmann, R., Orbital Interactions in Metal Dimer Complexes. *Journal of the American Chemical Society* **1975**, 97, (17), 4884-4899.
152. Noodleman, L., Valence bond description of anti-ferromagnetic coupling in transition-metal dimers. *Journal of Chemical Physics* **1981**, 74, (10), 5737-5743.
153. Gingsberg, A. P., Magnetic exchange in transition metal complexes vi: Aspects of exchange coupling in magnetic cluster complexes. *Inorganica Chimica Acta Reviews* **1971**, 5, 45-68.
154. Sherrill, C. D.; Lee, M. S.; Head-Gordon, M., On the performance of density functional theory for symmetry-breaking problems. *Chemical Physics Letters* **1999**, 302, (5-6), 425-430.
155. Fuchs, M.; Niquet, Y. M.; Gonze, X.; Burke, K., Describing static correlation in bond dissociation by Kohn-Sham density functional theory. *Journal of Chemical Physics* **2005**, 122, (9), 094116-094128.
156. Peach, M. J. G.; Teale, A. M.; Tozer, D. J., Modeling the adiabatic connection in H-2. *Journal of Chemical Physics* **2007**, 126, (24), 244104-244112.
157. Neese, F., Definition of corresponding orbitals and the diradical character in broken symmetry DFT calculations on spin coupled systems. *Journal of Physics and Chemistry of Solids* **2004**, 65, (4), 781-785.
158. Davidson, E. R.; Clark, A. E., Analysis of wave functions for open-shell molecules. *Physical Chemistry Chemical Physics* **2007**, 9, (16), 1881-1894.
159. Young, D., *Computational Chemistry: A Practical Guide for Applying Techniques to Real World Problems* Wiley-Interscience: 2001; Vol. 1, p 408.
160. Wu, Q.; Van Voorhis, T., Direct optimization method to study constrained systems within density-functional theory. *Physical Review A* **2005**, 72, (2), 024502-024505.
161. Lovell, T.; Han, W. G.; Liu, T. Q.; Noodleman, L., A structural model for the high-valent intermediate Q of methane monooxygenase from broken-symmetry density

- functional and electrostatics calculations. *Journal of the American Chemical Society* **2002**, 124, (20), 5890-5894.
162. Takeda, R.; Yamanaka, S.; Yamaguchi, K., Resonating broken-symmetry approach to biradicals and polyradicals. *International Journal of Quantum Chemistry* **2006**, 106, (15), 3303-3311.
163. Cory, M. G.; Zerner, M., Projected unrestricted Hartree-Fock calculations within the intermediate neglect of differential overlap model. *Journal of Physical Chemistry A* **1999**, 103, (36), 7287-7293.
164. Davidson, E. R.; Clark, A. E., Spin polarization and annihilation for radicals and diradicals. *International Journal of Quantum Chemistry* **2005**, 103, (1), 1-9.
165. Krylov, A. I., Spin-contamination of coupled-cluster wave functions. *Journal of Chemical Physics* **2000**, 113, (15), 6052-6062.
166. Kozłowski, P. M.; Pulay, P., The unrestricted natural orbital-restricted active space method: methodology and implementation. *Theoretical Chemistry Accounts* **1998**, 100, (1-4), 12-20.
167. Kaldor, U., Spin-optimized self-consistent-field function .2. hyperfine structure of atomic nitrogen. *Physical Review A* **1970**, 1, (6), 1586-1592.
168. Smeyers, Y. G., The Half Projected Hartree-Fock model for determining singlet excited states. In *Advances in Quantum Chemistry*, 2000; Vol. 36, pp 253-270.
169. Andrews, J. S.; Jayatilaka, D.; Bone, R. G. A.; Handy, N. C.; Amos, R. D., Spin contamination in single-determinant wave-functions. *Chemical Physics Letters* **1991**, 183, (5), 423-431.
170. Yamanaka, S.; Yamaki, D.; Shigeta, Y.; Nagao, H.; Yoshioka, Y.; Suzuki, N.; Yamaguchi, K., Generalized spin density functional theory for noncollinear molecular magnetism. *International Journal of Quantum Chemistry* **2000**, 80, (4-5), 664-671.
171. Rassolov, V. A.; Xu, F., Geminal model chemistry III: Partial spin restriction. *Journal of Chemical Physics* **2007**, 126, (23), 7.
172. Löwdin, P.-O., Quantum theory of many-particle systems. III. extension of the Hartree-Fock scheme to include degenerate systems and correlation effects. *Physical Review* **1955**, 97, (6), 1509-1520.
173. Isayev, O.; Gorb, L.; Zilberberg, I.; Leszczynski, J., Electronic structure and bonding of {Fe(PhNO₂)}(6) complexes: A density functional theory study. *Journal of Physical Chemistry A* **2007**, 111, (18), 3571-3576.

174. Ciofini, I.; Adamo, C.; Barone, V.; Berthier, G.; Rassat, A., Mapping the many-electron generalised spin-exchange Hamiltonian to accurate post-HF calculations. *Chemical Physics* **2005**, 309, (2-3), 133-141.
175. Moreira, I. P. R.; Illas, F., A unified view of the theoretical description of magnetic coupling in molecular chemistry and solid state physics. *Physical Chemistry Chemical Physics* **2006**, 8, (14), 1645-1659.
176. Illas, F.; Martin, R. L., Magnetic coupling in ionic solids studied by density functional theory. *Journal of Chemical Physics* **1998**, 108, (6), 2519-2527.
177. Ruiz, E.; Cano, J.; Alvarez, S.; Alemany, P., Broken symmetry approach to calculation of exchange coupling constants for homobinuclear and heterobinuclear transition metal complexes. *Journal of Computational Chemistry* **1999**, 20, (13), 1391-1400.
178. Neese, F., Importance of direct spin-spin coupling and spin-flip excitations for the zero-field splittings of transition metal complexes: A case study. *Journal of the American Chemical Society* **2006**, 128, (31), 10213-10222.
179. Ginsberg, A. P., Magnetic exchange in transition-metal complexes .12. calculation of cluster exchange coupling-constants with the X-Alpha-scattered wave method. *Journal of the American Chemical Society* **1980**, 102, (1), 111-117.
180. Noodleman, L.; Davidson, E. R., Ligand spin polarization and antiferromagnetic coupling in transition-metal dimers. *Chemical Physics* **1986**, 109, (1), 131-143.
181. Bencini, A.; Gatteschi, D.; Totti, F.; Sanz, D. N.; Mc Cleverty, J. A.; Ward, M. D., Density functional modeling of long range magnetic interactions in binuclear oxomolybdenum(V) complexes. *Journal of Physical Chemistry A* **1998**, 102, (51), 10545-10551.
182. Yamaguchi, K.; Takahara, Y.; Fueno, T.; Houk, K. N., Extended Hartree-Fock (Ehf) theory of chemical-reactions .3. Projected Moller-Plesset (Pmp) perturbation wavefunctions for transition structures of organic-reactions. *Theoretica Chimica Acta* **1988**, 73, (5-6), 337-364.
183. Rudberg, E.; Salek, P.; Rinkevicius, Z.; Agren, H., Heisenberg exchange in dinuclear manganese complexes: A density functional theory study. *Journal of Chemical Theory and Computation* **2006**, 2, (4), 981-989.
184. Ali, M. E.; Datta, S. N., Broken-symmetry density functional theory investigation on bis-nitronyl nitroxide diradicals: Influence of length and aromaticity of couplers. *Journal of Physical Chemistry A* **2006**, 110, (8), 2776-2784.
185. Wang, J. H.; Becke, A. D.; Smith, V. H., Evaluation of [S-2] in restricted, unrestricted Hartree-Fock, and Density-Functional based theories. *Journal of Chemical Physics* **1995**, 102, (8), 3477-3480.

186. Cohen, A. J.; Tozer, D. J.; Handy, N. C., Evaluation of $\langle S^2 \rangle$ in density functional theory. *Journal of Chemical Physics* **2007**, 126, (21), 214104-214107.
187. Theophilou, I.; Thanos, S.; Theophilou, A. K., Spin contamination for Hartree-Fock, optimized effective potential, and density functional approximations. *Journal of Chemical Physics* **2007**, 127, (23), 234103-234111.
188. Chipman, D. M., The spin polarization model for hyperfine coupling-constants. *Theoretica Chimica Acta* **1992**, 82, (1-2), 93-115.
189. Goursot, A.; Malrieu, J. P.; Salahub, D. R., Bonding in C_2 and Be_2 - Broken symmetry and correlation in DFT solutions. *Theoretica Chimica Acta* **1995**, 91, (3-4), 225-236.
190. Lynch, B. J.; Fast, P. L.; Harris, M.; Truhlar, D. G., Adiabatic connection for kinetics. *J. Phys. Chem. A* **2000**, 104, (21), 4811-4815.
191. Kant, A.; Moon, K. A., Dissociation-energies of gaseous CuH, AgH, AuH, and NiH. *High Temperature Science* **1979**, 11, (1), 52-62.
192. Fisher, E. R.; Armentrout, P. B., Reactions of Co^+ , Ni^+ , and Cu^+ with cyclopropane and ethylene-oxide - metal methyldene ion bond-energies. *Journal of Physical Chemistry* **1990**, 94, (4), 1674-1683.
193. Chen, Y. M.; Clemmer, D. E.; Armentrout, P. B., The Gas-Phase Thermochemistry of TiH. *Journal of Chemical Physics* **1991**, 95, (2), 1228-1233.
194. Kant, A.; Moon, K. A., Mass-spectrometric determination of the dissociation-energies of gaseous AlH, GaH, InH, ScH, and CoH and estimation of the maximum dissociation-energies of TiH, CrH, MnH, and FeH. *High Temperature Science* **1981**, 14, (1), 23-31.
195. Chen, Y. M.; Clemmer, D. E.; Armentrout, P. B., Gas-phase thermochemistry of VH and CrH. *Journal of Chemical Physics* **1993**, 98, (6), 4929-4936.
196. Sunderlin, L. S.; Armentrout, P. B., Reactions of Mn^+ with $i-C_4H_{10}$, $neo-C_5H_{12}$, $(CH_3)_2CO$, $cyclo-C_3H_6$, and $cyclo-C_2H_4O$: bond energies for $MnCH_2^+$, MnH, and $MnCH_3$. *Journal of Physical Chemistry* **1990**, 94, (9), 3589-3597.
197. Schultz, R. H.; Armentrout, P. B., The Gas-Phase Thermochemistry of FeH. *Journal of Chemical Physics* **1991**, 94, (3), 2262-2268.
198. Martin, R. L.; Hay, P. J., Relativistic contributions to the low-lying excitation-energies and ionization-potentials of the transition-metals. *Journal of Chemical Physics* **1981**, 75, (9), 4539-4545.
199. Jeng, H. T.; Hsue, C. S., Relativistic density-functional calculations of interconfigurational energies in transition-metal atoms. *Physical Review B* **2000**, 62, (15), 9876-9879.

200. Zou, W. L.; Liu, W. J., Theoretical study on the low-lying electronic states of NiH and NiAt. *Journal of Computational Chemistry* **2007**, 28, (14), 2286-2298.
201. Kadavathu, S. A.; Lofgren, S.; Scullman, R., Rotational Analysis of Some New Transitions in NiD - a Comparison between NiH and NiD. *Physica Scripta* **1987**, 35, (3), 277-285.
202. Gordon, I. E.; Le Roy, R. J.; Bernath, P. F., Near infrared emission spectra of CoH and CoD. *Journal of Molecular Spectroscopy* **2006**, 237, (1), 11-18.
203. Moore, C. E., *Atomic Energy Levels; National Bureau of standards*. 1949; Vol. I-III.
204. Herzberg, G., *Spectra of diatomic molecules*. 2nd ed ed.; D. Van Nostrand Company Inc.: Princeton, NJ, 1950.
205. Dedieu, A., *Transition Metal Hydrides*. VCH Publisher: France, 1990.
206. Gray, J. A.; Li, M. G.; Nelis, T.; Field, R. W., The electronic-structure of NiH - the (Ni+3d9 2d) supermultiplet. *Journal of Chemical Physics* **1991**, 95, (10), 7164-7178.
207. Beaton, S. P.; Evenson, K. M.; Brown, J. M., Rotational spectroscopy of the CoH radical in its ground 3-Phi state by Far-Infrared laser magnetic-resonance - determination of molecular-parameters. *Journal of Molecular Spectroscopy* **1994**, 164, (2), 395-415.
208. Ram, R. S.; Bernath, P. F.; Brault, J. W., Fourier-Transform emission-spectroscopy - the vibration-rotation of CuH. *Journal of Molecular Spectroscopy* **1985**, 113, (2), 269-274.
209. Alvaradoswaisgood, A. E.; Harrison, J. F., Electronic and geometric structures of ScH⁺ and ScH²⁺. *Journal of Physical Chemistry* **1985**, 89, (24), 5198-5202.
210. Scherlis, D. A.; Cococcioni, M.; Sit, P.; Marzari, N., Simulation of heme using DFT+U: A step toward accurate spin-state energetics. *Journal of Physical Chemistry B* **2007**, 111, (25), 7384-7391.
211. Kulik, H. J.; Cococcioni, M.; Scherlis, D. A.; Marzari, N., Density functional theory in transition-metal chemistry: A self-consistent Hubbard U approach. *Physical Review Letters* **2006**, 97, (10), 103001-103004.
212. Sorkin, A.; Iron, M. A.; Truhlar, D. G., Density functional theory in transition-metal chemistry: Relative energies of low-lying states of iron compounds and the effect of spatial symmetry breaking. *Journal of Chemical Theory and Computation* **2008**, 4, (2), 307-315.
213. Conradie, J.; Ghosh, A., DFT calculations on the spin-crossover complex Fe(salen)(NO): a quest for the best functional. *Journal of Physical Chemistry B* **2007**, 111, (44), 12621-12624.

214. Harvey, J. N., DFT computation of relative spin-state energetics of transition metal compounds. In *Principles and Applications of Density Functional Theory in Inorganic Chemistry I*, 2004; Vol. 112, pp 151-183.
215. Elkind, J. L.; Sunderlin, L. S.; Armentrout, P. B., Periodic trends in chemical-reactivity - reactions of Sc^+ , Y^+ , La^+ , and Lu^+ with H_2 , D_2 , and HD. *Journal of Physical Chemistry* **1989**, 93, (8), 3151-3158.
216. Elkind, J. L.; Armentrout, P. B., Effect of kinetic and electronic-energy on the reaction of V^+ with H^2 , HD, and D_2 . *Journal of Physical Chemistry* **1985**, 89, (26), 5626-5636.
217. Elkind, J. L.; Armentrout, P. B., Effect of kinetic and electronic-energy on the reactions of Cr^+ with H_2 , HD, and D_2 . *Journal of Chemical Physics* **1987**, 86, (4), 1868-1877.
218. Elkind, J. L.; Armentrout, P. B., Effect of kinetic and electronic-energy on the reactions of Mn^+ with H^2 , HD, and D_2 . *Journal of Chemical Physics* **1986**, 84, (9), 4862-4871.
219. Halle, L. F.; Klein, F. S.; Beauchamp, J. L., Properties and Reactions of Organometallic Fragments in the Gas-Phase - Ion-Beam Studies of Fe^+ . *Journal of the American Chemical Society* **1984**, 106, (9), 2543-2549.
220. Elkind, J. L.; Armentrout, P. B., Effect of kinetic and electronic-energy on the reactions of Ti^+ with H^2 , HD, and D^2 . *International Journal of Mass Spectrometry and Ion Processes* **1988**, 83, (3), 259-284.
221. Harrison, J. F., The electronic and geometric structures of the chromium cations CrF^+ , CrO^+ , CrN^+ , and CrC^+ . *Journal of Physical Chemistry* **1986**, 90, (15), 3313-3319.
222. Michael, D. H.; Robert, G. A. R. M.; Gustavo, E. S.; Mark, S. G., An ab initio study of TiC : A comparison of different levels of theory including density functional methods. *The Journal of Chemical Physics* **1996**, 104, (17), 6628-6630.
223. Panas, I.; Schule, J.; Brandemark, U.; Siegbahn, P.; Wahlgren, U., Comparison of the binding of carbon, nitrogen, and oxygen-atoms to single nickel atoms and to nickel surfaces. *Journal of Physical Chemistry* **1988**, 92, (11), 3079-3086.
224. Sosa, R. M.; Gardiol, P.; Beltrame, G., A theoretical study of the electronic structure of transition-element carbides MnC ($\text{M} = \text{Fe}, \text{Ni}, \text{Cu}, n = 1,5$; and $\text{M} = \text{Ti}, n = 1,7$) and their interactions with an O atom by DFT methods. *International Journal of Quantum Chemistry* **1997**, 65, (5), 919-928.
225. Zhao, Y.; Schultz, N. E.; Truhlar, D. G., Design of density functionals by combining the method of constraint satisfaction with parametrization for thermochemistry, thermochemical kinetics, and noncovalent interactions. *Journal of Chemical Theory and Computation* **2006**, 2, (2), 364-382.

226. Balasubramanian, K.; Feng, P. Y.; Liao, M. Z., Geometries and energy separations of 14 electronic states of Au₄. *Journal of Chemical Physics* **1989**, 91, (6), 3561-3570.
227. Kanai, Y.; Wang, X.; Selloni, A., Testing the TPSS meta-generalized-gradient-approximation exchange-correlation functional in calculations of transition states and reaction barriers. *Journal of Chemical Physics* **2006**, 125, (23), 234104-234111.
228. Staroverov, V. N.; Scuseria, G. E.; Tao, J. M.; Perdew, J. P., Comparative assessment of a new nonempirical density functional: Molecules and hydrogen-bonded complexes. *Journal of Chemical Physics* **2003**, 119, (23), 12129-12137.
229. Deka, A.; Deka, R. C., Structural and electronic properties of stable Au_n (n=2-13) clusters: A density functional study. *Journal of Molecular Structure: THEOCHEM* **2008**, 870, 83-93.
230. Wang, J. L.; Jellinek, J.; Zhao, J.; Chen, Z. F.; King, R. B.; Schleyer, P. V., Hollow cages versus space-filling structures for medium-sized gold clusters: The spherical aromaticity of the Au-50 cage. *Journal of Physical Chemistry A* **2005**, 109, (41), 9265-9269.
231. Idrobo, J. C.; Walkosz, W.; Yip, S. F.; Ogut, S.; Wang, J.; Jellinek, J., Static polarizabilities and optical absorption spectra of gold clusters (Au_n, n=2-14 and 20) from first principles. *Physical Review B* **2007**, 76, (20), 205422-205433.
232. Schwerdtfeger, P.; Hermann, H. L.; Schmidbaur, H., Stability of the gold (I) phosphine Bond. A comparison with other group 11 elements. *Inorganic Chemistry* **2003**, 42, (4), 1334-1342.
233. Stoll, H., Large-core vs. small-core pseudopotentials: A case study for Au₂. *Chemical Physics Letters* **2006**, 429, (1-3), 289-293.
234. Susumu, Y.; Takao, T.; Kimihiko, H., Investigation of the use of density functionals in second- and third-row transition metal dimer calculations. *Journal of Computational Chemistry* **2001**, 22, (16), 1995-2009.

LIST OF RELEVANT PUBLICATIONS

This thesis is based in part on the following publications:

1. Goel, S.; Velizhanin, K. A.; Piryatinski, A.; Tretiak, S.; Ivanov, S. A., DFT study of ligand binding to small gold clusters, *Journal of Chemical Physics Letters* **2010**, 1, (6), 927-931.
2. Goel, S.; Masunov, A. E., Pairwise spin-contamination correction method and DFT study of MnH and H₂ dissociation curves. *Lecture Notes in Computer Science* **2009**, 5545, 141-150.
3. Goel, S.; Masunov, A. E., Towards multiscale simulations of carbon nanotube growth process: A density functional theory study of transition metal hydrides. *Lecture Notes in Computer Science* **2009**, 5544, 765-774.
4. Goel, S.; Masunov, A. E., Potential energy curves and electronic structure of 3d transition metal hydrides and their cations, *Journal of Chemical Physics* **2008**, 129, (21), 214302-214315.
5. Goel, S.; Masunov, A. E., First principles study of transition metal diatomics as the first step in multiscale simulations of carbon nanotube growth process. *Fourth International Conference on MultiScale Material Modeling (MMM)* **2008**, pp.110-119.
6. Goel, S.; Masunov, A. E., Application of new pairwise spin-contamination correction approach to study the transition metal hydrides, *17th Conference on Current Trends in Computational Chemistry (CCTCC)* **2008**, pp. 155-159.
7. Goel, S.; Velizhanin, K. A.; Piryatinski, A.; Ivanov, S. A.; Tretiak, S., DFT study of optical transitions in bare and ligated small gold clusters, *Journal of Physical Chemistry Letters* – Submitted (2010)
8. Goel, S.; Masunov, A. E., Density functional theory study of small nickel clusters, *Journal of Physical Chemistry C* – Submitted (2010)
9. Goel, S.; Masunov, A. E., “Dissociation curves and binding energies of diatomic transition metal carbides from density functional theory”, *International Journal of Quantum Chemistry* – Submitted (2010)
10. Goel, S.; Velizhanin, K. A.; Piryatinski, A.; Tretiak, S.; Ivanov, S. A., Effect of ligand and solvent on geometry of Small Gold Clusters, *Journal of Physical Chemistry C* – in process
11. Goel, S.; Velizhanin, K. A.; Piryatinski, A.; Ivanov, S. A.; Tretiak, S., Benchmarking DFT functionals for optical study of ligated small gold clusters”, *Journal of Chemical Physics* – in preparation